

The University of Manchester Institute of Science and Technology

Printed by the University of Manchester, Manchester, M13 9PL, England



DTIC FILE COPY

APOSR-TR- 88-0663

AD-A196 726

A document has been approved
for public release and sale in
distribution is unlimited.

DTIC
ELECTE
JUN 30 1988
S E D



Approved for public release;
distribution unlimited.



FINAL SCIENTIFIC REPORT
1 July 1986 - 31 December 1987

[illegible]

EUROPEAN OFFICE OF AEROSPACE RESEARCH AND DEVELOPMENT
LONDON, ENGLAND

This document has been approved
for public release and sales in
distribution is unlimited.

DTIC
ELECTE
JUN 30 1988
S E D

88 6 29 143

UNCLASSIFIED
SECURITY CLASSIFICATION OF THIS PAGE

REPORT DOCUMENTATION PAGE				Form Approved OMB No. 0704-0188	
1a. REPORT SECURITY CLASSIFICATION Unclassified			1b. RESTRICTIVE MARKINGS		
2a. SECURITY CLASSIFICATION AUTHORITY			3. DISTRIBUTION / AVAILABILITY OF REPORT Approved for public release; Distribution unlimited		
2b. DECLASSIFICATION / DOWNGRADING SCHEDULE			5. MONITORING ORGANIZATION REPORT NUMBER(S) AFOSR-TR- 88 - 0663		
4. PERFORMING ORGANIZATION REPORT NUMBER(S)					
6a. NAME OF PERFORMING ORGANIZATION University of Manchester		6b. OFFICE SYMBOL (If applicable)		7a. NAME OF MONITORING ORGANIZATION AFOSR/NC	
6c. ADDRESS (City, State, and ZIP Code) Department of Physics PO Box 88, Manchester, M60 1QD			7b. ADDRESS (City, State, and ZIP Code) Building 410 Bolling AFB, DC 02332-6448		
8a. NAME OF FUNDING / SPONSORING ORGANIZATION AFOSR		8b. OFFICE SYMBOL (If applicable) NC		9. PROCUREMENT INSTRUMENT IDENTIFICATION NUMBER AFOSR-86-0193	
8c. ADDRESS (City, State, and ZIP Code) Building 410 Bolling AFB, DC 20332-6448			10. SOURCE OF FUNDING NUMBERS PROGRAM ELEMENT NO. 61102F PROJECT NO. 2310 TASK NO. A1 WORK UNIT ACCESSION NO.		
11. TITLE (Include Security Classification) A Study of the Identification and Development of Precipitation Using Dual Polarization Radar					
12. PERSONAL AUTHOR(S) Anthony J. Illingworth					
13a. TYPE OF REPORT FINAL		13b. TIME COVERED FROM 7/86 TO 12/87		14. DATE OF REPORT (Year, Month, Day) 88/01/20	
15. PAGE COUNT 147					
16. SUPPLEMENTARY NOTATION					
17. COSATI CODES FIELD GROUP SUB-GROUP			18. SUBJECT TERMS (Continue on reverse if necessary and identify by block number) Polarization Radar, Ice, Raindrops		
19. ABSTRACT (Continue on reverse if necessary and identify by block number) Polarisation radar measurements of precipitation enable ice to be differentiated from water and the size distribution of precipitation particles to be estimated. This report is divided into five parts: A. Observations of early convective echoes suggest that warm rain first develops as a very low concentration of large raindrops. B. A model is presented, suggesting that these early echoes of warm rain can form by the sweep out of cloud water by ultra-giant (10-100µm) nuclei. C. Drop size distributions in heavy rain are derived from radar observations using newly available drop shape measurements. The statistics on the natural variability of spectra are presented. D. Artefacts in polarisation measurements due to triple scattering. E. First results of the correlation of time series measurements of horizontal and vertical reflectivities are analysed.					
20. DISTRIBUTION / AVAILABILITY OF ABSTRACT <input checked="" type="checkbox"/> UNCLASSIFIED/UNLIMITED <input type="checkbox"/> SAME AS RPT <input type="checkbox"/> DTIC USERS			21. ABSTRACT SECURITY CLASSIFICATION Unclassified		
22a. NAME OF RESPONSIBLE INDIVIDUAL Lt Col James P. Koerner			22b. TELEPHONE (Include Area Code) (202) 767-4960		22c. OFFICE SYMBOL NC

DD Form 1473, JUN 86

Previous editions are obsolete.

SECURITY CLASSIFICATION OF THIS PAGE

UNCLASSIFIED

PREFACE

This final report describes work performed with the Chilbolton dual polarisation radar under contract number AFOSR-86-0193. In addition to measuring the conventional radar reflectivity factor, Z , this radar can measure the differential reflectivity, ZDR , which senses the shape of the precipitation particles. ZDR may be used to differentiate water from ice, to measure the mean size of raindrops and to provide more accurate estimates of rainfall rates.

This report is divided into five self-contained parts, each with its own set of diagrams and references. The first four parts consider analysis of Z and ZDR data obtained in 1983 and 1984; the final part describes the first results of a new parameter observed with the reconfigured radar in the fall of 1987.

PART A

Polarization Radar Studies of Precipitation Development in Convective Storms

A detailed account of the implementation and interpretation of the Z and ZDR measurements for raindrops and ice particles is given. An analysis of Z and ZDR for evolving convective storms observed in 1983 shows:

- (i) First echoes are, on occasion, characterised by a low Z /high ZDR signature indicating that warm rain first forms as a low concentration (less than one per cubic meter) of large (greater than 4mm) raindrops. Normal raindrop concentrations are several thousand per cubic meter. Recent data from the MIST program in the USA gathered in 1986 supports this suggestion.
- (ii) During vigorous convection ZDR radar measurements show that large supercooled raindrops can extend to heights where the

temperature is -12°C . These supercooled raindrops could constitute an icing threat to aircraft. This finding has also been confirmed in the MIST data in the USA, and it has been suggested (Wilson, Boston Radar Conference, Am Met Soc, Nov 1987) that these narrow columns of positive ZDR (which indicate the presence of supercooled raindrops) can be used to predict downbursts.

PART B

Radar Observations and Modelling of Warm Rain Initiation

Additional data acquired in 1984 on the development of precipitation by the low Z / high ZDR route are described. A model is presented suggesting that this rain forms by the ultra-giant nuclei (size 10-100 μm , present in very low background concentration) sweeping out cloud water.

PART C

Polarization Radar Measurements of Raindrop Size Spectra and Rainfall Rates in Heavy Rain

A precise knowledge of raindrop shape is required for the application of the ZDR technique. From our radar results we had suggested that large raindrops must be more oblate than previously believed; independent theory now confirms this. These new drop shapes agree well with the radar data. We present statistics on the variability of drop size distributions observed in convective storms.

PART D

ZDR Artefacts due to Triple Scattering

In severe storms a spurious 'flare' echo has been observed

behind storms. It is believed that this signal results from scattering from the intense echo down to the ground, then from the ground back to the intense echo, and finally from the intense echo back to the radar; because of the extra time delay this return appears to be on the same radial as the high echo but further away from the radar. This triple scattering is confined to the horizontal polarisation and so gives positive ZDR artefacts. For an S band radar these artefacts are a rare occurrence, but calculations suggest they will be more troublesome at the shorter wavelengths.

PART E

Radar Measurements of the Breadth of the Size Distribution of Participation Particles

Very recent data of $p(H,V)$, the correlation between time series data for ZH and ZV (the radar reflectivities measured at horizontal and vertical polarisations, respectively), is presented. First measurements confirm that, as expected from theory, this correlation is unity when all the particles have the same size as in drizzle, but falls when a distribution of sizes is present as in the melting layer. This parameter, and others derived from the time series data, promise additional information on the shapes, sizes and concentration of precipitation particles.

ACKNOWLEDGEMENTS

The implementation and interpretation of differential reflectivity measurements at Chilbolton was pioneered by S M Cherry and J W F Goddard of the Rutherford Appleton Laboratory; without their painstaking work and co-operation this study would not have been possible.

PART A

POLARIZATION RADAR STUDIES OF PRECIPITATION
DEVELOPMENT IN CONVECTIVE STORMS

Accession For	
NTIS GRA&I	<input checked="" type="checkbox"/>
DTIC TAB	<input type="checkbox"/>
Unannounced	<input type="checkbox"/>
Justification	
By	
Distribution/	
Availability Codes	
Dist	Avail and/or Special
A-1	



1 INTRODUCTION

Our present knowledge of how precipitation develops within clouds has been obtained using both radar and instrumented aircraft. Measurements of the radar reflectivity, Z , provide an indication of the rainfall rate; air motions can be computed from multiple doppler radar, and hydrometeor types and sizes may be obtained from probes mounted on aircraft. However, information on hydrometeors is generally available only for a very limited number of one dimensional penetrations through the less vigorous regions of a cloud, and a complete history of the hydrometeor evolution throughout the volume of the cloud can only be built up by extrapolation from these limited samples (e.g. Hallett et al, 1978; Knight and Squires, 1982; Heymsfield and Hjelmfelt, 1984, and for hail growth, Browning et al, 1976, Browning 1978).

Several radar scans through a cloud do provide a reasonably complete three dimensional picture of the extent and intensity of the radar reflectivity, Z , but Z itself gives no information on hydrometeor types, sizes or concentrations. Several empirical relationships are available which relate Z to the rainfall rate R , but because Z is proportional to the product ND^6 summed over particles of all sizes (where N is the concentration of hydrometeors of diameter D), the use of such Z - R relationships is error prone and is equivalent to assuming that all hydrometeor size distributions are identical. The same Z could result from many different size distributions having widely varying equivalent rainfall rates. An additional ambiguity occurs if mixed phase clouds are present, because liquid water has a reflectivity 6.7dB greater than ice; for melting particles interpretation of Z is even more error prone.

In this paper we present measurements not only of Z but of the differential radar reflectivity, Z_{DR} , of evolving convective clouds. This additional parameter can reduce considerably the ambiguities present in the interpretation of Z alone.

Differential radar reflectivity, Z_{DR} , expressed in decibels, is defined as

$$Z_{DR} = 10 \log (Z_H/Z_V) \quad (1)$$

where Z_H and Z_V are the radar reflectivity factors (in $\text{mm}^6 \text{m}^{-3}$) for horizontally and vertically polarised transmission respectively. Because raindrops are distorted and fall with a larger horizontal diameter than a vertical one, they give rise to positive Z_{DR} , and since drop shape is uniquely related to drop size the magnitude of Z_{DR} can be used to estimate a mean drop diameter. Z_{DR} is a ratio and is therefore independent of hydrometeor concentration, and so for rain, once the drop size is known the concentration can be derived from a knowledge of Z . Interpretation of the Z_{DR} signal for frozen hydrometeors is more difficult because shape is no longer a defined function of size and the fall mode is variable. For example larger ice particles tend to tumble and thus give very low or zero values of Z_{DR} . In the next Section we consider the implementation and interpretation of the Z_{DR} measurement in more detail, and then in Section 3 we present results of the rapid evolution of convective storms obtained in the summer of 1983.

2 THE DIFFERENTIAL REFLECTIVITY TECHNIQUE

(a) The Chilbolton Radar

The measurement of Z_{DR} is not trivial. The radar reflectivity fluctuates as the hydrometeor targets re-arrange, and so an accurate estimate of Z_{DR} is only possible if the polarisation is switched in a time short compared to this re-shuffling time. The first fast switching Z_{DR} measurements were reported by Hall et al (1980) using the Chilbolton radar. The radar, which is situated in Hampshire, England, has a quarter degree beamwidth and operates at 9.75cm; at this wavelength, Rayleigh scattering theory is generally a valid approximation and attenuation by precipitation can normally be neglected. At 3cm differential attenuation of the horizontally and vertically polarised incident radiation would introduce serious errors in the

measurement. Each range-gate data sample comprises a spatial average (linear power) over 300m (four pulse volumes). At 60km the sample volume is typically a cube of side 300m in length. Time averaging (linear power) for each data sample is over 210ms every 240ms (i.e. 64 transmitted pulses on each polarisation). The worst case systematic errors in measuring Z and Z_{DR} were estimated to be 0.7dB and 0.1dB, respectively, while the standard deviations of the random errors when measuring rain echoes were estimated to have the same values. A detailed study of the accuracy of the measurement has been given by Cherry and Goddard (1982).

Herzogh and Carbone (1984) have shown that when strong reflectivity gradients in Z are present, a mismatch of the polarisation characteristics of the antenna sidelobes may give rise to totally false Z_{DR} values. In this case it is possible for the main beam to be sensing a low reflectivity region, but for a significant part of the reflected signal to be due to the sidelobe detecting the high Z region. They give examples from the 1° beamwidth CP2 radar where mismatched sidelobes result in spurious regions of high positive and negative Z_{DR} on either side of a reflectivity maximum. Very much higher reflectivity gradients would be required to produce such effects for the quarter degree beamwidth of the Chilbolton radar, but we shall return to this potential problem when discussing the observations in Section 3.

(b) Z_{DR} of Rain

If hydrometeors are assumed to be oblate spheroids, having their figure axes vertical, then application of Gans scattering theory gives the curves in Figure 1 (from Hall et al, 1984) showing the value of Z_{DR} as a function of axial ratio for liquid water and air-ice mixtures. The Figure clearly demonstrates that for a given shape this ratio is much larger for liquid water than for ice. For rain it is probably valid to assume that the drops fall with their figure axes aligned in the vertical, but any canting or tumbling will lead to lower values of Z_{DR} : in the extreme case of random tumbling, which may occur for ice particles, Z_{DR} will be zero.

The most accurate laboratory measurement of equilibrium raindrop shapes is provided by Pruppacher and Pitter (1971). In a series of comparisons of radar observations for values of Z_{DR} up to 2dB, with both groundbased distrometers (Goddard et al, 1983) and airborne measurements (Cherry et al, 1984) Goddard and Cherry (1984a) found significantly improved agreement if they used slightly more spherical shapes than those of Pruppacher and Pitter. This modified relationship between drop diameter and Z_{DR} is displayed on the abscissa of Figure 2. Oscillations of raindrops are believed to be asymmetric, and if these are excited then a time averaged shape should be more spherical than the equilibrium one, and this could reduce the observed value of Z_{DR} (Beard et al, 1983). It could be argued that because oscillations are collision induced, any correction to Z_{DR} would have to be concentration dependent. Direct photography of raindrops at the ground (Jones, 1959) indicates that a degree of canting is present, but the wind shear at the ground may not be representative of conditions within clouds; computations (Beard and Johnson, 1983) suggest that shear produced by turbulence would lead to small canting angles distributed around a mean zero value. However, the changes proposed by Goddard and Cherry are actually within the experimental error of the Pruppacher and Pitter measurements, and so there is no evidence that canting or collision induced oscillations affect the Z_{DR} measurement of rain. The calibration of Z_{DR} is so sensitive to drop shape that at present it is able to detect changes in shape that cannot be resolved by direct photography.

If both Z and Z_{DR} are measured for rain then the data can be fitted to any two parameter raindrop distribution. Figure 2 considers one extreme example, the monodispersed spectrum, and for a given Z_{DR} the curves show the expected values of Z for a rainfall rate of 1mm hr^{-1} and for drop concentrations of 1 and 100 per cubic meter. Because Z_{DR} is independent of concentration, the values of N and R scale linearly with Z . There is uncertainty over the average shape of drops having an equivalent diameter above 4mm. Some recent aircraft measurements (Cooper et al, 1983) suggest that they are more oblate than the equilibrium shapes of Pruppacher and Pitter, with a 6mm drop having a Z_{DR} of 5.8dB instead of 3.8dB,

and an indication that the values of 7mm drops should be 7.7dB rather than 4.18dB. The two dotted branch to the curves in Figure 2 for Z_{DR} above 2.5dB are computed using these more oblate shapes.

The Marshall Palmer raindrop size distribution is given by

$$N(D) = N_0 (\exp(-3.67 D/D_0)) \quad (2)$$

where N_0 is $8000\text{m}^{-3} \text{ mm}^{-1}$ and constant, and D_0 depends upon the rain rate and is equivalent to a median drop size such that an equal volume is contained in drops smaller and larger than D_0 . If both Z and Z_{DR} are available then a fit to a generalised exponential distribution with both N_0 and D_0 as variables is possible (Seliga and Bringi, 1976). In Figure 3 the abscissa shows the relationship between Z_{DR} and D_0 obtained by weighting the Z - D dependence in Figure 2 and truncating the exponential spectra at 8mm diameter. As above, because they scale linearly with Z , the values of N_0 and R may be obtained by linear extrapolation of the plotted curves. According to this Figure values of Z_{DR} above 5dB cannot be fitted to realistic exponential raindrop size distributions if the drop shapes of Pruppacher and Pitter are used.

Some caution should be exercised in interpreting these curves for Z_{DR} values above 3dB because of the uncertainty in the precise shapes of the larger drops and the sensitivity of the curves to the truncation of the exponential. If the exponential is not truncated at 8mm then, for D_0 above 4mm, because the very few drops above 8mm are so distorted, their contribution determines Z_{DR} . Consequently in very intense rain the shape of the drops at the truncation limit of 8mm-fixes the maximum possible value of Z_{DR} to about 3.5dB for Pruppacher-Pitter shapes. If the more oblate shapes of Cooper et al are used then an 8mm truncation limit would lead to a maximum Z_{DR} of around 6dB.

The sensitivity of predicted values of Z_{DR} in very intense rain to the rather arbitrary choice of the truncation limit of the exponential is rather artificial; the observed concentrations of these very large drops are in fact smaller. Ulbrich and Atlas (1984) have suggested introducing this effect more naturally by the use of gamma distributions of the form:

$$N(D) = N_0 D^m \exp(-(3.67 + m) D/D_0) \quad (3)$$

The third variable, m , is zero for a pure exponential and infinity for monodispersed spectra and is a measure of spectral width. Ulbrich and Atlas (1984) suggested using $m = 2$, but Goddard and Cherry (1984b) obtained even better agreement with measured rainrates for a value of $m = 5$. The magnitudes of N , N_0 and R calculated from Figures 2 and 3 ($m = \text{infinity}$ and zero) represent limits, with the true value of the total drop concentration probably lying between these two extremes. We note that for an observed Z and Z_{DR} combination the choice of the monodispersed spectrum will result in predicted rainfall rates typically 3dB greater than for the exponential spectrum.

(c) **Measurements of Hydrometeors above the 0° isotherm**

The shape of an ice particle and its mode of fall is not a unique function of its size and so the analysis of the Z_{DR} signal is complicated. Hall et al (1984) consider the problem in detail, and Figure 1 taken from their paper, demonstrates some of the possible ambiguities. Even if the particles were all aligned with the major axis horizontal we see that Z_{DR} would depend not only on the particle shape but also on the density. If they are not perfectly aligned as they fall, then the value of Z_{DR} will be lower, falling to zero for random tumbling. Further complications and ambiguities would arise if the actual ice particle shapes were used rather than idealised oblate spheroids.

From experience with the Chilbolton data Z_{DR} is usually very close to zero in regions of convective clouds where the temperature is below zero, indicating nearly spherical or randomly orientated tumbling ice particles. In the next Section we shall be considering transitory regions of high positive Z_{DR} above 4dB within convective clouds which extend both above and below the zero degree isotherm and occur where Z is moderate or high. We shall now consider the types of hydrometeor which could give rise to such signals.

(i) **Dry ice particles**

From Figure 1 snow cannot give a Z_{DR} above 1dB, but a Z_{DR} of +4dB can result from dry aligned oblate spheroids of ice having axial ratios of 0.15 for an ice-air mixture of density 0.5g cm^{-3} or spheroids of solid ice with a ratio of 0.4. For example, Hall et al (1984) found regions of high positive Z_{DR} in the upper regions of stratiform clouds where Z is low and suggested that these may be due to small ice crystals in the form of plates which fall with their larger dimension horizontally aligned. Direct aircraft observations (Bader et al, 1986) flying through such clouds in 1984 have confirmed this suggestion. However, such small particles can give only low values of Z and on melting would acquire a water coating and give much larger values of Z_{DR} just below the 0°C isotherm before subsequently collapsing to smaller raindrops. Hall et al (1984) do find regions of positive Z_{DR} in association with the bright band in Z which are obviously caused by melting particles, but for the observations we shall present there was no bright band and the positive Z_{DR} extended 2km above the zero degree isotherm.

The various habits of ice crystal growth can result in extremely oblate shapes but because of their size would be associated with low values of Z . Larger ice particles are formed by aggregation or riming and there is no evidence from aircraft measurement that they would have both such a degree of oblateness and also be aligned when they fall. Although the fall mode of larger

frozen hydrometeors and hailstones is not well known (Thwaites et al, 1977, Matson and Huggins, 1980), most evidence suggests that discs tumble when the Reynolds number exceeds 1000 (Pruppacher and Klett, 1980).

(ii) **Ice in wet growth**

Hail or graupel particles in wet growth will have a Z_{DR} of 4dB if the axial ratio is 0.65. This could happen in two ways; either sufficient water builds up on a spherical particle, or a surface layer of water on a quite asymmetric hail pellet stabilises it and stops it tumbling. The particles would probably shed any excess water, but if for the sake of argument, we extend the analysis of Bailey and Macklin (1968) to smaller particles with a fall velocity of $V = 1.43 (D)^{0.8}$ where D is in mm and V in $m s^{-1}$ (Pruppacher and Klett, 1980), we find that if the surface is to be wet, then for diameters of 2, 4 and 10mm, a cloud liquid water content of 13, 7.3 and $3.2 g m^{-3}$ respectively is required. Even higher values would be needed for a reasonable thickness of water to build up, and for rough particles with higher ventilation coefficients these values should be increased threefold. From sonde ascents made on the days in question the maximum adiabatic liquid water content at $0^{\circ}C$ and $-10^{\circ}C$ cannot exceed $5g$ and $7g m^{-3}$. We conclude that small graupel particles in wet growth require unrealistic liquid water contents and would also melt to give much smaller Z_{DR} below the freezing level. Computation (Mason, 1956) shows that for solid ice spheres to fall 2km below the freezing level without melting completely, the original diameter must be at least 4mm; for graupel of density $0.3g cm^{-3}$ the equivalent size is 8mm. However, interpretation of these signals in terms of hail of diameter greater than 5mm which is in wet growth cannot be ruled out.

(iii) **Supercooled raindrops**

A simpler explanation of such signals would be to assume they are due to large supercooled raindrops, a $Z_{DR} + 4\text{dB}$ being equivalent to a diameter of about 6mm; and when analysing these results we shall adopt this approach. We shall return to consider the wet growth aspects in the discussion Section.

3 RESULTS OBTAINED IN 1983

The aim of the 1983 studies was to trace the development of isolated convective clouds. Typical echoes from these clouds have horizontal diameters of about 5km and about 5 vertical sections (RHIs) at different azimuths were sufficient to identify the maximum echo and its spatial extent. Each RHI takes about 30 seconds, so an observation at any particular azimuth was obtained every 2 or 3 minutes. Occasional horizontal sections (PPIs) served to confirm the isolated character of the storms. Hall et al (1980) reported that pillars of $+veZ_{DR}$ extending higher than the 0°C isotherm were occasionally observed, and suggested that they were due to supercooled raindrops. One particular goal was to find out if these columns of large $+veZ_{DR}$ were a common occurrence and to study their persistence. Because there is no area of preferred convection over Southern England the location of first echoes is difficult, but in these examples the problem was alleviated, because winds were very light leading to minimal advection of cells, and on 6 and 7 July a slight shear resulted in the development of sequences of daughter cells.

3(a) 7 July - 1635 to 1655

On this day the 1200 hrs GMT sonde ascent from Crawley, 80km to the east of Chilbolton, showed that a further rise in surface temperature of 2 or 3 degrees would be sufficient to lift the moist low level air to the condensation level of 1.1km, this air could then, in the absence of mixing, rise to the 250mb level. Winds throughout the troposphere were very light from between 250 and 270° and at no height exceeded 5 m s^{-1} . The freezing level was at 3.3km, with unmixed cloudy air perhaps 2° warmer. In the afternoon a few vigorous showers developed.

Two weak isolated echoes 30 and 40km East of Chilbolton are clearly visible in Figure 4 which is a 2° elevation PPI. A further ten kilometers distant at 50km range is a much more extensive row of vigorous cells having reflectivities above 50dBZ. This PPI shows that at an altitude of 1.4km an isolated echo at 40 km range and 5km lateral distance has areas where Z is 20 to 30dBZ accompanied by anomalously high Z_{DR} values above 3dB. This combination is so far from the predictions of a Marshall-Palmer raindrop size distribution (see Figure 3) that 42 RHI and 3 PPI scans were made through this cell in 30 minutes in order to trace its evolution; each RHI being separated by only 1°, which is equivalent to a distance of 700m at this range. The isolated cell at 30km range and -6km lateral distance has Z values above 20dBZ but is not accompanied by any unexpectedly high values of Z_{DR} .

The first vertical section through the most intense part of this weak echo obtained at 1635-40 (all times are GMT), three minutes before the PPI, is displayed in Figure 5. A vertical profile of Z and Z_{DR} at the gate where the maximum Z occurs is plotted in Figure 6. RHIs at neighbouring azimuths show lower Z

values. These data confirm that the cell had a Z which only locally reached 34dBZ whereas the value of Z_{DR} widely exceeds 2dB with a maximum of 4.1dB where Z is less than 30dBZ. In Figure 5 the high Z_{DR} region extends in a narrow column almost to the ground. Half-melted ice particles might give such a large Z_{DR} but they would need to be large to survive such a fall without complete melting, and raindrops would need to have a diameter of about 5 or 6mm to assume such an oblate shape. In either case the low values of Z must imply that such large particles are present in very low concentrations.

This cell subsequently intensified rapidly, but because of the light westerly winds did not change azimuth appreciably and the range only increased by about 1km every 10 minutes or so. The actual 30dBZ echo in Figure 5 did not grow, but, perhaps not surprisingly in view of the large particles below the maximum echo, it fell to the ground in the following five minutes, as did the subsidiary 10dBZ echo at 37km range. Instead of these echoes growing, a local maximum in Z of 24dBZ at 2.5km altitude accompanied by a Z_{DR} of over 3dB located 1.4km to the south (2° in azimuth) increased rapidly in intensity and areal extent, so that by 1641-10 the vertical section in Figure 7 was observed with the development of a narrow vertical column of positive Z_{DR} . The vertical profile displayed in Figure 8 taken through the most intense part of this column confirms values of Z_{DR} of 4dB above the freezing level with Z reaching 38dB at 4.8km altitude. Two minutes later the vertical sections indicate little change in the column but show that the maximum height of the 20dBZ contour has risen by just over 1km, equivalent to a vertical velocity of almost 10m s^{-1} . This contour is growing up into an area where no echo was previously detectable, so an alternative explanation in

terms of particle growth in situ seems unlikely.

A typical RHI obtained a further five minutes later at 1648-10 is displayed in Figure 9 and shows a quite different character. Although the cloud has grown further and at 3km height Z has reached 54dBZ, a traditional hail signature (Geotis, 1963), the column of positive Z_{DR} has vanished. The vertical profile of Z and Z_{DR} plotted in Figure 10 highlights this transformation. the Z_{DR} signature is now typical of that commonly observed in mature glaciated cumulonimbus clouds. Above the freezing level Z_{DR} is generally within 0.1dB of zero, this is usually interpreted as tumbling hail or graupel pellets. If the particles were small raindrops, then to give a 40dBZ echo, their concentration would need to be so high that the rainfall would be over 1000 mm hr^{-1} . Below the zero degree isotherm Z_{DR} gradually increases from 0 to 5dB over a distance of 2km, consistent with the particles slowly melting to form large oblate raindrops near to the ground. Three minutes later Z values of 61dBZ were observed. The Z_{DR} gradient in Figure 10 should be contrasted with the very abrupt fall off in Z_{DR} above 5km in Figure 8, which is difficult to explain in terms of particles falling and melting. A more plausible interpretation is to consider the sharp change occurring at the boundary where a rising parcel of air containing super-cooled raindrops penetrates upwards into the glaciated region of the cloud.

The evolution from the first RHI in Figure 5 to the mature cloud in Figure 9 took only 12 minutes with the echo top rising nearly 4km at an average velocity of 5 m s^{-1} . The two minute period when there was a column of positive Z_{DR} extending towards the -10°C isotherm appeared to coincide with the most vigorous growth with the Z echo rising at about 10 m s^{-1} . It is

interesting to note that the second isolated weak Z echo in the PPI of Figure 4 which is at a range of 30km and a lateral distance of -6km, which was not accompanied by any large positive Z_{DR} , failed to develop.

3(b) 6 July - 1606 to 1615

The 1200 sonde ascent from Crawley indicated a similar structure to that on the 7 July described above. The calculated freezing level was 3.2km and the winds again were less than 5 m s^{-1} , but from a direction between 170° and 180° . An isolated daughter cell was first detected in the 5° elevation PPI which is displayed in Figure 11. This cell is at 30km range and 7km lateral distance, at larger lateral distances no returns were detected, but at 2km lateral distance only 3km from the cell is the start of a long narrow band of intense echoes extending about 50km to the south. No echo was detected at the position of the isolated cell in the 4° elevation PPI where the height of the beam at this range would be about 2km. Because the 5° elevation showed such anomalously high Z_{DR} values of 2.4dB accompanied by a Z echo of 25dBZ, a series of 25 RHI scans through the cell was made in the 12 minutes following the PPI. Each RHI was separated by 2° , equivalent at this range to a horizontal distance of 1km. As the southerly wind was so light, the echo was remained between azimuths 141° and 149° throughout this period, advecting by less than 1km in 20 minutes.

Fig 12 displays the contours in Z and Z_{DR} for the first RHI at 1607-00 through the most intense section of this daughter cell. The daughter cell has a maximum Z of 33dBZ but, as in the example of 7 July, is accompanied by much higher values of Z_{DR} than would be predicted by most commonly observed raindrop size

distributions. This is further demonstrated by the vertical profiles in Z and Z_{DR} in Figure 13, where values of Z_{DR} of 3dB are found where Z is only 30dBZ. By similar arguments to those employed in Section 3(a) these particles must be large raindrops or large melting ice particles and so the low Z value implies the particles are present in very low concentrations.

This daughter cell grew rapidly and the vertical section in Figure 14 was obtained 6 minutes later at 1613-20 with the highest Z value of 51dBZ coinciding with the maximum observed Z_{DR} of 5.1dB. Again the Z_{DR} contours show a well developed narrow vertical column containing the highest values of differential reflectivity which extends over 1.5km above the freezing level to where the temperature is about -10°C . As this feature is virtually absent on the neighbouring RHIs we conclude that the diameter of the column is only about 1km. An RHI 2 minutes later (not illustrated) still shows the Z_{DR} column, while Z has further increased to 61dBZ and the echo top has risen a further 1 km implying an upward velocity of close to 10 m s^{-1} .

The evolution is simpler than the previous example in that only one maximum in the echo could be distinguished, though by the time of Figure 14 the anvil from the band of more active cells visible in the earlier PPI is only 2km away from the daughter cell. The maximum echo in this anvil is about 20dBZ, and Figure 15 shows that by 1618-20 it had merged with this developing cell which now has a maximum echo of 65dBZ. The Z_{DR} in this Figure is quite revealing. At 30km range the positive Z_{DR} is confined to regions below the freezing level indicating ice above, but at 33km the positive Z_{DR} extends to a height of 4km with a maximum of 5dB at 2.3km altitude; above this there is a region of negative Z_{DR} with a peak value of -1.4dB occurring at

5km where Z is 62dBZ. These various regimes of Z_{DR} can be clearly identified in the vertical profile of Z and Z_{DR} passing through this region of negative Z_{DR} which is displayed in figure 16. Above 6km altitude, Z is high and Z_{DR} is very close to zero, and this probably results from tumbling graupel and hail pellets; below the freezing level (which is at 3.2km altitude), Z_{DR} increases rapidly and this is consistent with large raindrops or large oblate melting hydrometeors.

Negative values of Z_{DR} such as those between 3.2 and 6km in figure 16 have not been previously observed with the Chilbolton radar. In Section 4 we will analyse all possible effects which could give rise to artificial spurious values of negative Z_{DR} , but if for the moment we assume that the data is valid, then the only plausible explanation is that this negative value is due to oblate or conical hailstones falling with some degree of alignment. From Figure 1, solid ice spheroids with vertical diameters 20% greater than the horizontal would have a Z_{DR} of about -1dB. Prolate spheroids would give similar values. This feature is very localised and quite transitory. No negative values of Z_{DR} can be found at the neighbouring azimuths only 1km away, and in the previous RHI at the same azimuth as Figure 16 but two and a half minutes before, there is just one gate showing a negative value of -0.7dB.

The major evolution appears to be similar to the 7 July case previously described, in that a cell having low Z but high Z_{DR} grew very rapidly. The highest value of Z observed in the cell increased from 31dB to 65dBZ in only 12 minutes.

3(c) 22 August - 1358 to 1414

The evolution of an isolated shower on this day is shown in Figures 17, 18 and 19. Sonde ascents showed that the wind was

again very light at all levels and that the freezing level was about 3.1km. The convection was of quite limited depth with the 20dBZ echo contour never rising above 6.6km altitude, but in spite of this the plots show the development of an intense echo of over 60dBZ which is associated with a Z_{DR} of 8.3dB, the highest yet recorded with the Chilbolton radar.

The first RHI through the most intense part of the isolated developing cell obtained at 1358-40 is displayed in Figure 17 and shows a large area above the freezing level where values of Z_{DR} exceed 4dB and Z is 40dBZ. The echo top (20dBZ) is at 5.6km, but above 5km values of Z_{DR} are essentially zero. Although the high values of Z_{DR} extend down to the ground the values of Z are much less at these lower altitudes, indicating that the major part of the precipitation is still above the zero degree isotherm but that a few large precipitation particles are reaching the ground. Six minutes later, as shown in Figure 18, the values of Z in the centre of the cell reach over 63dBZ but the echo top at this azimuth is only 5km. These high values of Z were accompanied by a Z_{DR} value of 8.3dB at one gate. This gate was at 2.8km altitude, very close to the freezing level, and was situated in the centre of a region 900m wide and 600m deep where Z_{DR} was above 6dB. If we use the more oblate drop shapes implied by Cooper et al, then this region with Z_{DR} values of 6dB could be due to raindrops. The single value of 8.3dB may be an unrepresentative sample of a Z_{DR} value which is fluctuating about a 6dB mean; these fluctuations are thought to arise when a broad spectrum of drops is present.

On this day the winds were very light and, in the absence of shear, the intense echo in Figure 18 fell to ground and the cell decayed. The compact region of Z_{DR} above 6dB fell 1km by the time

of the next RHI 140 seconds later, and after a further 140 seconds it was just discernible 1.2km lower at an altitude of only 600m. By this time Z_{DR} was everywhere zero above the freezing level, with positive values confined to altitudes below 3km. This is the pattern usually observed with mature convective storms. Figure 19 was obtained eleven minutes after Figure 18, and shows that the highest values of Z_{DR} were only 2dB where Z was above 50dBZ implying raindrop size distributions much closer to the Marshall-Palmer. From Figure 3 if N_0 is $8000 \text{ m}^{-3} \text{ mm}^{-6}$ then the contours of 1dB and 2dB in Z_{DR} should be near to the contours of 35dBZ and 48dBZ respectively. This approximates to the situation in Figure 11.

4. POSSIBLE ARTIFACTS IN DIFFERENTIAL REFLECTIVITY MEASUREMENTS.

Before embarking upon an interpretation of the rather unexpectedly high values of Z_{DR} reported in the above convective clouds, we consider whether these observations could have been influenced by any possible spurious factors. Beard et al (1983) have suggested that raindrops oscillate and that their mean shape should be slightly more spherical than the equilibrium one; if this effect was significant then a given value of Z_{DR} should correspond to an even larger raindrops size than that assumed in this paper.

We now examine the effect of side lobes in the presence of reflectivity gradients. The symbols superposed on the five figures showing the vertical profiles represent each separate data point recorded for every quarter degree increment in antenna elevation. This angular resolution is equal to the beamwidth of the Chilbolton antenna. In all these profiles changes in reflectivity of 20dBZ never occur over such small angular

changes, so for the Chilbolton antenna, the signal detected by the side lobes is always much less than that sensed by the main beam. Consequently the contribution to the measured differential reflectivity by any mismatched polarisation characteristics of the sidelobes is negligible. It is also clear from Figure 16 that the negative values of Z_{DR} coincide with the maximum values of Z of over 60dBZ. Similarly the maximum values of Z_{DR} in Figure 12 occur where Z attains its highest value. If these features in Z_{DR} were artifacts due to side lobes then they should be found where Z is changing rapidly.

Differential attenuation can result in an apparent reduction in the values of Z_{DR} . If large oblate precipitation particles lie between the cell and the radar antenna, then the incident horizontal radiation will be attenuated by more than the vertical and, consequently, the received power reflected even from spherical particles will be less in the horizontal than in the vertical, leading to an apparent negative value of Z_{DR} . In Figure 14, where we have tentatively ascribed the negative Z_{DR} to conical hail, there is no echo between the cell and the antenna and so differential attenuation cannot be responsible. It is worth commenting that even using 10cm radiation this effect can occasionally be important, but is a sensitive function of the oblateness of the intervening precipitation. Calculations assuming an exponential raindrop size distribution show that for a rainfall of 100mm/hr having a ZDR of 1dB the differential attenuation is only 0.01dB/km, but if ZDR is 3dB then the differential attenuation is increased tenfold. These figures are an order of magnitude higher at 5.6cm. Negative values of ZDR of below -0.2dB can be detected in the PPI in figure 11, at a range of 29 to 30km and a lateral range of -7km; the lowest

value recorded being -0.6dB at one gate. The radiation between this region and the antenna has traversed a 2km region having a Z of over 50 dBZ and a differential reflectivity above 3dB . A differential attenuation of 0.1dB/km can account for the slightly negative values of Z_{DR} . In none of the other sections discussed is this effect important.

The observation in mature intense convective storms that the values of Z_{DR} are so close to zero for all values of Z up to 65dBZ gives us additional confidence that there is no systematic bias between the processing of the signals of the vertical and horizontal polarisations. We conclude that the reported differential reflectivity observations are valid.

5. INTERPRETATION OF THE 1983 RESULTS.

The three evolutions described in Section 3 are the examples where the echoes were located and observed at an early stage in their growth. The most striking aspects of the evolution are the occurrence of high positive values of Z_{DR} accompanied by fairly modest values of Z as shown in Figures 5, 12 and 17. In view of the arguments advanced in Section 2 we believe that these high values of Z_{DR} imply large particles. In the early stages the high values of Z_{DR} occur in a broad region extending up to 2km both below and above the zero degree isotherm indicating that their origin is not in the melting layer. Smaller ice particles would melt to small raindrops in falling 2km, and larger ice particles would tumble. There is a possibility that the high Z_{DR} is due to large ice particles which are in wet growth above the 0°C isotherm and are melting below it, but the observation that hail falling to the ground is accompanied by zero Z_{DR} does not support this. We shall offer an explanation assuming that these high values of Z_{DR} are due to large raindrops, but shall retain the possibility that they are due to even larger wet ice particles.

Figure 5 and the accompanying vertical profile in Figure 6 show that in this first RHI of the 7 July example, Z values near to 30dBZ were accompanied by Z_{DR} of about 3dB. Assuming a monodispersed distribution of raindrops then Figure 2 indicates that the cloud contains drops of about 4mm diameter present in a concentration of rather less than one per cubic meter. The more commonly observed exponential distribution plotted in Figure 3 using Pruppacher and Pitter drop shapes predicts a value of N_0 of about 8 (instead of 8000 in the normal Marshall Palmer

distribution) and a rainfall rate of 0.2 mm/hr. Even with the more oblate drop shapes of Cooper et al N_0 is 40 and R is 0.35 mm/hr. The first RHI obtained in the 6 July example in Figure 12 and the profile in Figure 13 again show a Z of slightly less than 30dBZ where Z_{DR} is just above 3dB. These observations again suggest, using either the monodispersed or exponential model that there is a very low concentration of large (above 4mm) supercooled raindrops present in the cloud. In this case the rainfall rate is considerably less than 1mm/hr, whereas an empirical Z - R relationship would indicate about 2.5mm/hr.. The example on the 22 August shows a similar deviation from the Marshall-Palmer distribution. In the centre of the echo is a large area having Z values of about 40dBZ occurring where Z_{DR} is about 4dB, suggesting a mean raindrop size of 5 or 6mm. Figure 3 shows that this data cannot be fitted to an exponential raindrop size distribution if the Pruppacher and Pitter drop shapes are used, but a fit is possible using the more oblate shapes of Cooper et al, and implied values of N_0 are at least two orders of magnitude lower than the Marshall-Palmer value. The high Z_{DR} values of 6dB observed on 22 August are compatible with raindrops providing the Cooper et al shapes are used.

An analysis of the average values of Z_{DR} for a given Z using data on all convective clouds obtained on many different days, shows that the mean data does follow the Marshall-Palmer dotted curve in Figure 3 with $N_0 = 8000$ (Caylor and Illingworth, 1986). Individual data points are scattered around this mean curve, but further analysis (unpublished) of the distribution of the data reveals that the inferred raindrop size distributions are normally quite close to the Marshall-Palmer. The combinations of Z and Z_{DR} to which we have drawn attention in Section 3 are

really quite exceptional, and only seem to occur during the early development of the clouds. When the observations for all clouds are analysed, then 99% of the data points having a Z of 30 and 40dBZ, are accompanied by Z_{DR} values below 3 and 4dB, respectively.

The sizes and concentration of raindrops calculated above relate to the region of the cloud where the reflectivity is a maximum; in other parts of the cloud the implied concentrations are even lower. Evaporating rainshafts could lead to small concentrations of large drops, but these should be fairly local phenomena not occurring near the reflectivity maximum of a developing cloud. Such a low concentration of large drops would be difficult to confirm with aircraft because the cloud is evolving very rapidly and conventional probes would not obtain a statistically significant sample in a single 1 or 2km penetration.

The evolution which emerges from this limited study is rather unusual. A small number of large (4mm) drops form, which are liquid even at -10°C . Rapid intensification of the echo follows, with Z rising at a rate of up to 30dBZ in ten minutes, with subsequent glaciation and disappearance of positive values of Z_{DR} above the zero degree isotherm. The most rapid upward growth of the echo (at a velocity of about 10m s^{-1}) appears to coincide with partial glaciation, when there is a narrow vertical column of positive Z_{DR} extending to an altitude where the temperature is about -10°C ; outside this column the values of Z_{DR} are essentially zero where the temperature is below freezing.. This column is a transitory phenomenon persisting for less than ten minutes; it is of circular cross section with a diameter of

between 1 and 2km, but the values of Z_{DR} typically reach 4dB within the column. As the cell loses its vigour the echo descends and the area of high Z_{DR} also subsides towards the ground without any very marked change in its magnitude.

In the examples presented the echoes were initially isolated, but in the second case we drew attention to the proximity of an existing cell with which the developing cloud subsequently merged. There is always the possibility that a very small number of ice crystals, far below the radar level of detectability, entered the isolated echoes, melted and then grew rapidly by coalescence. It is difficult to test such a hypothesis directly as the particles would be virtually invisible. Growth of the large drops by the normal condensation-coalescence process seems more likely.

It seems reasonable that a rapidly rising parcel of moist air could rise to an altitude where the temperature is -10°C before any of the surrounding ice particles mix in and cause rapid glaciation. It could be argued that even larger ice particles in wet growth can account for these observations, although the implied concentrations would be even lower than those calculated for the raindrops and their presence would be equally difficult to explain at these early stages of cell growth. As suggested before the evidence that hail falling to the ground has a low value of Z_{DR} implies that any surplus water should be shed. Furthermore as the particles fall and melt, the value of Z_{DR} should rise even further, which is not observed.

Once the clouds in this study glaciate the ice particle spectrum will initially be similar to the raindrop spectrum. Federer and Waldvogel (1975) report mean spectra for hail of size less than 22mm having an average N_0 of $12.1\text{m}^{-3}\text{mm}^{-1}$ and a D_0 of

8.73mm. Similar values of D_0 and N_0 are apparent from Figure 3 for the initial raindrop spectra in these three examples. There is some evidence from aircraft penetrations of developing cells (Musil et al, 1976) that the value of N_0 may be as low as 10 or 100 m^{-3} . If even smaller concentrations of large supercooled raindrops do exist in the early stages of precipitation development then they would be the natural favoured embryos which could then grow rapidly into hail without exhausting the supply of liquid water. Consequently the requirement of embryo sorting (Browning, 1978) for hail growth may not be quite so stringent. Macklin et al (1960) found that most hailstones collected in England had clear growth centres suggesting large frozen drop embryos.

In one example we infer that hail causes a negative value of Z_{DR} , although this seems to be a rare occurrence. More normally the value of Z_{DR} is nearer to zero, indicating that hail tumbles as it falls or is lacking in average orientation. A much more reliable hail signature at low altitudes in the cloud is a region of zero Z_{DR} where Z is very high, instead of the more normal positive Z_{DR} in heavy rain (Bringi et al, 1985; Illingworth et al, 1986).

6. CONCLUSION.

From a study of a number of vigorous isolated convective storms over the UK during the summer of 1983 we draw the following tentative conclusions.

a) Isolated weak echoes having moderate Z but accompanied by large positive differential reflectivity (Z_{DR}) are likely to intensify very rapidly.

b) These anomalous low Z / high positive Z_{DR} first echoes indicate very low concentrations of large precipitation particles. Although we cannot rule out the possibility that they are large ice particles in wet growth this seems most unlikely, and we propose that they are large (greater than 4mm) supercooled raindrops. Inferred drop size distributions within mature convective clouds are normally very much closer to the Marshall-Palmer distribution.

c) Such low concentrations of large drops could be very efficient hail embryos, growing to large hailstones after freezing because of the lack of competition for the cloud water. This may relax requirements for embryo sorting.

d) Narrow columns of positive Z_{DR} extending by up to 2km above the zero degree isotherm occur during vigorous convection when the echo top is rising rapidly and tend to precede high values of Z . They are generally circular in cross section and of diameter between 1 and 2km, the remainder of the cloud at these heights having Z_{DR} values very close to zero. We believe that these columns may be due to large supercooled raindrops in an ascending updraught, and that their subsequent disappearance indicates rapid glaciation.

Further data sets obtained with the Chilbolton radar should provide more evidence on the size, concentration and types of hydrometeors during the evolution of convective clouds. The additional measurement of the linear depolarisation should differentiate between particles falling with and without a vertical axis of symmetry; this may help to distinguish supercooled rain from wet ice.

REFERENCES

- Bader, M J, Clough, S A, and Cox, G P 1986 Aircraft and dual polarisation radar observations of hydrometeors in light stratiform precipitation. Submitted to Quart. J.R. Met Soc.
- Beard, K V, Johnson, D B, and Jameson A R 1983 Collisional Forcing of Raindrop Oscillations J. Atmos. Sci., 40, 455-462.
- Beard, K V, and Jameson, A R 1983 Raindrop Canting, J. Atmos. Sci., 40, 448-454.
- Bailey, I H and Macklin, W C 1968 Heat transfer from artificial hailstones. Quart. J. R. Met. Soc., 94, 93.
- Browning, K A 1978 The structure and mechanism of hailstorms, Am. Met. Soc. Monograph, 38.
- Browning, K A and Foote, G B 1976 Airflow and hail growth in supercell storms, Quart. J. R. Met. Soc., 102, 499-533.
- Cherry, S M and Goddard, J W F 1982 Design features of dual-polarisation radar, URSI Conference, Bournemouth, United Kingdom.
- Cherry, S M, Goddard J W F and Ouldrige, M 1984 Simultaneous measurements of rain by airborne distrometer and dual-polarisation radar. Radio Sci, 19, 169-176.
- Cooper, W A, Bringi, V N Chandrasekhar, V and Seliga, T A 1983 Analysis of raindrops parameters using a 2-D precipitation probe with application to differential reflectivity. 21 Conf on Radar Meteorol, AMS, Boston.
- Federer, B and Waldvogel, A 1975 Hail and raindrop size distributions from a Swiss multicell storm. J. App. Met 14, 91.
- Goddard, J W F and Cherry, S M 1984a The ability of dual-polarisation radar (coplanar linear) to predict rainfall rate and microwave attenuation. Radio Sci, 19, 201-8.
- Goddard, J W F and Cherry, S M 1984b Quantitative Precipitation Measurements with dual linear polarisation radar. 22nd Conf on Radar Meteorol. AMS, Boston.
- Goddard, J W F, Cherry, S M and Bringi, V N 1983 Comparisons of dual-polarisation radar measurements of rain with ground-based distrometer measurements. J. App. Met., 21, 252-256.
- Hall, M P M, Cherry, S M Goddard, J W F and Kennedy, G R 1980 Rain drop sizes and rainfall rate measured by dual-polarisation radar. Nature., 85, 195-198.
- Hall, M P M, Goddard, J W F and Cherry, S M 1984 Identification of hydrometeors and other targets by dual-polarisation radar. Radio Sci, 19, 132-140.
- Hallett, J, Sax, R I, Lamb, D and Murty, A S R 1978 Aircraft measurements of ice in Florida cumuli. Quart. J.R. Met. Soc. 104, 631-651.
- Herzogh, P H and Carbone, R E 1984 The influence of antenna illumination function characteristics on differential reflectivity measurements. 22nd Conf on Radar Meteorol. AMS, Boston.
- Heymsfield, A J and Hjelmfelt, M R 1984 Processes of Hydrometeor Development in Oklahoma Convective Clouds, J. Atmos. Sci. 41, 2811-2835.

- | | | |
|---|------|--|
| Illingworth, A J, Goddard, J W F, and Cherry, S M | 1986 | Detection of hail by dual-polarisation radar, <i>Nature</i> , <u>320</u> , 431-433. |
| Jameson, A R and Beard, K V | 1982 | Raindrop Axial Ratios, <i>J. Appl. Meteorol.</i> 21, 257-259. |
| Jones, D M A | 1959 | The shape of raindrops. <i>J. Meteor.</i> 16, 504-510. |
| Knight, C A and Squires, P | 1982 | Thunderstorms of the High Plains, Vol. 1 Colorado Associated University Press 282 pp. |
| Macklin, W C, Strauch, E and Ludlam, F H | 1960 | The density of hailstones collected from a summer storm. <i>Nubilia</i> <u>3</u> , 12. |
| Matson, R J and Huggins, A W | 1980 | The direct measurement of the sizes, shapes and kinematics of falling hailstones. <i>J. Atmos. Sci.</i> <u>37</u> , 1107-1125. |
| Musil, D J, May, E L, Smith, P L and Sand, W R | 1976 | Structure of an evolving hailstorm, Part IV: Internal structure from penetrating aircraft. <i>Mon Wea Rev.</i> <u>104</u> , 596-602. |
| Pruppacher, H R and Klett, J D | 1980 | Microphysics of clouds and precipitation. Reidel, Dordrecht, Holland. |
| Pruppacher, H R and Pitter, R L | 1971 | A semi-empirical determination of the shape of cloud and rain drops. <i>J. Atmos. Sci.</i> 28, 86-94. |
| Seliga, T A and Bringi, V N | 1976 | Potential use of radar differential reflectivity measurements at orthogonal polarisation for measuring precipitation. <i>J. App. Met.</i> 15, 69-76. |
| Thwaites, S, Carras, J N and Macklin, W C | 1977 | The aerodynamics of oblate hailstones. <i>Quart. J. R. Met. Soc.</i> <u>103</u> , 803-808. |
| Ulbrich, C W | 1983 | Natural variations in the analytical form of the raindrop size distribution. <i>J Clim. & Appl. Met.</i> <u>22</u> , 1764-1775. |
| Ulbrich, C W and Atlas, D | 1984 | Assessment of the contribution of differential polarisation to improved rainfall measurements. <i>Radio Sci.</i> <u>19</u> , 49-57. |

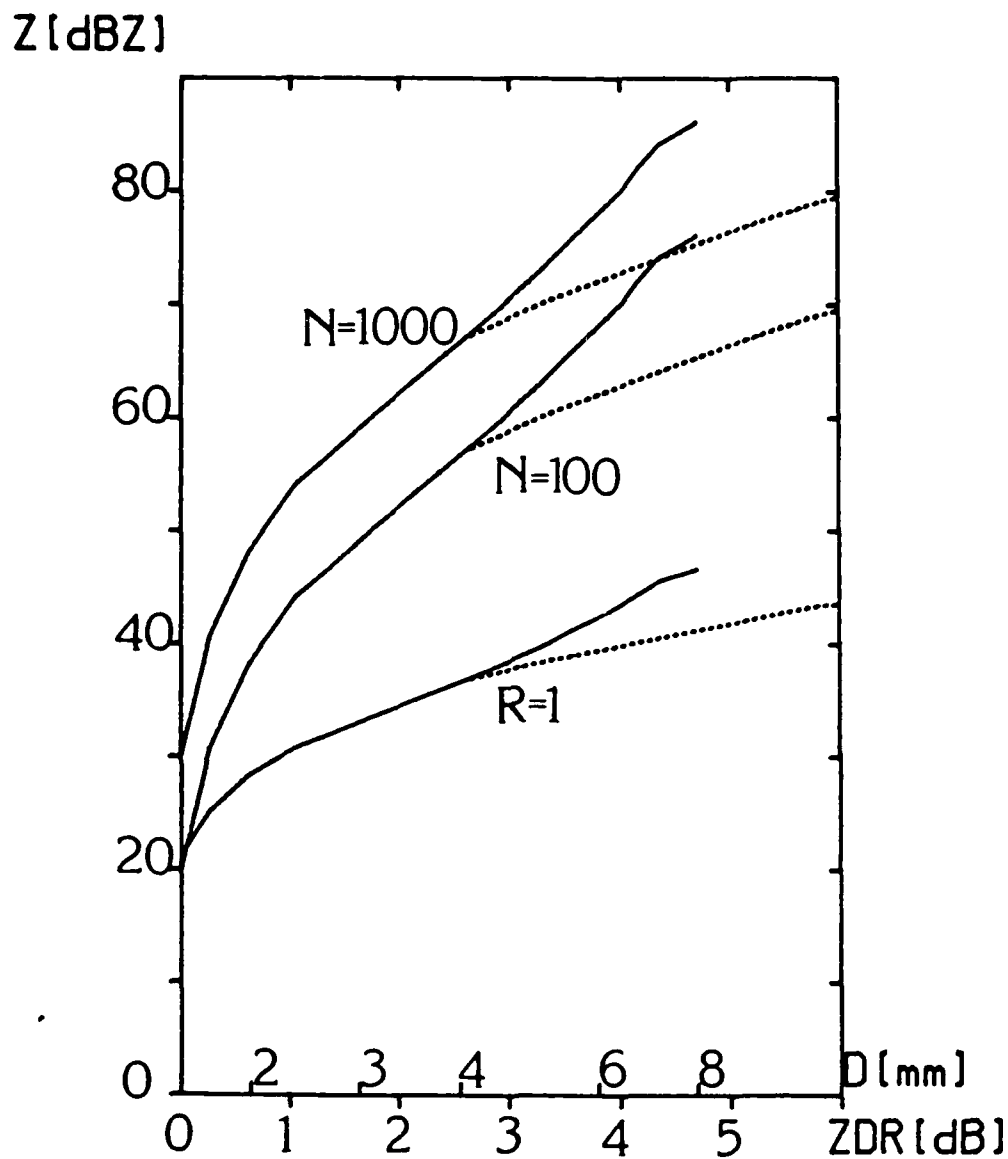
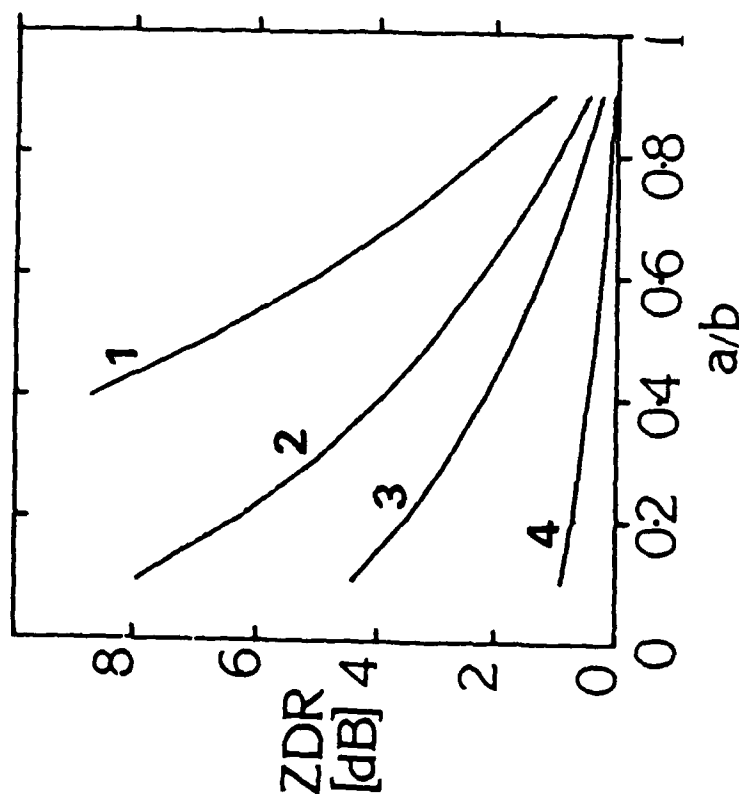


Figure 2

The variation of reflectivity, Z , with differential reflectivity, Z_{DR} , for a monodispersed distribution of raindrops having equivalent diameter D . R : Rainfall rate of 1 mm hr⁻¹. N : drop concentrations of 100 and 1000 m⁻³. Solid curves Pruppacher and Pitter shapes, dotted curves shapes extrapolated from Cooper et al.

Figure 1

The values of Z_{DR} predicted from Gans scattering theory for oblate spheroids as a function of their minor to major axis ratio, (a/b) . Minor axis vertical. Water - curve 1; solid ice of 0.92 g cm^{-3} - curve 2; ice air mixture of 0.5 g cm^{-3} - curve 3; and an ice air mixture of 0.19 g cm^{-3} - curve 4. (From Hall et al, 1984, with changes).



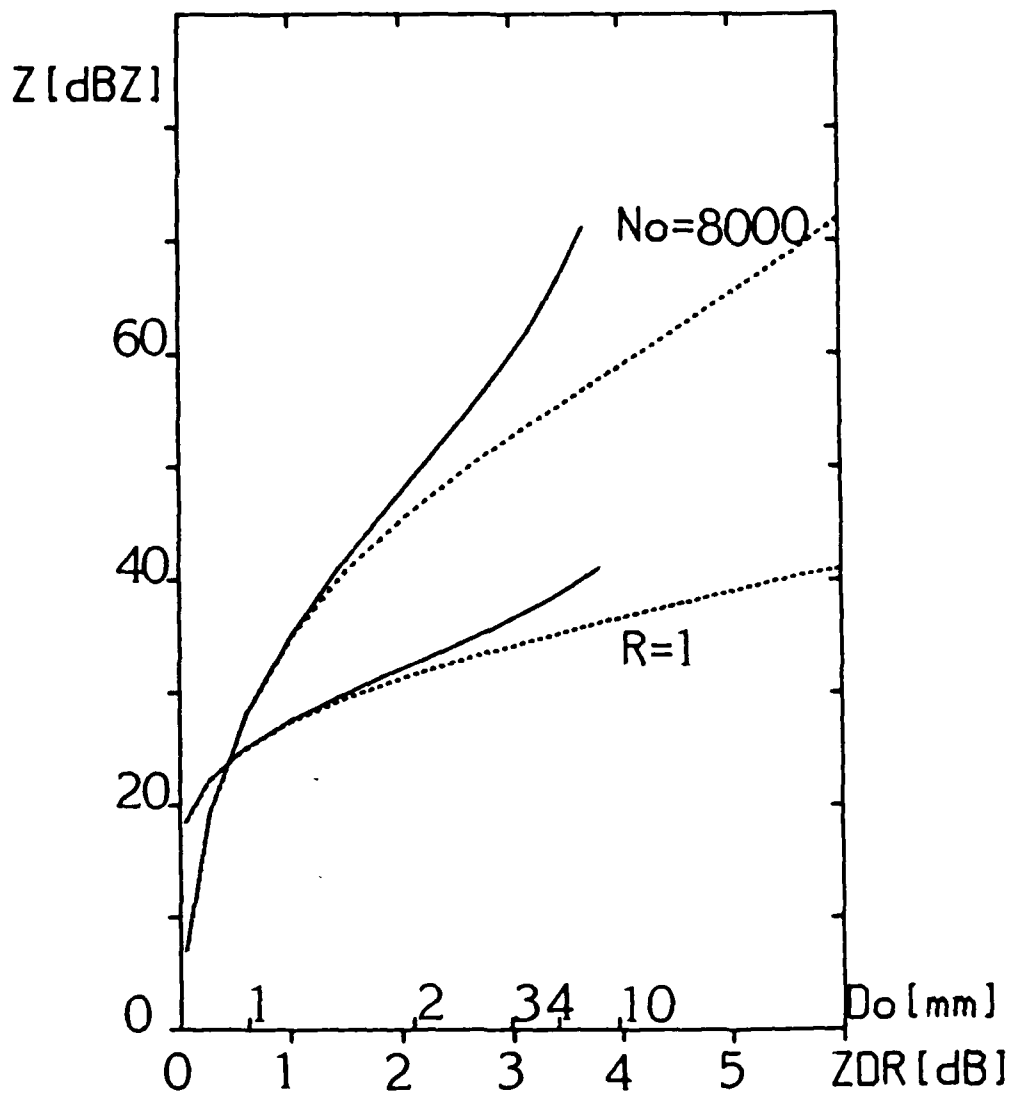
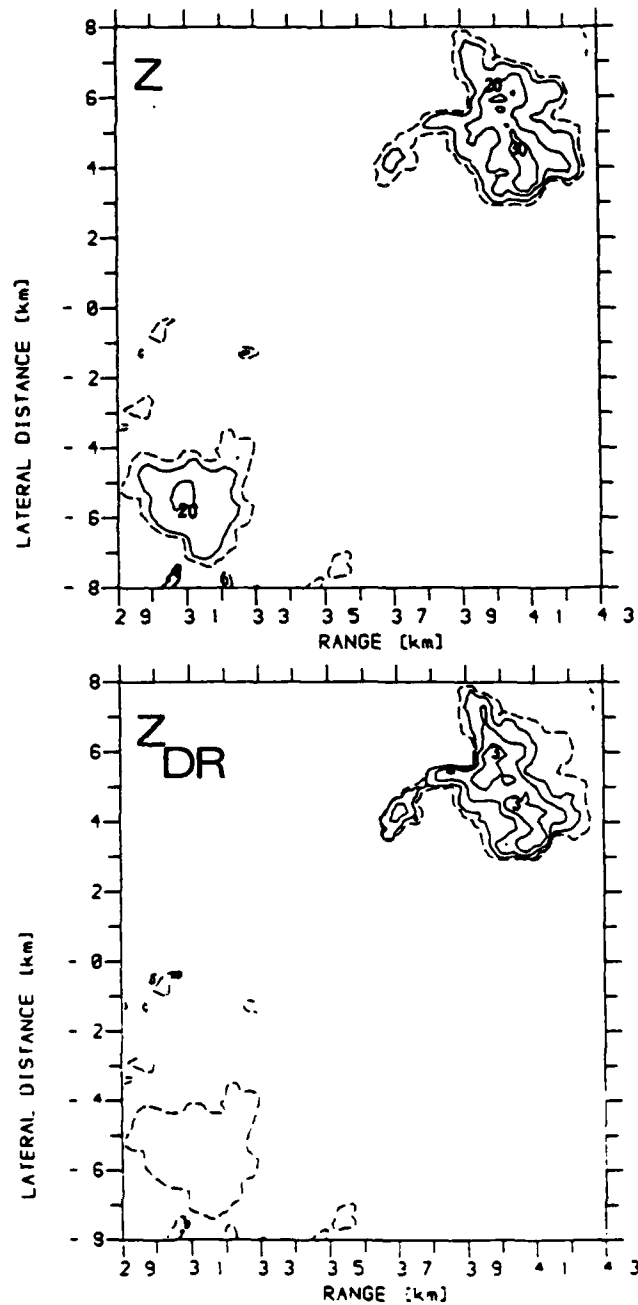


Figure 3

The variation of Z with Z_{DR} predicted for the exponential distribution of raindrops in Equation (2). Solid curves for $N_0 = 8000 \text{ m}^{-3} \text{ mm}^{-1}$ and $R = 1 \text{ mm hr}^{-1}$ using Pruppacher and Pitter shapes, dotted branches for the more oblate shapes of Cooper et al.

Figure 4

A horizontal section (PPI) at 2° elevation at 1638-00 GMT on 7/7/83 showing two isolated cells. In this and the following figures the solid contour lines in Z are drawn every 10dBZ starting at 10dBZ, and in Z_{DR} every 1dB starting at 1dB. The broken contour line in both the Z and the Z_{DR} plots is for $Z=5$ dBZ and serves to delineate the extent of the cloud.



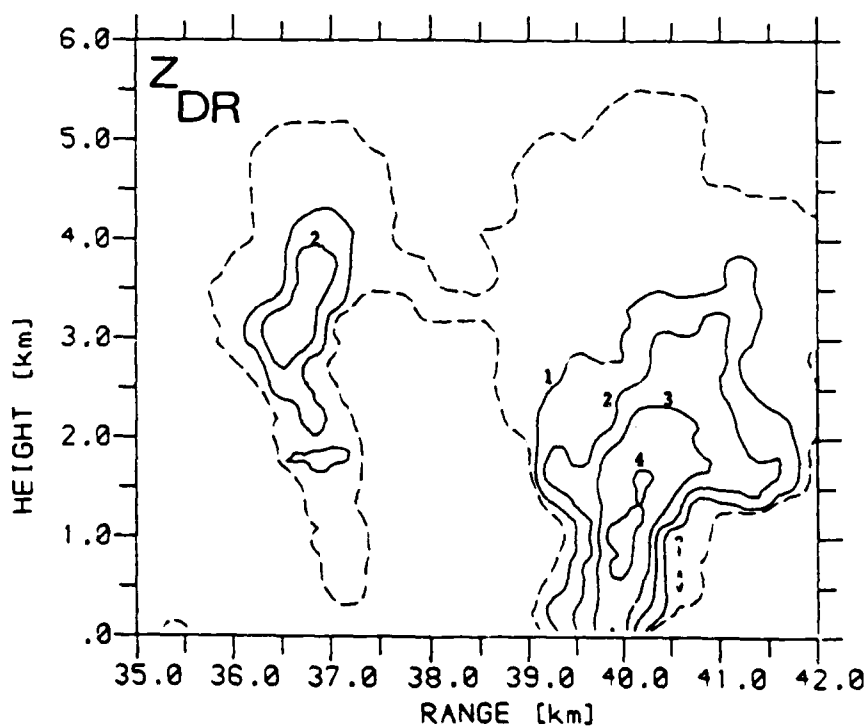
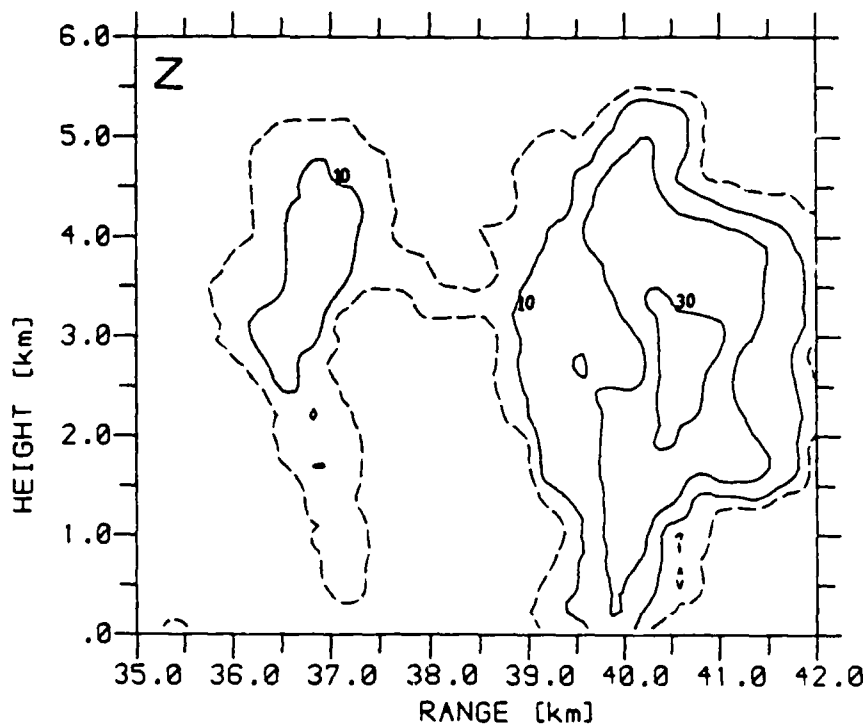
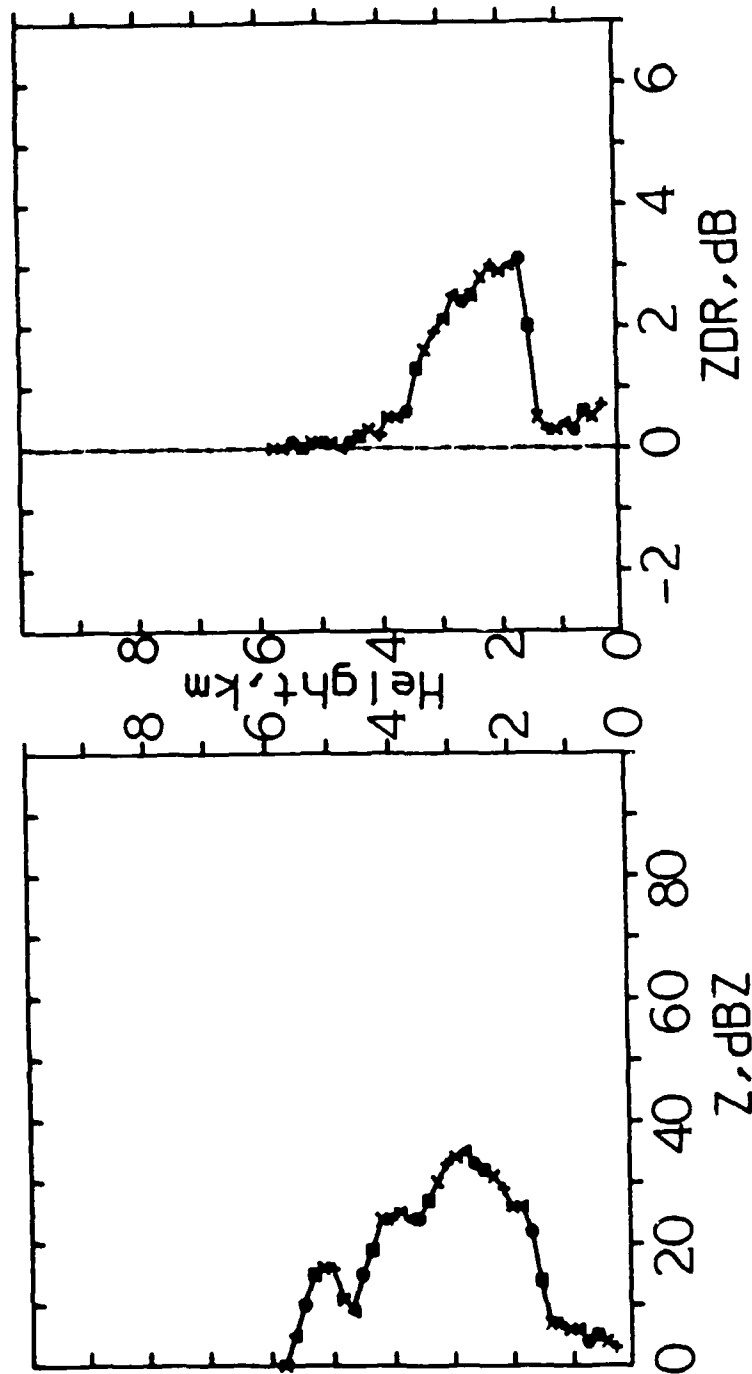


Figure 5

A vertical section at 1635-40, azimuth 93°, through the most intense part of the echo at 40 km range in figure 4. Contours of Z and Z_{DR} as in Figure 4

Figure 6

A vertical profile of Z and Z_{DR} at 40.8km range, the gate where Z is a maximum in Figure 5. Below 3km altitude values of Z_{DR} are anomalously high.



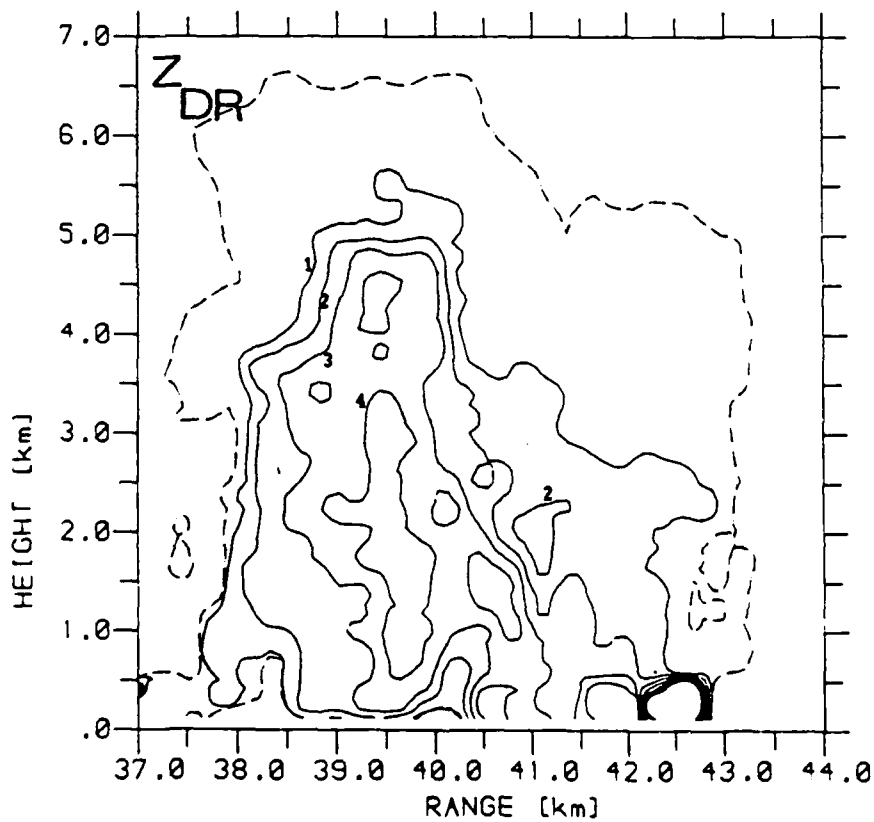
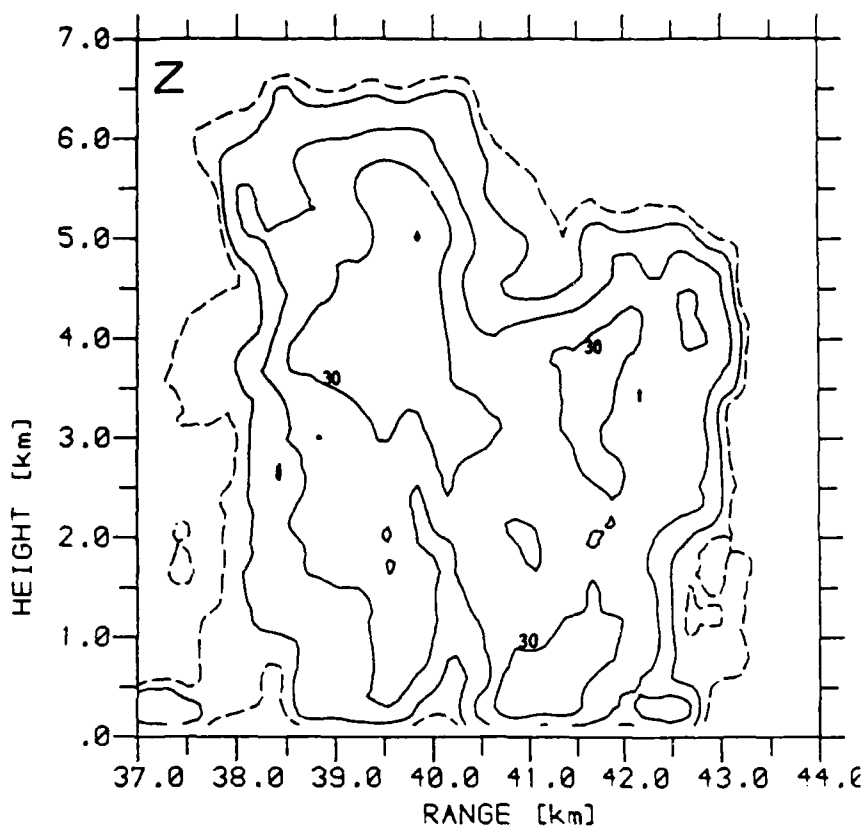
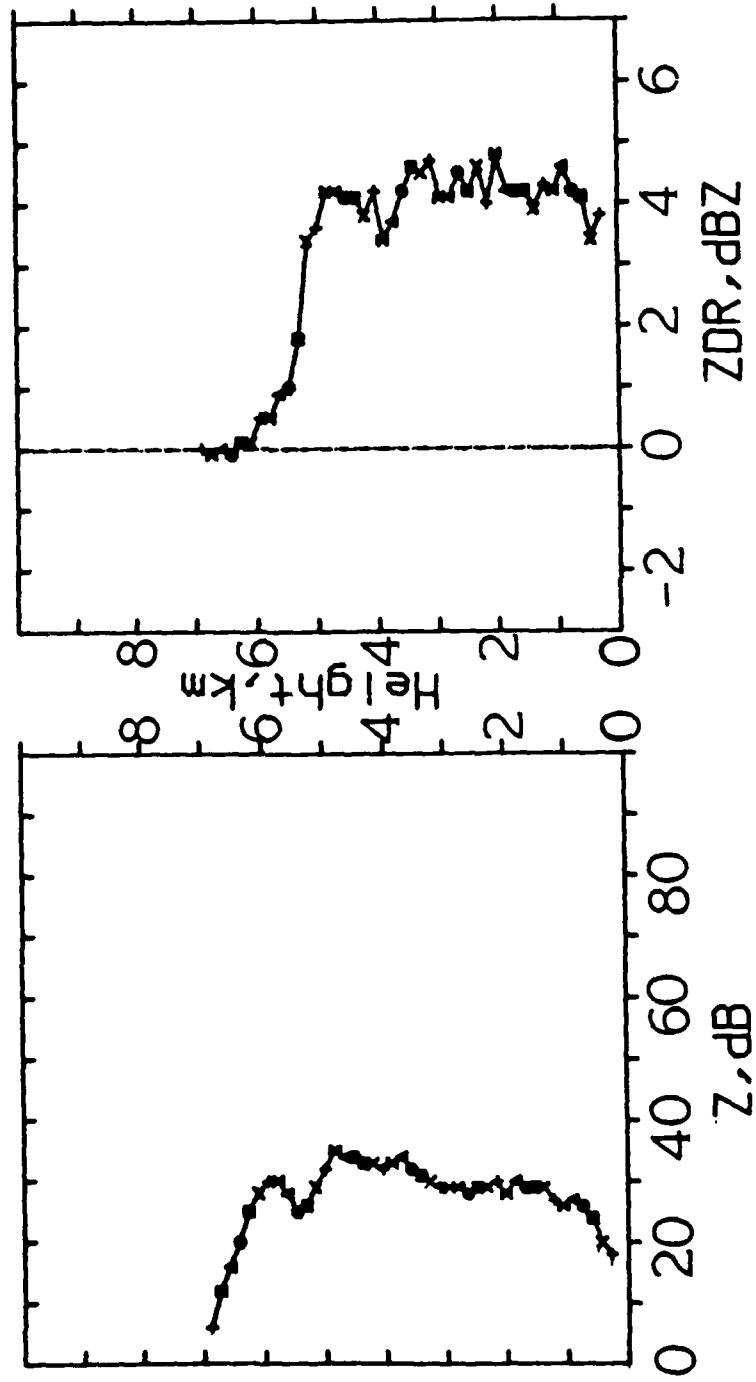


Figure 7

An RHI at 1641-10 through the cell in Figure 5 at azimuth 95° showing the development of a narrow column of positive Z_{DR} above 4dB which extends almost 2km above the freezing level.

Figure 8

A vertical profile of Z and Z_{DR} at range 39.9km through the column of positive Z_{NR} in Figure 7.



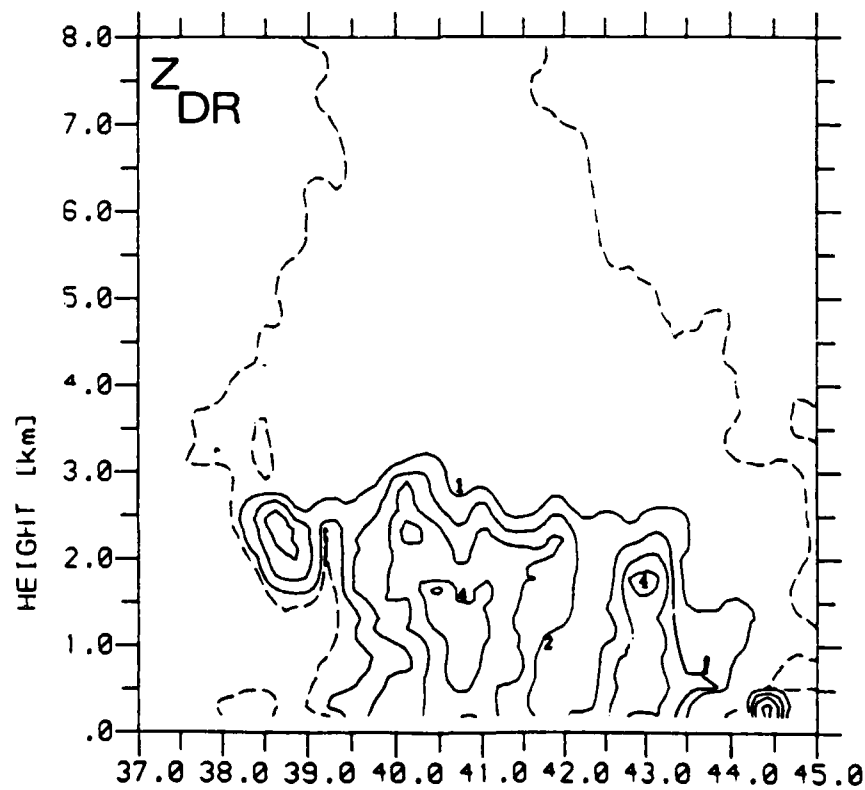
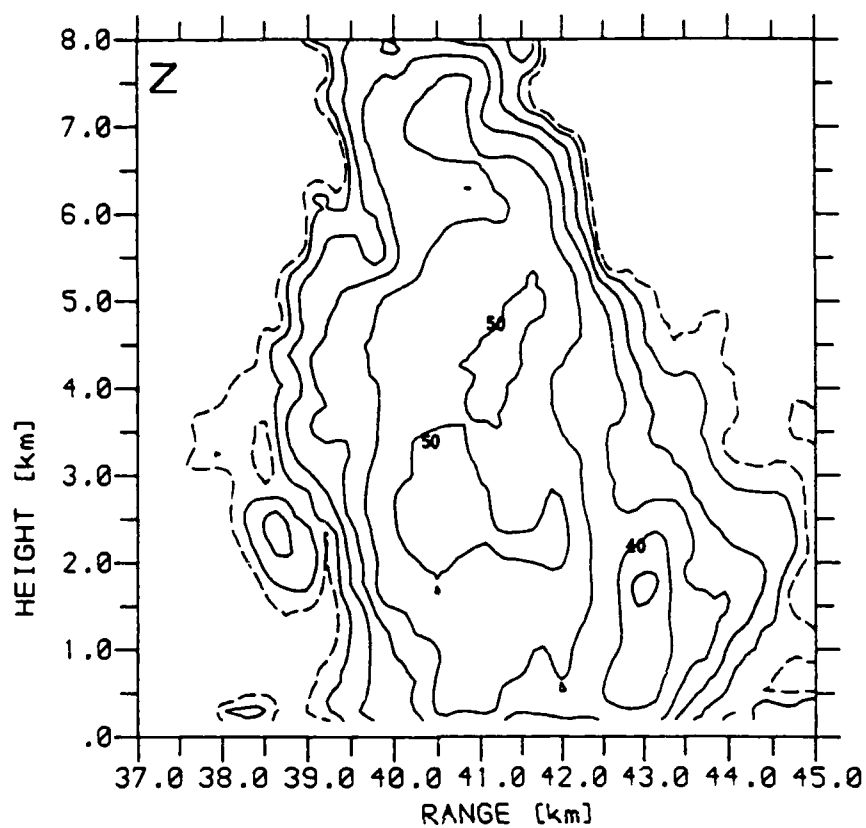


Figure 9

An RHI obtained at 1648-10 and azimuth 94° through the same cell as the previous five figures, but now Z and Z_{DR} are more typical of a mature glaciated cloud, with Z_{DR} only positive below the freezing level.

Figure 10

A vertical profile of Z and Z_{DR} at a range of 40.8 km in Figure 9. Z_{DR} values are zero above 3 km consistent with tumbling graupel, but become increasingly positive below 3 km as the particles melt.

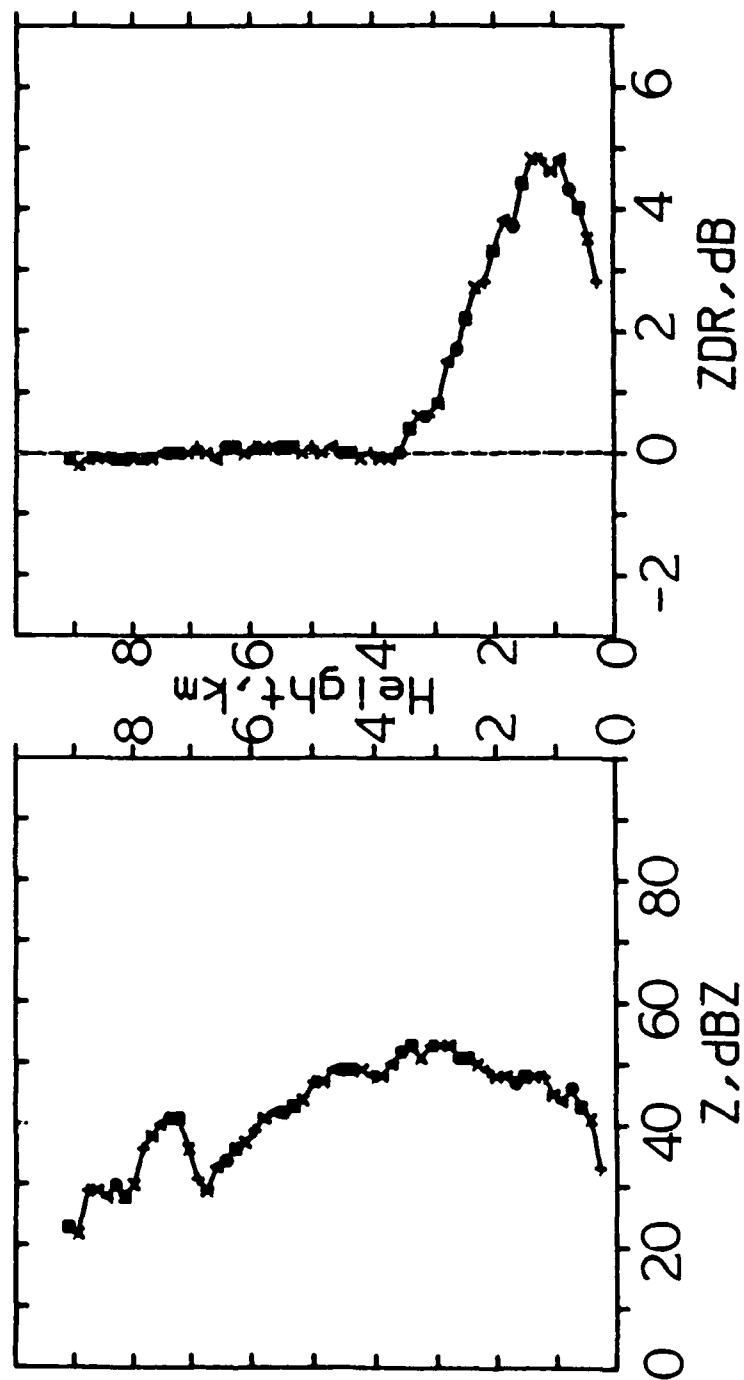


Figure 11

A PPI obtained at 1606-00 on 6/7/83 showing an isolated cell with unexpectedly high Z_{DR} at 30km range and 7km lateral distance, separated by 3km from an extensive area of intense echoes. An area of negative Z_{DR} at 29km range and lateral distance -7km (marked with an N) is believed due to differential attenuation and is discussed in Section 4.

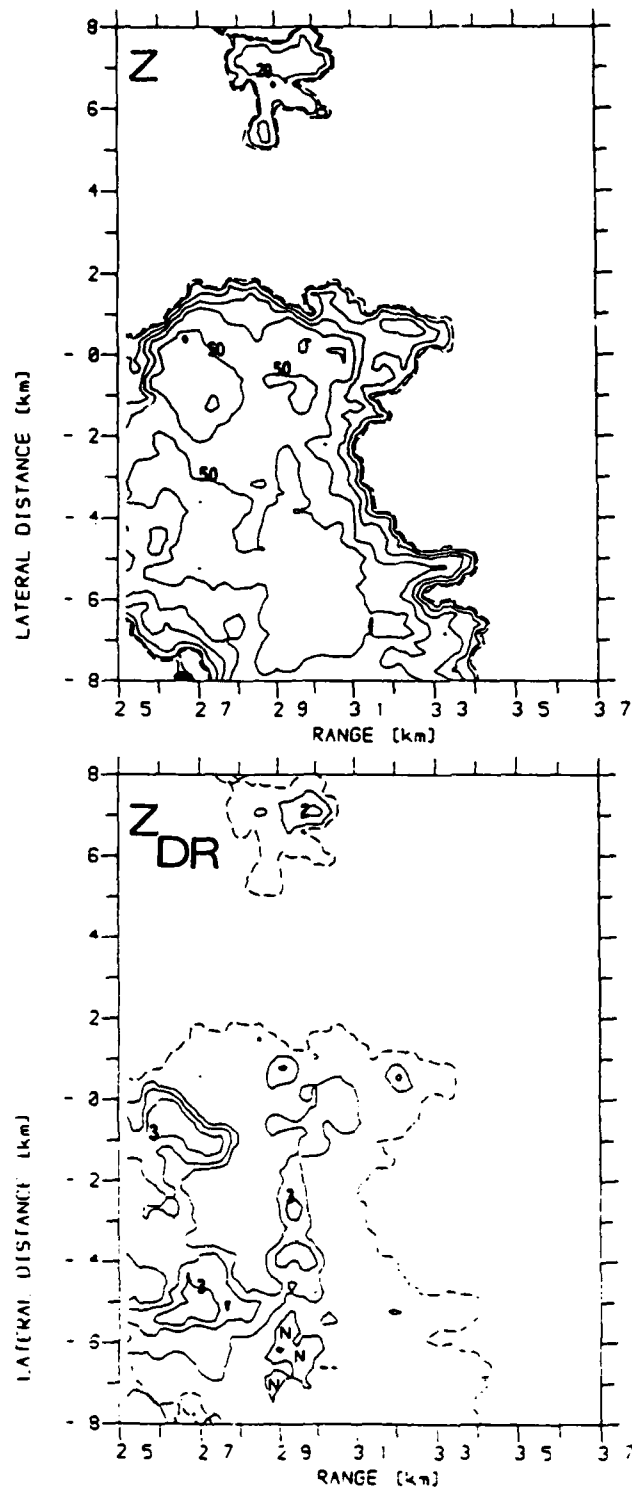


Figure 12

An RHI at 1607-00, azimuth 148° , through the most intense part of the isolated cell in figure 11. High positive Z_{DR} accompanies a weak Z .

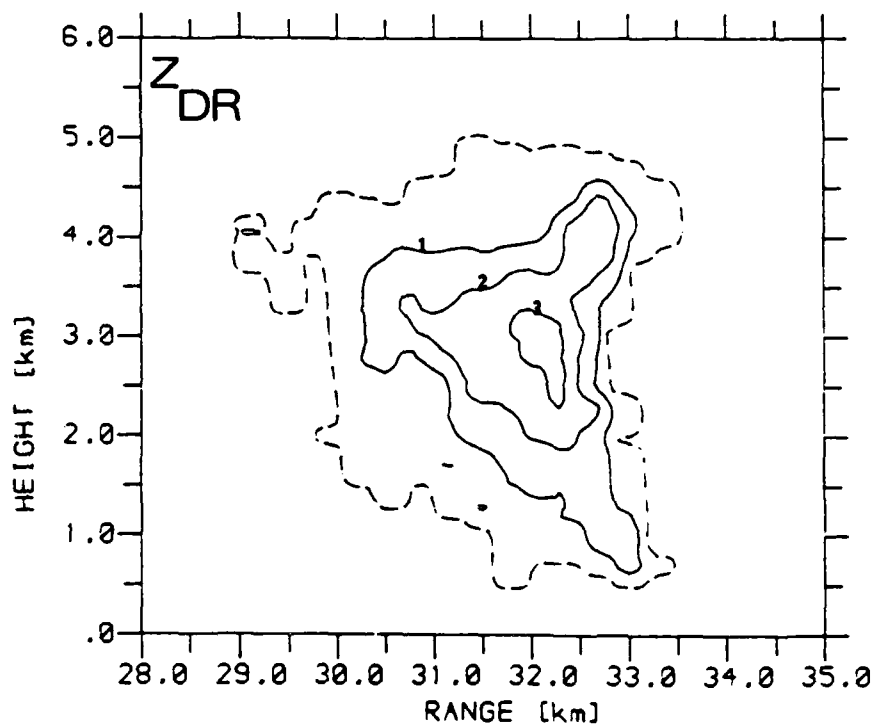
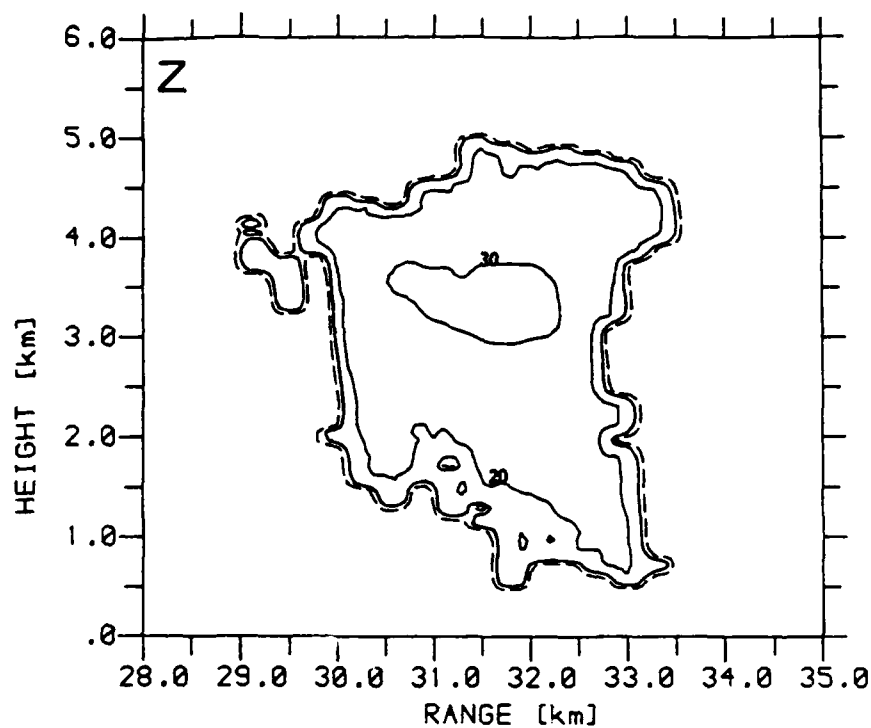
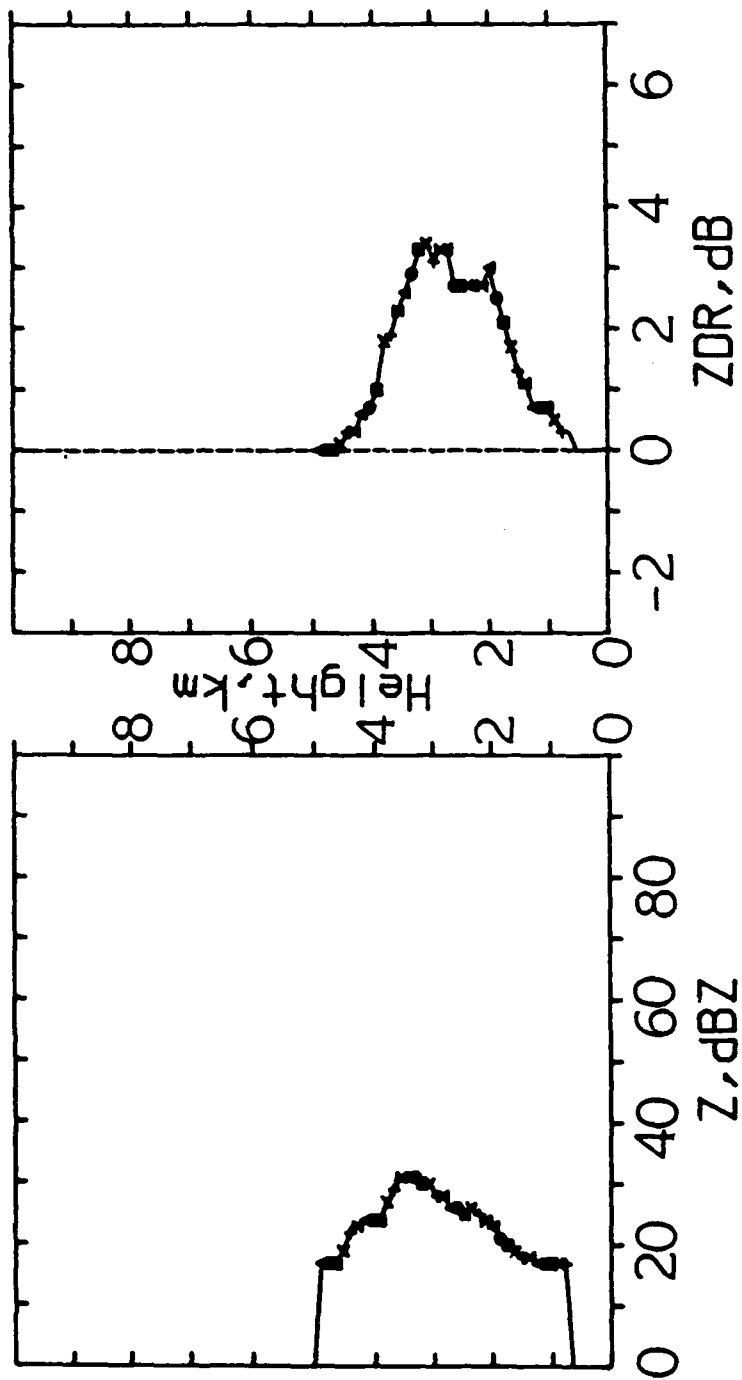


Figure 13

A vertical profile of Z and Z_{DR} at 32.1km range through the maximum Z echo in Figure 12. Comparison with Figure 3 confirms the anomalously high values of Z_{DR} .



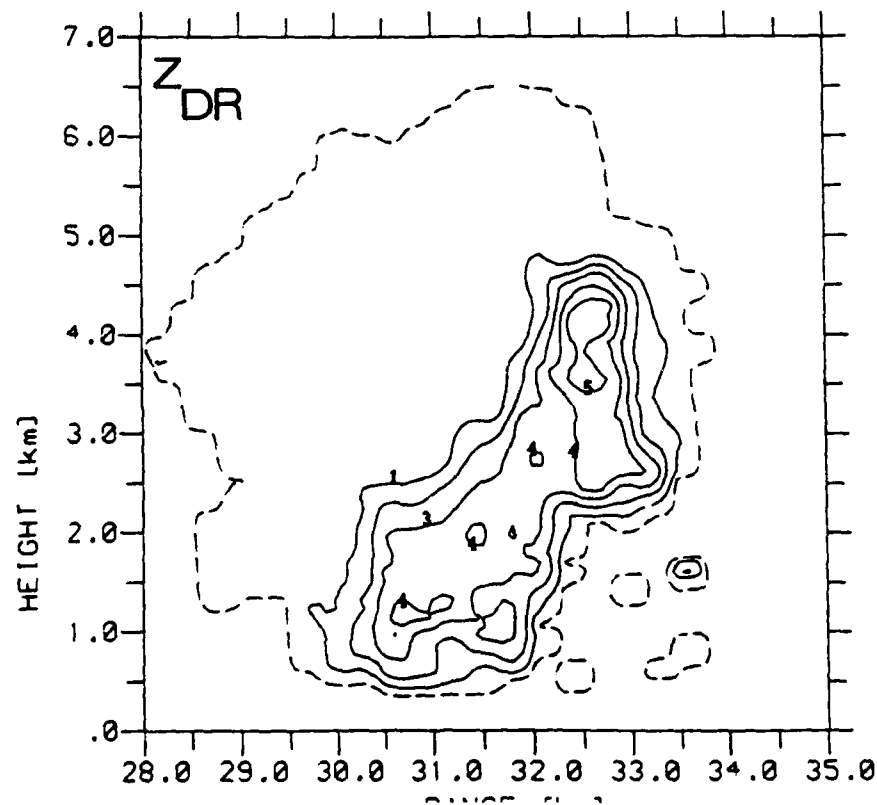
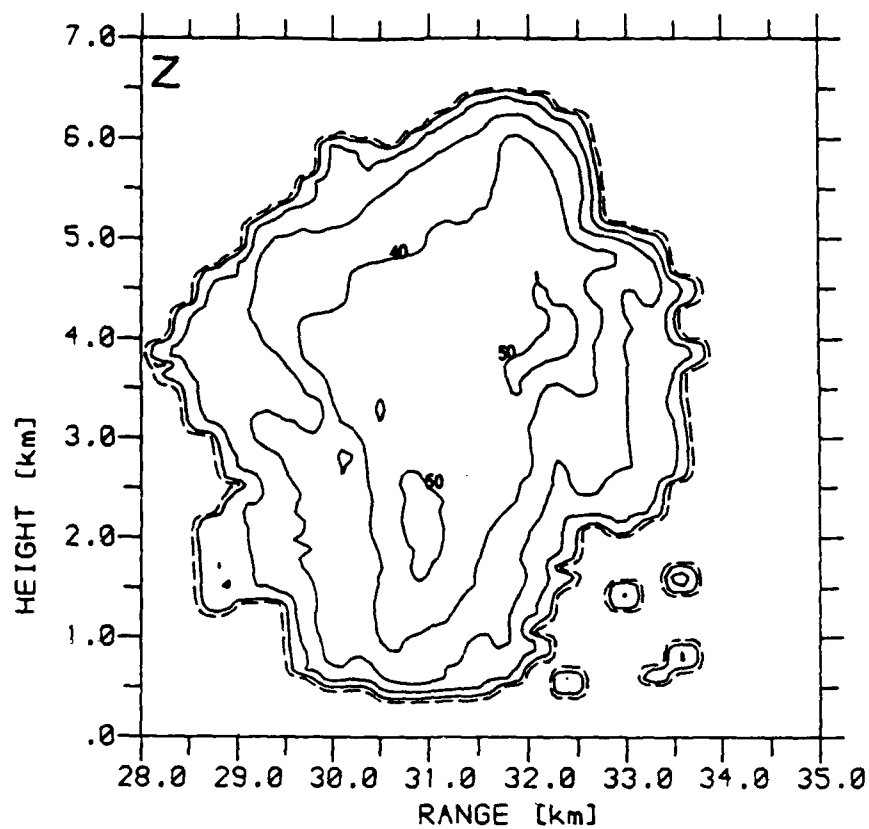


Figure 14

An RH1 at 1613-20, azimuth 146°, showing the development of a narrow column with Z_{DR} values exceeding 5dB which extends over 1.5km above the freezing level.

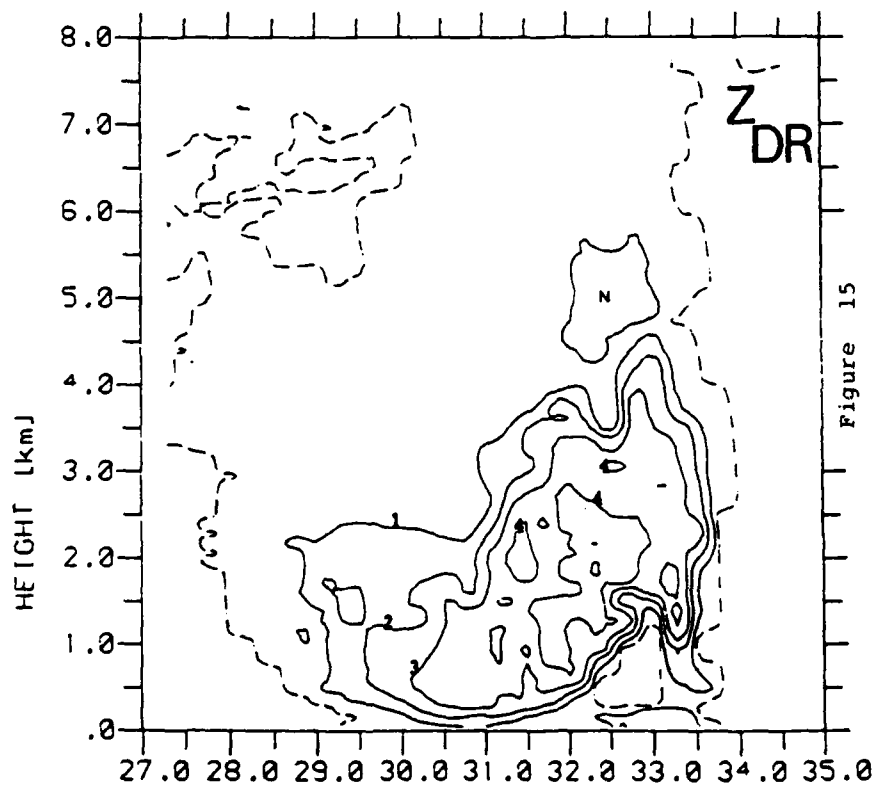
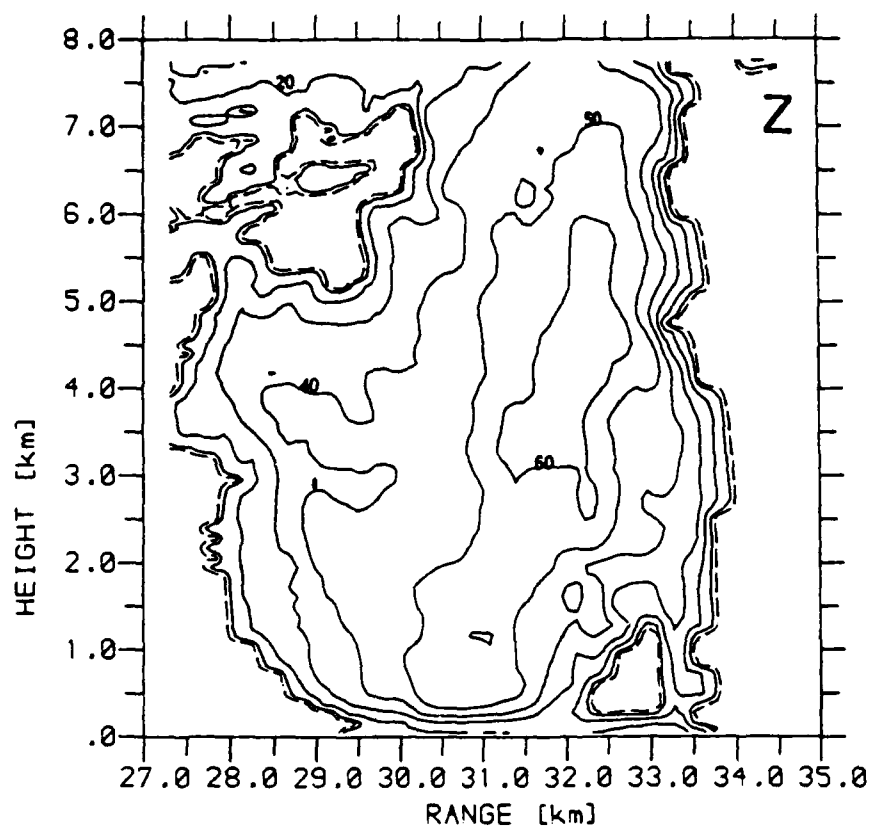
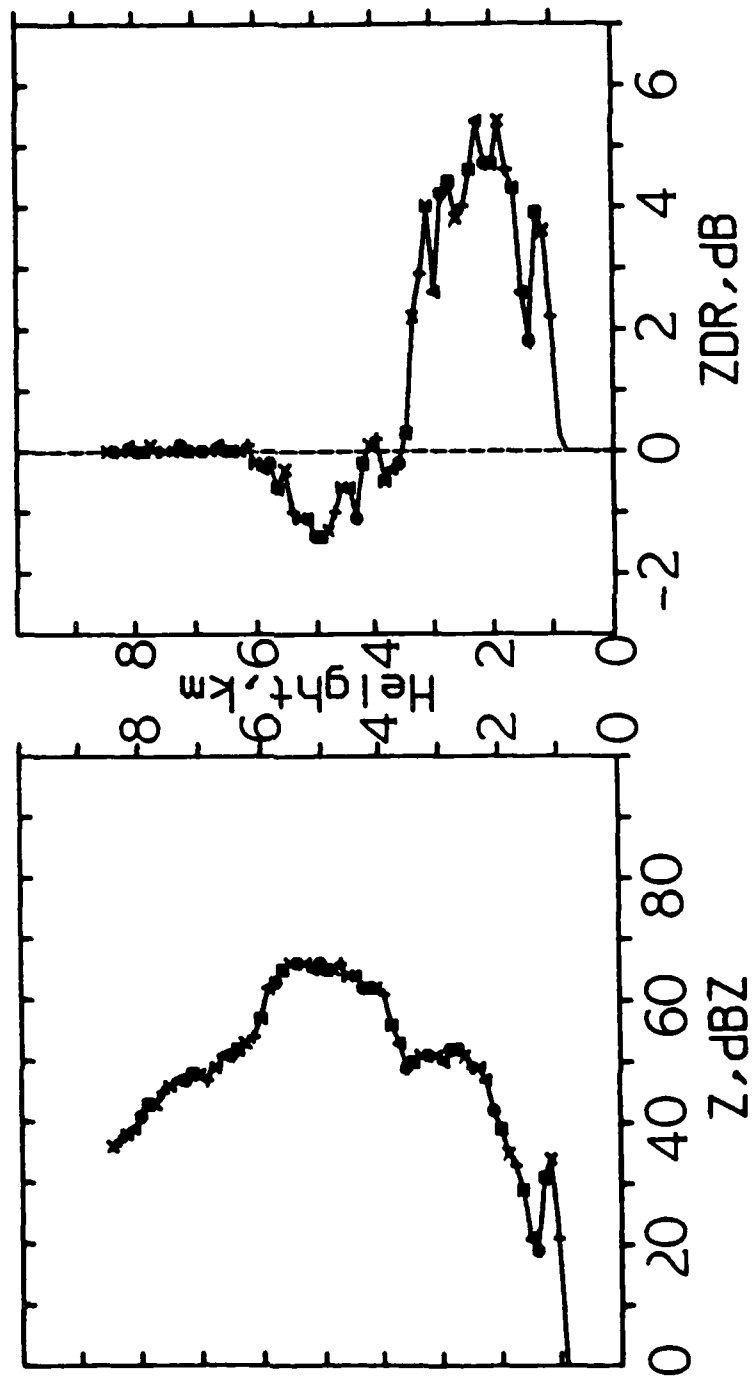


Figure 15

An RHI at 1618-20, azimuth 145°, through the same cell as the previous four Figures. An additional -0.5dB contour in Z_{DR} is plotted (marked with an N), and occurs where Z is above 60dBZ. The negative Z_{DR} is believed to be due to conical hail.

Figure 16

A vertical profile of Z and Z_{DR} at 33km range through the negative Z_{DR} region in Figure 14, demonstrating that the negative Z_{DR} occurs where Z is a maximum.



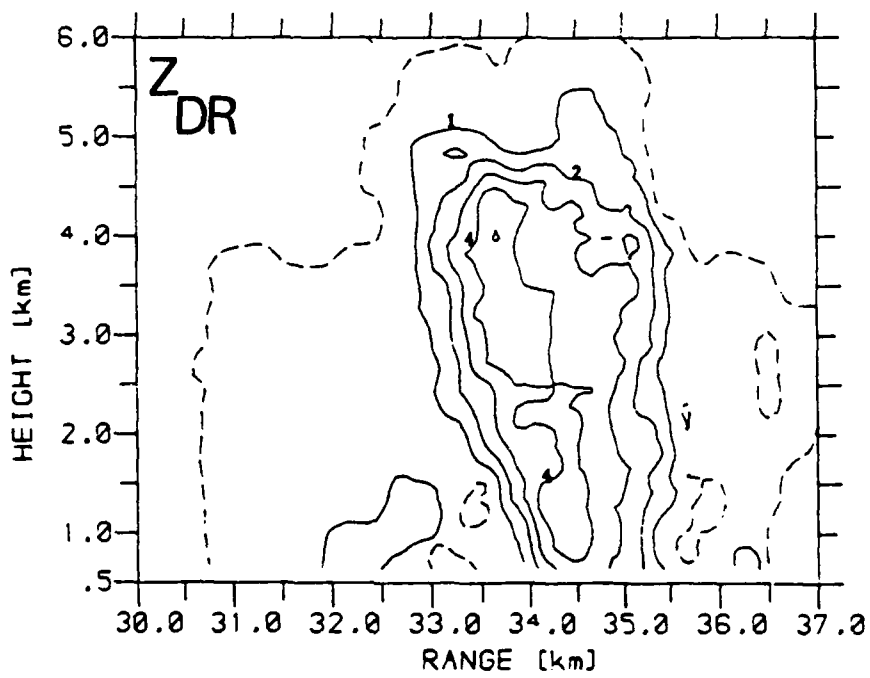
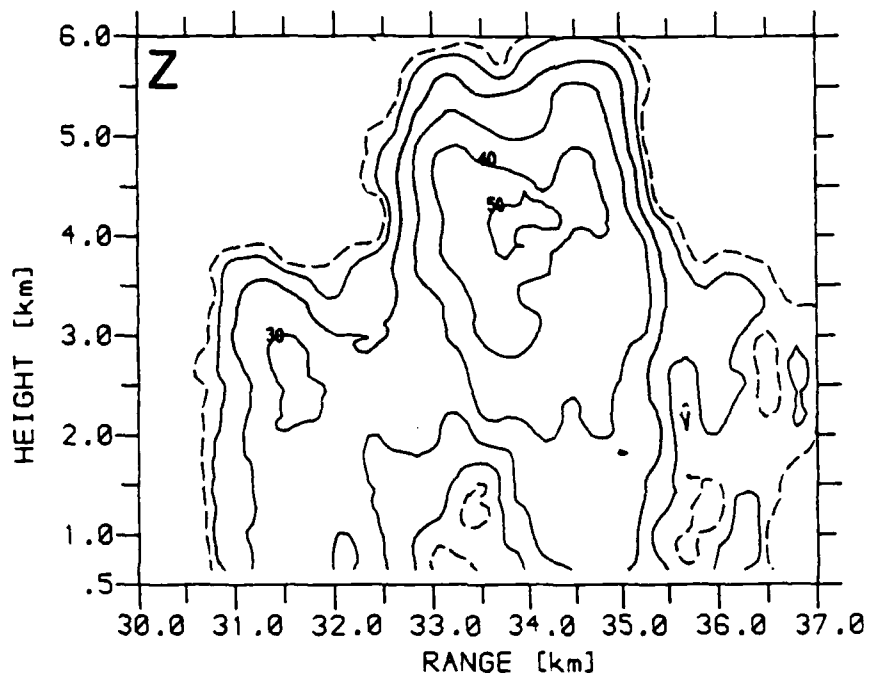


Figure 17

The first RH1 through a developing cell at 1358-40 on 22/8/83, azimuth 78°. Note the high Z_{FR} above the freezing level.

Figure 18

An RHI through the cell in figure 17 obtained at 1404.40, azimuth 78° . The highest Z_{DR} contour is 7dB with a maximum value at one gate of 8.3dB. Echo top is only 5km.

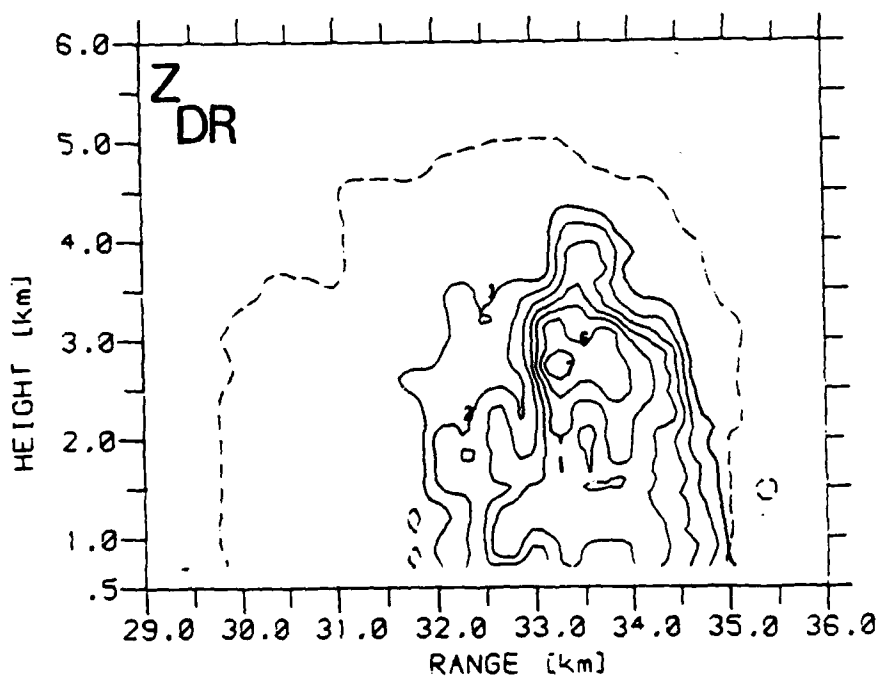
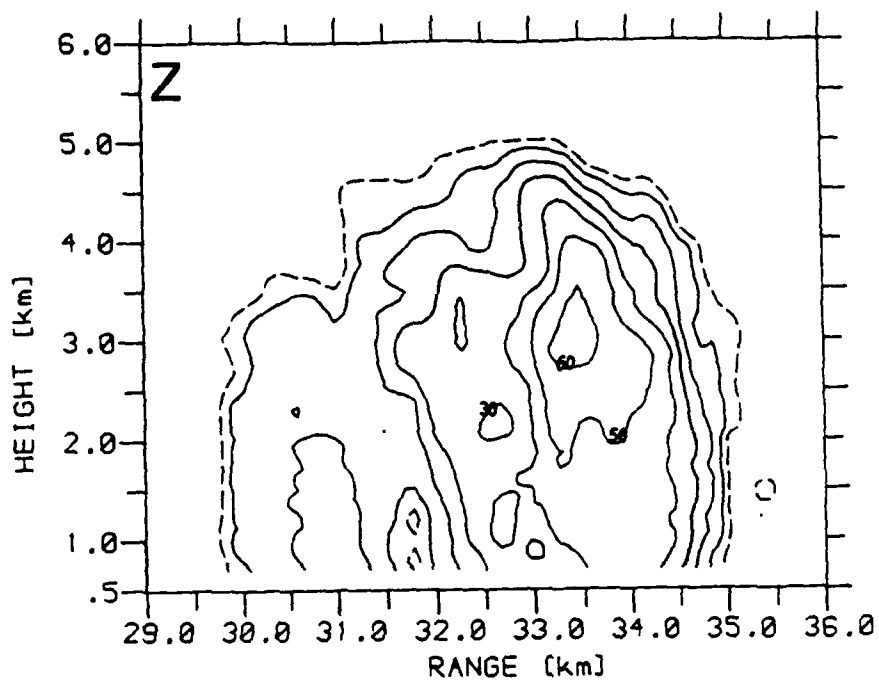
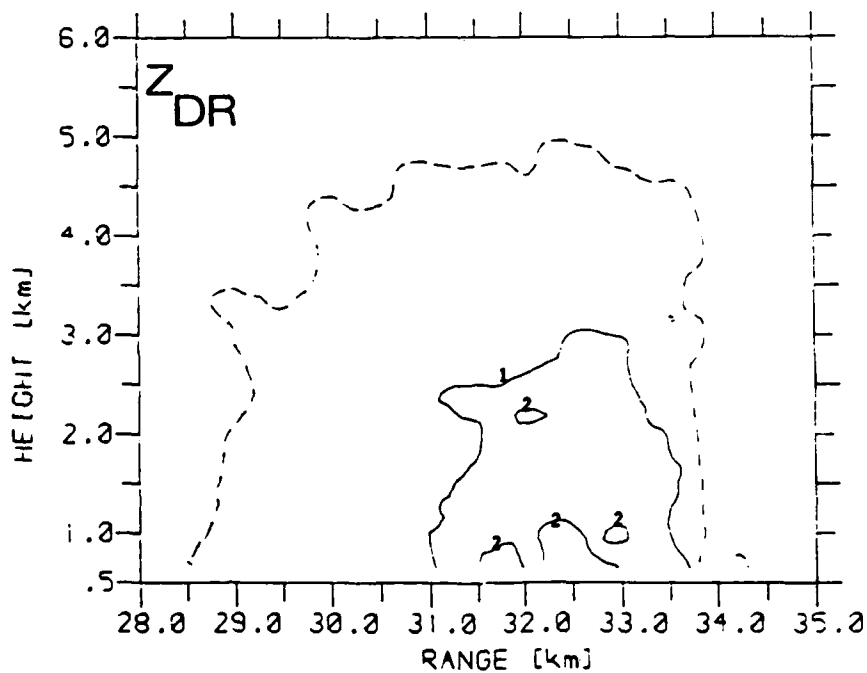
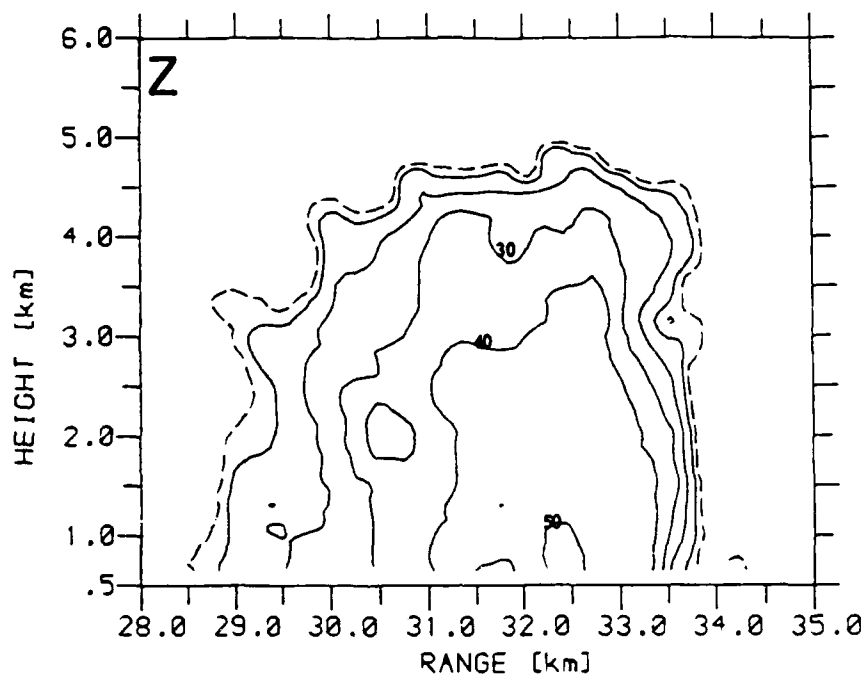


Figure 19

An RHI obtained 11 minutes later than Figure 18 at 1415.40, azimuth 80° . The large precipitation particles have fallen to ground and Z and Z_{DR} are much closer to those expected for a Marshall-Palmer drop size distribution.



PART B

RADAR OBSERVATIONS AND MODELLING OF
WARM RAIN INITIATION

ABSTRACT:

Differential reflectivity radar data are presented which indicate that some initial echoes of convective clouds consist of a small number of very large raindrops; these raindrops may be supercooled. Typically raindrop concentrations are three orders of magnitude lower than the average Marshall-Palmer drop size distribution found in mature clouds. An explanation of these observations in terms of the sweep out of cloud droplets by a low concentration of ultra-giant nuclei of radii between 30 and 100 μ m is offered. A simple model of this process, initiated using the average background levels of these nuclei, gives good agreement with the radar data. The model is not critically dependent upon the choice of collection efficiencies of the nuclei for the cloud droplets nor on the precise form of the ultra-giant nucleus spectrum. The ultra-giant nuclei seem capable of explaining the appearance of the raindrops without invoking complex mixing processes within clouds or appealing to the stochastic nature of the collisions between cloud droplets.

1. INTRODUCTION

It is well established that rain can fall from convective clouds which do not contain the ice phase, but the precise nature of the mechanism involved is still not clear. There must be two stages in the development of such "warm rain"; the growth of cloud droplets by condensation and the subsequent coalescence of cloud droplets to form raindrops. The rate of droplet growth by condensation is inversely proportional to the droplet radius, and so condensation alone will tend to produce a stable monodispersed droplet spectrum. If coalescence is to occur then a broader spectrum is needed with some drops large enough so that

they have a reasonable terminal velocity and can collide with the smaller droplets.

One suggestion is that a sufficiently broad spectrum of droplets is indeed produced by condensation, whereas other researchers have proposed that a few giant condensation nuclei must be present to give a small number of large droplets which can trigger the coalescence process. Ludlam (1951) concluded that droplets of up to 20 μ m radius could grow by condensation on hygroscopic salt nuclei and such droplets would then be able to capture 8 μ m radius cloud droplets and subsequently grow into rain drops. In contrast East (1957) believed that if the cloud liquid water content was high enough such 20 μ m droplets could grow by condensation without invoking giant nuclei. A critical parameter in such work is the value of the collection efficiency, E , which is the fraction of smaller cloud droplets in the path of the larger droplet which are actually collected.

Thirty years of intensive research has revealed that the processes involved are far more complicated than in these early formulations, but in spite of our increased knowledge the question has not been resolved. The following major difficulties can be identified.

(a) The collection efficiencies are not well known. The early workers used Langmuir's (1948) values, using, for example, a near unity value of E for a 20 μ m droplet collecting an 8 μ m droplet, whereas many of the detailed recent calculations (reviewed in Pruppacher and Klett, 1978) suggest it is nearer 0.01. Unfortunately this lower value is in the very sensitive transition region for significant coalescence to start. In the laboratory formidable practical difficulties arise in the measurement of such low values of E for these small droplets, and so we cannot

check the validity of the theoretical models.

(b) Extensive measurements of cloud droplet spectra within clouds reveal that the spectra are not as narrow as would be expected by condensation alone, but that there is a broad maximum extending from 5 to about 15 μ m. This size range coincides with the region where precise values of E are critical but uncertain. When so many small droplets are present, it is difficult, using existing instrumentation, to obtain a statistically significant sample of the concentration of any occasional larger droplets with radii from 20 to 100 μ m. Turbulence and entrainment of dry air may account for the broadening of the spectrum (Baker and Latham, 1979; Paluch and Knight, 1986a; Hill and Choularton, 1986; Telford et al, 1984), but the complexity of the analysis is such that it cannot at present be extended to consider the coalescence process and the development of raindrops. Paluch and Knight (1986b), who provide a useful review of this topic, found that the spectrum does broaden towards the smaller sized drops, but could not observe any broadening towards the larger sizes. It should be pointed out that the lowest droplet concentration they could measure was 0.02 cm^{-3} , so the larger droplets could escape detection if they were only present in the same concentration as raindrops.

Young (1975) provides the most comprehensive model of rain-drop evolution; it includes condensation, coalescence and even collision induced break-up of the larger raindrops. He finds that it is not necessary to invoke the presence of giant nuclei, but that rain can develop providing that the "stochastic" nature of the random collision process is analysed - a few fortunate droplets experiencing more collisions than average and triggering the coalescence. Such a conclusion could of course be affected by

uncertainties in the values of collection efficiency which were discussed above. This model starts with the activation of the cloud condensation nuclei, and initially calculates the supersaturation and the droplet growth by condensation. The possibility of coalescence is critically dependent upon the size distribution of these droplets, but unfortunately the predicted droplet spectra are not given in the paper, and so it is not possible to compare them with those actually observed.

Faced with these difficulties, Johnson (1982) revived and extended an earlier idea, suggesting that the large droplets arise quite naturally on large aerosol particles. This proposal was prompted by observations that the natural aerosol spectrum does not terminate at 10 μ m radius, and that there is a small but finite concentration of particles of up to 100 μ m. Nuclei of such a size would not need to be hygroscopic, but could themselves collect cloud water and grow into raindrops. When reviewing such aerosol data Junge (1972), noting that the concentration of aerosol particles with radii above 50 μ m is less than one per cubic meter, considered that such large particles should not be important in the warm rain process. Johnson realised that such a low concentration of raindrops could, if they were of sufficient size, have an appreciable radar reflectivity, and his model shows that collection of the cloud water by such giant particles can produce high radar reflectivities within fifteen to twenty minutes. The predicted growth of the radar reflectivity factor, Z , with time is remarkably similar in both Young's stochastic model and Johnson's giant nuclei model. But whereas Young found that if the stochastic formulation was not included then the echo failed to grow above 0dBZ, Johnson's computations of the collection of cloud droplets by the giant nuclei could be accurately

described by a simpler continuum model; the incorporation of the stochastic effect making a negligible difference to the growth of the giant nuclei.

In this paper we analyse some differential reflectivity radar measurements of the development of convective precipitation which should distinguish between the two growth mechanisms described above. The radar reflectivity factor, Z , is proportional to the product ND^6 , where N is the concentration of drops of diameter D , summed over all values of D . Z is usually expressed in dB relative to $1 \text{ mm}^6 \text{ m}^{-3}$. If Z alone is measured it is not possible to derive values for N and D . The differential reflectivity (Z_{DR}) provides an estimate of hydrometeor shape, and, because raindrops are oblate to a degree which depends upon their size, the diameter can be derived from Z_{DR} . If Z and Z_{DR} are available then an estimate of both the size and concentration of raindrops in the cloud is possible. It is to be expected that the two mechanisms of rain growth would lead to different values of Z_{DR} for a given Z . If the giant nuclei are important in the release of the rain then a given value of Z would be caused by a low concentration of unusually large drops, but if the stochastic growth mechanism is dominant the raindrop size distribution would be more normal. There are some reports in the literature indicating anomalous particle size concentrations. Mordy and Eber (1954) measured raindrop sizes at the ground during warm rain in Hawaii and commented that light intensity rains frequently consisted of raindrops which were relatively large but few in number. Browning and Atlas (1965) observed a low reflectivity early echo core which appeared to descend rapidly, and interpreted this as indicating a smaller-than-usual particle concentration.

In Section 2 we describe the new polarisation radar

technique; some new radar observations of the development of convective showers are presented in Section 3. Computations of the raindrop size distributions expected from the two mechanisms are considered in Section 4 and their applicability is considered in the final Section.

2. THE DIFFERENTIAL RADAR REFLECTIVITY TECHNIQUE

The differential reflectivity measurement is defined as

$$Z_{DR} = 10 \log (Z_H/Z_V) \quad (1)$$

where Z_H and Z_V are the radar reflectivity factors measured with horizontally and vertically polarised radiation respectively. In this paper we shall describe results obtained using the Chilbolton radar situated in Hampshire, England. A full description of the implementation of the Z_{DR} technique and its accuracy is given by Cherry and Goddard (1982).

The differential reflectivity provides a measure of mean hydrometeor shape. As raindrops increase in size they become increasingly distorted with the horizontal diameter exceeding the vertical so Z_{DR} is positive. Because the differential reflectivity is a ratio it is independent of hydrometeor concentration, and so for rain the magnitude of Z_{DR} gives an estimate of the mean raindrop size. The Z_{DR} of ice particles is more complicated because the shape is no longer a unique function of size and, in addition, the various forms of frozen precipitation may have different densities and fall modes. Experience with the Chilbolton radar (e.g. Hall et al, 1984) shows that in regions of convective clouds where the temperature is below freezing, the values of Z_{DR} are very close to zero (indicating that the ice particles are nearly spherical or randomly tumbling), and that positive values are usually confined to the rain below the zero

degree isotherm.

The Chilbolton radar can normally estimate Z_{DR} to an accuracy of 0.1dB. A drop of 1.3mm diameter has a Z_{DR} of 0.1dB rising to 2dB for a 3.3mm drop; consequently, if the raindrops were all the same size, the radar would be able to estimate the size of drops larger than 1.3mm to an accuracy of 0.1mm. If the concentration of raindrops, N , of diameter D , is assumed to follow an exponential raindrop size distribution

$$N(D) = N_0 \exp(-3.67D/D_0) \quad (2)$$

then, once the drop shapes are known, we can calculate Z_{DR} for various values of D_0 (the equivolumetric diameter). N_0 is then chosen to give the observed value of Z . A long series of observations comparing the radar data with direct drop size measurements made at the ground (Goddard et al, 1982) has confirmed the validity of the technique for values of Z_{DR} up to 2.5dB; the best agreement was obtained using raindrop shapes slightly less oblate than those reported in the laboratory measurements of Pruppacher and Pitter (1971). The original ground-based measurements of Marshall and Palmer (1948) suggested that the average value of N_0 is about $8000 \text{ m}^{-3} \text{ mm}^{-1}$, and the dotted line in Figure 1 is the computed value of Z_{DR} as a function of Z using this value of N_0 . Drops of 4mm diameter have a Z_{DR} of 2.5dB, but a limited series of aircraft measurements of drops shapes by Cooper et al (1983) indicated that drops larger than this size were rather more oblate than the Pruppacher and Pitter (1971) shapes. The dotted line in Figure 1 was obtained using these more oblate shapes. The individual data points obtained by the radar are scattered around this $N_0=8000$ line. The solid line in Figure 1 joins the mean values of Z_{DR} for each 2dBZ increment in Z for 150000 data points obtained during many different days of widespread heavy convec-

tive rain when no bright band was present; weak isolated echoes were not included in the analysis. The radar observations show reasonable agreement with the theoretical computations; further details are provided in Caylor and Illingworth (1986). For values of Z below 15dBZ, Z_{DR} is essentially zero when consideration is given to the observational error of 0.1dB. The values of N_0 for a given Z scale linearly with Z , so for each individual data point it is possible to derive the appropriate value of N_0 , and, if required, the total drop concentration, $N_0 D_0 / 3.67$.

3. RADAR OBSERVATIONS OF CONVECTIVE CLOUDS

In an analysis of differential reflectivity observations of the evolution of convective storms using the Chilbolton radar, Illingworth et al (1984, 1987) drew attention to some anomalously high values of Z_{DR} in isolated developing convective clouds. In contrast to the situation in mature convective clouds, these high values of Z_{DR} extended a couple of kilometers either side of the zero degree isotherm, and the conclusion was drawn that they were due to large raindrops present in low concentrations which had probably grown by the warm rain process. Any interpretation in terms of even lower concentrations of very large frozen hydrometeors in wet growth being most unlikely at such an early stage in the echo development.

The largest deviations from a Marshall-Palmer raindrop size distribution (ie $N_0 = 8000$) occurred in these isolated developing cumulus clouds. This is demonstrated in Figure 2 (from Illingworth et al, 1987) which shows values of Z and Z_{DR} obtained in a vertical section (RHI) through the most intense section of a daughter cell; neighbouring RHIs separated by 2° in azimuth had much lower values of Z . The region where Z_{DR} exceeds 1.5dB

straddles the zero degree isotherm (3km altitude on this day) and is accompanied by values of Z below 30dBZ. At one data point Z reaches 33dBZ and here the value of Z_{DR} is just over 3dB. It was argued in the paper that these particles were large raindrops present in very low concentrations. For monodispersed rain, values of Z_{DR} of 2 and 3dB correspond to diameters of about 3.3 and 4.5mm respectively, present in concentrations of 0.77 and 0.12 m^{-3} to give a Z of 30dBZ. The curves in Figure 1 for the more realistic exponential distribution imply a value of N_0 three orders of magnitude below the 8000 Marshall-Palmer value.

The echo shown in Figure 2 grew rapidly; by 1618 GMT the highest value of Z was 65dBZ and the 40dBZ contour had reached 8km altitude. This evolution is depicted in a different manner in Figure 3, where the individual data points of Z and Z_{DR} are plotted for three successive RHI scans through the most active portion of the cloud. To aid comparison the solid curve from Figure 1 which represents the average data for many different storms on many different days is also plotted. The data at 1611 lie far below this average curve, but the data points at 1613 and 1619 show a tendency for the points to evolve towards the 'average'. Each data point in Figure 3 represents the Z and Z_{DR} measurement for a sample volume of 300m between range gates and a beamwidth of about 150m. To minimise confusion in the diagram, data points with Z_{DR} below 2dB have not been plotted, most of these points have low values of Z and lie on the periphery of the cloud. In addition by 1611 the cloud had started to glaciate, and by 1619 the process was complete; so that above the freezing level although values of Z are high, the values of Z_{DR} are below 0.1dB. Accordingly, we only plot data points below 2km altitude, where we are reasonably sure that the precipitation is liquid

water. We have already commented when discussing Figure 2 that the 1607 data imply low values of N_0 . These data points would lie in a tight cluster in Figure 3 with Z values mostly between 25 and 30dBZ and Z_{DR} in the range 2 to 2.5dB, but in order to avoid cluttering the diagram they have not been plotted. Figure 3 demonstrates that at 1611 the concentrations were equally low, but the particles were rather larger with values of Z_{DR} of up to 4.5dB. Subsequently the values of Z grew rapidly without any great change in the spread of Z_{DR} ; the data points tending to move up towards the solid line, closer to the Marshall-Palmer value of $N_0 = 8000$. By 1619, the Z and Z_{DR} points are scattered close to the average curve and would not, by themselves, elicit any particular attention.

Illingworth et al (1987) reported similar low values of N_0 in two other isolated echoes which also developed rapidly. Such extreme deviations from the values of Z and Z_{DR} predicted from the Marshall-Palmer distribution are quite unusual and appear to be confined to early echoes of developing convective clouds. Further analysis of the 150000 data points which were averaged to produce the solid curve in Figures 1 and 3 shows that, for a given Z , the Z_{DR} values are approximately log-normally distributed about the mean values plotted on the curve. For values of Z between 30 and 32dBZ only 2% of the data points have a Z_{DR} above 3dB, and for Z in the range 20 to 22dBZ only 2% have a value of Z_{DR} exceeding 2dB, thus confirming the unusual properties of these early echoes.

The data presented so far appear compatible with an evolution in terms of the sweep out of cloud water by ultra-giant nuclei, in that a very small number of large raindrops seem to form in the early stages of precipitation development. In at-

tempting to test such a hypothesis more rigorously problems arise. Once the value of Z exceeds about 40dBZ the clouds glaciate and growth of raindrops via the ice mechanism and subsequent melting occurs. Furthermore, even in the absence of glaciation when Z is above 40dBZ, for a Marshall-Palmer raindrop size distribution the number of collisions between pairs of large raindrops which might lead to the production of several small satellite drops can become significant. It may well be that such collisions are responsible for the tendency of N_0 to rise as Z values become large, but so little is known about the statistics of drop collisions and satellite production that it seems premature to attempt to model the process.

We now report some additional radar data obtained during the few days when it was possible to operate the radar in 1984. Of particular interest were the observations on 20 June 1984. The midday sonde ascent for Crawley, 80km to the east of Chilbolton, shown in Figure 4 reveals the existence of a dry layer at about 700mb, at an altitude of 3.2km and temperature of 0°C , which prevented any great vertical development of the clouds. On this day it was possible to observe an isolated echo for over 20 minutes. Although it had anomalously high values of Z_{DR} it only evolved slowly, with Z values remaining low enough so that collision induced break-up should be negligible.

On 20 June 1984 the radar was performing a series of wide area low elevation PPIs to identify any convective clouds. A PPI at 1738 GMT revealed an isolated echo which was approximately circular and of diameter 2km, the maximum Z was only 12.3dBZ but was accompanied by a Z_{DR} of 2.2dB. The next PPI at 1743 is displayed in Figure 5 and shows that the diameter of this echo, which is 33km north and 11km west of the radar, had grown to

about 3km and the highest value of Z had risen to 23.2dBZ which occurred where Z_{DR} was 2.9dB. Two other echoes are visible in Figure 5. A small echo 24km to the north and 14 km west of the radar has only a very few gates above 15dBZ but again has unexpectedly high values of Z_{DR} ; no vertical sections were made through this cell. The larger echo 38km to the north and 22km to the west is more normal with a few gates above 35dBZ and Z_{DR} around 2dBZ, implying drop concentrations only a factor of ten below the Marshall-Palmer. Attention was initially focused on the weak echo 33km to the north in Figure 5, and the values of Z and Z_{DR} in the first RHI obtained at 1745 through the maximum Z of the weak echo are displayed in Figure 6. Values of Z above 10dBZ only occur in a narrow column extending from the freezing level at 3.2km altitude down to ground; the highest value of Z is 31.5dBZ is found where Z_{DR} is 3.4dB. For most regions where Z exceeds 20dBZ the values of Z_{DR} are over 3dB, and the highest value of Z_{DR} of 4.7dB occurs where Z is only 23.6dBZ. This cloud changed relatively slowly and in the next 20 minutes it was possible to obtain 28 separate RHIs and 6 PPis through the cell, a total of 2700 individual data points. During this time all significant echoes were confined to regions below the freezing level, although there was a rather diffuse region having Z values of about 0 to 7dBZ up to 5km altitude. The final sequence of RHIs showed the Z echo subsiding at about 500 meters a minute in a manner consistent with large raindrops falling to ground in the absence of an updraught.

Before proposing any mechanism for the development and persistence of the echoes displayed in Figures 5 and 6, which apparently contain such a small concentration of large drops, let us consider if the echo could be non meteorological in origin.

Ground echoes show great spatial variability in differential reflectivity, with values ranging between +4dB and -4dB, and changes of 2 or 3dB between adjacent range gates (Hall et al, 1984). Similarly, echo characteristics of burning chaff (Hall et al, 1984) have larger spatial variability in Z_{DR} than the echoes presented in this paper. Furthermore, although the echo in Figure 6 shows no shear, it did advect by about 1km during the observation period; such an advection is inconsistent with a fixed source of particles on the ground such as a fire. Echoes due to insects are generally much more localised (Mueller and Larkin, 1985). A systematic bias in the radar transmission and reception hardware can lead to differing sensitivity for horizontal and vertical polarisations, but this would result in all Z_{DR} values being shifted; this possibility can be ruled out because no negative values of Z_{DR} were observed, and most weak echoes had a value of Z_{DR} within 0.1dB of zero, confirming that the gains of the two polarisation channels were precisely matched. Finally we note that the descent towards the ground and the subsequent disappearance of the echo in Figure 6 on 20 June 1984 seems consistent only with the presence of precipitation.

It is difficult to interpret the data in Figures 5 and 6 in terms of ice particles. A Z_{DR} of +3dB could result from: a) solid ice spheroids with an axial ratio of 0.5, b) graupel of density 0.3 gm cm^{-3} and an axial ratio of 0.26, or c) wet oblate spheroids having axial ratios of 0.82. In view of the feeble values of Z_{DR} above the freezing level it seems unlikely that ice particles can grow large enough to survive the three kilometer fall to the ground without complete melting. In any event, most evidence suggests that discs tumble when the Reynolds number exceeds 1000 (Pruppacher and Klett, 1978), which would give zero

Z_{DR} , so that an explanation in terms of large oblate graupel particles does not seem acceptable. The various habits of ice crystal growth can result in extremely oblate shapes but these particles would melt fairly rapidly and collapse to spherical raindrops. At no time was a bright band in Z or Z_{DR} in evidence, instead the high values of Z_{DR} persisted down to the ground. Any interpretation in terms of melting ice or ice in wet growth seems equally hard to sustain. The wet growth would only occur for large particles above the zero degree isotherm, and, as remarked above, unless the ice particles are very large they will melt completely before reaching the ground. The only tenable conclusion is to consider that the hydrometeors are large raindrops.

If we pursue our interpretation in terms of raindrops, then Figure 7 shows the average values of Z_{DR} for each 2dBZ increment in Z for the 2700 data points obtained during the sequence of RHIs on 20 June 1984, together with the 'average' curve for rain used in Figure 1 for comparison. To emphasise the abnormality of this particular echo, we note that the data points with a Z between 20 and 22dBZ have an average Z_{DR} of 2.9dB; yet for the 10000 points used to find the average over this interval the mean value of Z_{DR} of less than 0.2dB. Less than 2% of the total data set had values of Z_{DR} exceeding 2dB. Note that when observational errors are taken into account, the values of Z_{DR} for the 'average' curve are not significantly different from zero, once Z is below 15dBZ. If we assume the particles are raindrops, then this Figure implies that for twenty minutes raindrop concentrations were extremely low, with values of N_0 remaining three orders of magnitude below the Marshall-Palmer values.

By the time the data set displayed in Figure 7 had been gathered the cloud had virtually disappeared, and it was possible

to make a few vertical scans through a new cell at about 10km greater range. When the PPI in Figure 5 was taken this new cell was only visible as two gates with an echo of 4dBZ, but 27 minutes later the vertical section in Figure 8 shows that the echo was more extensive. Sections at neighbouring azimuths confirm that the echo was isolated and approximately circular in cross-section. Figure 8 reveals the abnormal character of this new echo; Z exceeds 15dBZ at only a few gates, but these gates have values of Z_{DR} of over 2.5dB. The six sections made through this cell give mean values close to those plotted in Figure 7 for the cell which was observed for a longer period.

A series of PPIs scanning the area during the afternoon of 20 June 1984 demonstrated that all echoes were weak and isolated; none having a Z above 45dBZ, and no echoes were detected above 5km altitude. One possibility to be examined is that a very small flux of ice crystals, falling from higher level clouds, could melt to produce a low concentration of embryonic raindrops. Several factors preclude this suggestion: the limited vertical growth on this day, the absence of any detectable anvils, the isolated nature of the echoes, and the dryness of the air above 700mb. From the sonde ascent cloud base should have been at about 1.5km altitude where the temperature was 10° , with the zero degree isotherm at 3.2km; in the absence of any mixing the adiabatic cloud liquid water content at 0°C should have been about 3g m^{-3} .

4. MODEL OF RADAR PARAMETERS BY GROWTH ON GIANT NUCLEI

This model is of an extremely rudimentary nature. The aim is to examine whether the radar data, and in particular the variation of Z with Z_{DR} in Figure 7, can be explained in terms of

the simple sweep out of liquid water by ultra-giant nuclei. We shall pay particular attention to the robustness of the model, and explore the sensitivity of the predictions to uncertainties in such parameters as the collection efficiencies, variations in the precise form of the ultra-giant nucleus spectrum, and changes in the spectrum of the smaller cloud droplets.

The basic growth equation when a larger drop of radius R , collects smaller cloud droplets of size r , having liquid water content LWC, is:

$$dR/dt = 0.25 (LWC) E(R,r) (V(R)-v(r))/\rho_w \quad (3)$$

where $E(R,r)$ is the collection efficiency for the two sizes of drops, V their velocities, and ρ_w is the density of the water. Initially we shall consider the small cloud droplets to be monodispersed with $r=6\mu m$ and the LWC to be constant at $2 g m^{-3}$. The line marked 'J' in Figure 9 is the average spectrum of giant nuclei taken from Junge's (1972) data, with the concentrations (in units m^{-3} per unit log interval of radius) ranging from 10^3 for $R=10\mu m$ to 3×10^{-2} for $R=100\mu m$. Junge's data were gathered above the trade-wind inversion and probably represent the true background aerosol which may be of continental origin or produced within the atmosphere. The other two lines have different gradients and are intended to encompass the variation in gradients likely to be encountered in both continental and maritime conditions; the concentration at $100\mu m$ is unchanged, but, to model steeper gradients, spectrum H has higher concentrations of smaller particles with the $10\mu m$ concentration being increased by a factor of ten; for the lower gradient (spectrum L) this concentration is decreased by a factor of ten. As we have indicated earlier, drop growth can be critically dependent upon the choice of collection efficiency, E ; the values used in these calcula-

tions are plotted in Figure 10 and were extrapolated from the table in Mason (1971). Later we shall consider how the computations are affected by this choice. A time step of 5 seconds was used throughout, tests with a one second increment showing virtually identical results; similarly, dividing the nucleus spectrum between 10 μ m and 200 μ m into 14 logarithmic bins gave the same values as 66 bins.

The computations were only carried out for the early stages of the growth of the radar echo and were terminated when Z reached 40dBZ. In this case the number of collisions between raindrops which could result in break-up and the formation of smaller satellite drops was always negligible. As a worst case it was assumed that all collisions between drops with radii exceeding 0.5mm resulted in the production of 10 satellite drops, but even then, because the concentration of such drops only ever rose to 0.3 m^{-3} , such collisions were so rare and the total number of satellites produced was always less than 1% of the number of raindrops. These low raindrop concentrations also meant that the depletion of the liquid water content of the cloud, LWC, by the raindrops never exceeded 1% of the initial value of the LWC. Similarly, depletion of the LWC by condensation on to the giant nuclei was negligible. Termination at a Z of 40dBZ thus leads to simplifications and linearisation of the processes involved.

The nucleus spectrum between 10 and 200 μ m was split up into 66 logarithmic bins, and the growth history of each bin computed using Equation 3, the number of particles in each bin remaining constant. At each time step the values of Z and Z_{DR} were computed. This predicted evolution of Z and Z_{DR} with time is of limited practical use; in the absence of dynamical Doppler infor-

mation we have no way of knowing from our radar data which parts of the cloud are young and which are old; of more importance are the predicted values of Z_{DR} for a given Z . Because of the linearity of the equations, if we change the value of the LWC then the time at which a given value of Z or Z_{DR} is reached will alter, but the curve of Z against Z_{DR} will be the same. In a real cloud the LWC might be expected to increase as a parcel of air rises, and although this will change the unverifiable Z and Z_{DR} evolution with time, the Z versus Z_{DR} prediction is unaffected by the time history of the LWC. In a similar manner the linearity lessens the sensitivity of the calculations to the choice of nucleus spectrum. If all nucleus concentrations are increased by the same factor, then the value of Z at any time is scaled up by the same amount; the values of Z_{DR} , which depend upon the ratio of differently sized drops, are unaffected, and so the result is that the overall shape of the Z versus Z_{DR} curve is unchanged, but the values of Z are scaled up. Of more importance to the predicted values of Z_{DR} is the slope of the nucleus spectrum.

The computed increases in the size of the nuclei as they collect liquid water are displayed in Figure 11 as a function of time. In this Figure the computations are initiated with the Junge spectrum, J , of Figure 9, and a liquid water content of the cloud of 2 g m^{-3} , but three different cloud droplet sizes are considered. In each case the result is broadly similar; the nuclei smaller than about $30 \mu\text{m}$ fail to grow appreciably, but those larger than this size grow rapidly to produce a small concentration of large raindrops. Once their size is more than a few hundred micrometers E rises to between 0.6 and 0.7 and is nearly constant, then, as predicted by Equation 3, the radius

grows at a rate proportional to the terminal velocity; this terminal velocity itself becoming relatively constant when the radius exceeds 1.5mm. Consequently once the raindrops exceed 1.5mm radius, the drops in each bin experience almost the same increase in size for each time increment. The small variations in the curves between Figures 11A, B and C for the different cloud droplet sizes reflect differences in collection efficiencies and droplet concentrations. The size difference between those nuclei which grow and those which do not is quite sharp; for cloud droplet radii of 4 and 6 μ m this critical nucleus size is 37 and 28 μ m respectively, and corresponds to a value of E of about 0.01. For the 10 μ m cloud droplets the critical size is reduced to 24 μ m corresponding to an E of about 0.04; this higher value of E being required because the concentration of these larger droplets is much reduced, and so the collision rate will be much lower. These curves in Figure 11 suggest that the effect of quite large changes in E will be merely to shift the critical nucleus size by a few microns, but will not make a significant difference to the total concentration of large raindrops which is produced. This was confirmed by numerical tests.

The sensitivity of the predictions to the choice of the nucleus spectrum is explored in Figure 12, in which the evolution of Z and Z_{DR} with time is calculated for the three different nucleus spectra (H, J and L) in Figure 9, assuming the cloud droplet radius to be 6 μ m and the LWC to be 2 g m⁻³. For all three spectra Z reaches 30 or 40dBZ after about 30 minutes; a prediction not significantly different from that of the models of Young and Johnson. Increasing the nucleus concentrations by a factor of ten would merely multiply the Z value at a given time by ten and so would not affect this time by more than 5 or 6 minutes.

The data in Figure 12 are expressed in another form in Figure 13 which displays the predicted variation of Z_{DR} with Z for the three different ultra-giant nucleus spectra. For comparison the 'average' curve and the anomalous data of 20 June 1984 are also plotted. It is clear that the rain that develops from all three spectra consists of a small concentration of large raindrops, and the shape of the curves are in agreement with the 20 June 1984 data, with drop concentrations several orders of magnitude lower than expected for the Marshall-Palmer curve. The predicted concentrations are rather lower than observations, but this is within the margin of error of our knowledge of the absolute concentration of the giant nuclei. The changes introduced by varying the slope of the spectra are relatively small, but, as expected, if the gradient of the spectrum is reduced, then the ratio of large drops to small ones is increased; this results in a larger mean raindrop size and larger values of Z_{DR} .

The effect of changing the liquid water content of the cloud but keeping the standard Junge aerosol spectrum is depicted in Figure 14. As the liquid water content is increased the evolution proceeds more rapidly, but, because of the linearity discussed above, a plot of the values of Z_{DR} against Z for different values of the LWC follows exactly the same curve as the J spectrum in Figure 12. For different liquid water contents we proceed along the same curve but move along it at a different rate.

We have already remarked upon the effect of changing the cloud droplet size when discussing the evolution of the spectra in Figure 11. A more comprehensive model would be expected to consider a spectrum of cloud droplets similar to those observed in real clouds; in view of the uncertainties and arbitrariness in any choice of values of E , we have carried out a simpler test.

The cloud droplets are still monodispersed with an LWC of 2 g m^{-3} and the standard Junge nucleus spectrum was used, but the evolution was computed for cloud droplet radii of $r=4, 6$ and $10 \mu\text{m}$ (Figure 11). These values could be considered as extreme limits to any reasonable condensate spectra. The cloud consisting only of $10 \mu\text{m}$ droplets grew much faster reaching 30dBZ in 22 minutes compared to 50 minutes for the $4 \mu\text{m}$ droplets. The slower growth with the smaller sized cloud droplets results from the lower values of collection efficiencies; another effect of the lower values of E for the $4 \mu\text{m}$ droplets is that less large drops are produced than for a cloud of $10 \mu\text{m}$ droplets, thus leading to an increase in the value of Z_{DR} for a given Z . This effect can be seen in Figure 15 where the corresponding values of Z and Z_{DR} are plotted for different sized cloud droplets and compared with the average values for the cloud observed on 20 June 1984. Even for these values of droplet radii, which must be taken as extreme limits, for a given value of Z_{DR} the values of Z changes by only about 10dBZ. In all three cases the curves lay well below the Marshall-Palmer values but are still consistent with the radar observations. Additional numerical experiments changing all values of E by a factor of 10 up and down, gave very large differences to the rate of development of the echo, but had a relatively small effect on the Z v Z_{DR} curve. For example such large changes in E had little effect on the $6 \mu\text{m}$ curve in Figure 15; even with these changes it still lay between the 4 and $10 \mu\text{m}$ curves.

5. CONCLUSION

The radar observations indicate that on occasion first echoes consist of a small number of large raindrops; these echoes

having raindrop concentrations three orders of magnitude lower than the average Marshall-Palmer size spectra found in mature clouds. This is a large deviation and cannot be explained by any uncertainties in the shape of raindrops having diameters above 4mm (Z_{DR} above 2.5dB) which were discussed in Section 2. A simple model which considers the collection of cloud water by the spectrum of ultra-giant nuclei reported by Junge (1972) appears to simulate this process accurately. The model is fairly robust. Whereas alterations in the liquid water content and collection efficiencies have a marked effect on the rate at which the echo grows; the values of Z for a given value of Z_{DR} do not change markedly and are in agreement with the radar observations. The values of Z remain three orders of magnitude below those encountered in average mature precipitating clouds.

It appears that the critical value of collection efficiency which governs whether an aerosol particle will grow appreciably is about 0.01; for our choice of E this means that aerosol particles larger than 30 μ m grow to raindrops, but smaller ones stay the same size. Values of E of this magnitude are virtually impossible to measure in the laboratory, and any numerical computations of E are open to doubt, but fortunately the effect of quite large changes in E on this model is relatively small. Altering the cloud droplet radius from 4 to 10 μ m changes the threshold size of nuclei which can grow by collecting droplets from 37 to 24 micrometers respectively. As a result it is the numbers and sizes of ultra-giant particles above 30 μ m which govern the developing raindrop size spectra until collision induced break-up of raindrops becomes important. The Junge aerosol spectrum used is an average of many observations and is representative of conditions above the boundary layer; close to the sea and to the

ground there may be higher concentrations. Changing the slope of this spectra to cover most naturally occurring spectra does not change the predictions appreciably. The truncation of the spectrum at 100 μ m or 200 μ m does not affect the conclusions; in all cases the numbers of these 100 μ m or 200 μ m particles are so low compared to the 50 μ m ones that raindrops grown on them make a negligible contribution to Z and Z_{DR} , the principal component to these parameters coming from drops formed on the 50 μ m aerosol particles.

It should be stressed that we do not have a large enough data set to assert that all first echoes form on these large nuclei, but that the case studies presented do seem consistent with such a mechanism. It is also not possible to state that a small concentration of large drops could not result from the stochastic nature of the collisions between more normally sized cloud droplets. Indeed it is probable that a combination of collection efficiencies could be found that would give such a result. The stochastic models in the literature discuss the various techniques used to optimise the formidable computations but do not tend to dwell upon the sensitivity of the results to a particular choice of E . A modeller who simulates the interactions between the 10^8 or 10^9 droplets in a cubic meter needs considerable courage to predict with confidence that one and only one of these droplets will grow to a raindrop. Any attempt to incorporate collision induced breakup of large raindrops to predict raindrop size distributions requires full statistical information on the numbers and sizes of the satellite drops produced. Such information is not yet available. Young (1975) based his formulation upon laboratory simulations of colliding drops, but in these experiments the raindrops were not falling

vertically nor were they at the correct terminal velocities. Johnson (1982) assumed that as soon as a raindrop reached a radius of 2.5mm it spontaneously split into four equally sized fragments; this would introduce two unrealistic steps into any computed raindrop spectrum. It seems that any modelling of the final raindrop spectra which includes collision induced drop break-up is premature and must await improved experimental data.

Some tropical locations, such as Hawaii, appear particularly favourable for testing the mechanism of warm rain development on ultra-giant nuclei; the dynamics are relatively straightforward and it should be possible to monitor the nucleus concentrations before the air enters the cloud, and also to trace the growth of Z and Z_{DR} as the drops move through the orographically induced cloud. Using aircraft Hallett et al (1978) have observed large supercooled raindrops inside Florida clouds and differential reflectivity measurements in this location would help to identify the mechanism responsible for their growth.

The situation is not so well defined in temperate regions: the depth of cloud below the freezing level is rather restricted, and, as seen in one of the case studies in this paper where supercooled raindrops were inferred to be present, glaciation can follow warm rain initiation. The model suggests 20 or 30 minutes is required for the large raindrops to develop, and, providing the temperature is warmer than -10°C , the raindrops should not freeze spontaneously during this time (Vali and Stansbury, 1966). In the second case, on 20 June 1984, there was about 1.5km of cloud warmer than 0°C with computed values of liquid water content at 3 g m^{-3} , so again the raindrops of the size inferred from the radar could develop in about twenty minutes. It is difficult to see how aircraft measurement could provide confirmation of the

deductions made from the radar; even supposing the aircraft could be directed towards the particular echo, the sampling volume of most aircraft probes is so small that they would not obtain a significant sample of these low raindrop concentrations. Similar difficulties would be encountered when attempting to monitor the ultra-giant nuclei entering a particular cloud. On 6 July 1983 the echoes of interest were daughter cells forming near much larger storms; it may be that the outflow preferentially lifted large nuclei up into the daughter cell. On 20 June 1984 two of the echoes in Figure 5 had anomalous differential reflectivity, one more intense echo had drop concentrations a factor of ten below normal; other much weaker echoes had zero values of Z_{DR} but the magnitude of Z was below 8 dBZ. Doppler studies might reveal that the origin of the air was different for the two classes of echo on this day, or that the normal echoes had lower values of Z because the updraughts were much weaker and so no precipitation developed. Previously the radar has tended to concentrate on the more intense echoes because of their importance to communications problems, but it is clear that a more lengthy period of observations of early echoes is required. This would enable statistics to be gathered on which types of early echoes develop and which do not, and if any echoes do develop via the warm rain process without having anomalously high values of differential reflectivity, or if the appearance of a low concentration of large raindrops is the only route.

REFERENCES

- Baker, M B and Latham, J (1979) The evolution of droplet spectra and the production of embryonic raindrops in small cumulus clouds. J. Atmos. Sci., 36, 1612-1615.
- Browning, K A and Atlas, D (1965) Initiation of precipitation in vigorous convective clouds. J. Atmos. Sci., 22, 678-683
- Caylor and Illingworth (1986) Observations of the growth and evolution of raindrops using dual-polarisation radar. 23rd Conf. on Radar Meteorology, A.M.S., Boston. 22-26 Sep.
- Cherry, S M and Goddard, J W F (1982) Design features of dual polarisation radar, URSI, Open Symposium on Multiple-Parameter Radar Measurements of Precipitation, Bournemouth, U.K. 23-27 Aug.
- Cooper, W A, Bringi, V N, Chandrasekhar, V and Seliga, T A (1983) Analysis of raindrop parameters using a 2-D precipitation probe with application to differential reflectivity. 21st Conf on Radar Meteorology, A.M.S., Boston. 19-23 Sep
- East, T W R (1957) An inherent precipitation mechanism in cumulus clouds. Q.J.R.Meteorol.Soc., 83, 61-76
- Goddard, J W F, Cherry, S M and Bringi, V N (1982) Comparison of dual-polarisation radar measurements of rain with ground-based disdrometer measurements. J.Appl.Meteorol., 21, 252-256.
- Hall, M P M, Goddard, J W F and Cherry, S M. (1984) Identification of hydrometeors and other targets by dual-polarisation radar. Radio Sci., 19, 132-140.
- Hallett, J, Sax, R L, Lamb D, and Murty A S R (1978) Aircraft measurements of ice in Florida cumuli. Q.J.R.Meteorol.Soc., 104, 631-651
- Hill, T A and Choulaton, T W (1986) A model of the development of the droplet spectrum in a growing cumulus turre. Q.J.R.Meteorol.Soc., 112, 531-554.
- Illingworth, A J, Goddard, J W F and Cherry, S M (1984) Dual linear polarisation radar studies of the evolution of convective storms. 22nd Conf. on Radar Meteorology, A.M.S., Boston. 10-14 Sep
- Illingworth, A J, Goddard, J W F and Cherry, S M (1987) Polarisation-radar studies of precipitation development in convective storms. Q.J.R.Meteorol.Soc. (in press)
- Johnson, D B (1982) The role of giant and ultra-giant aerosol particles in warm rain initiation. J.Atmos.Sci, 39, 448-460
- Junge, C E (1972) Our knowledge of the physico-chemistry of aerosols in the undisturbed marine environment. J.Geophys. Res., 77, 5183-5200.

- Langmuir, I (1948) The production of rain by a chain reaction in cumulus clouds at temperatures above freezing. J.Meteorol.,5,175-192.
- Ludlam, F H (1951) The production of showers by the coalescence of cloud droplets. Q.J.R.Meteorol.Soc., 77, 402-417.
- Marshall, J S and Palmer, W.McK (1948) The distribution of raindrops with size. J.Meteorol.,5,165-166.
- Mason, B J (1971) The Physics of Clouds, Clarendon Press, Oxford.
- Mordy, W A and Eber, L E. (1954) Observations of rainfall from warm clouds. Q.J.R.Meteorol.Soc.,80,48-57.
- Mueller, A E and Larkin, R P (1985) Insects observed using dual-polarisation radar. J.Atm.Ocean.Tech.,2,49-54.
- Paluch, I R and Knight, C A (1986a) Mixing and the cloud droplet size spectrum: Generalisations from the CCOPE data. J.Atmos.Sci.,43,1984-1993.
- Paluch, I R and Knight, C A (1986b) Does mixing promote cloud droplet growth. J.Atmos.Sci.,43,1994-1998.
- Pruppacher, H R and Klett, J D (1978) Microphysics of clouds and precipitation. Reidel, Dordrecht.
- Pruppacher, H R and Pitter, R L (1971) A semi-empirical determination of the shape of cloud and rain drops. J.Atmos.Sci., 28, 86-94.
- Telford, J W, Keck, T S and Chai, S K (1984) Entrainment at cloud tops and the droplet spectra. J.Atmos.Sci.,41,3170-3179.
- Vali G, and Stansbury, E J (1966) Time-dependent characteristics of the heterogeneous nucleation of ice. Canad.J.Phys.,44,477-502.
- Young, K C (1975) The evolution of drop spectra due to condensation, coalescence and breakup. J.Atmos.Sci., 32, 965-973.

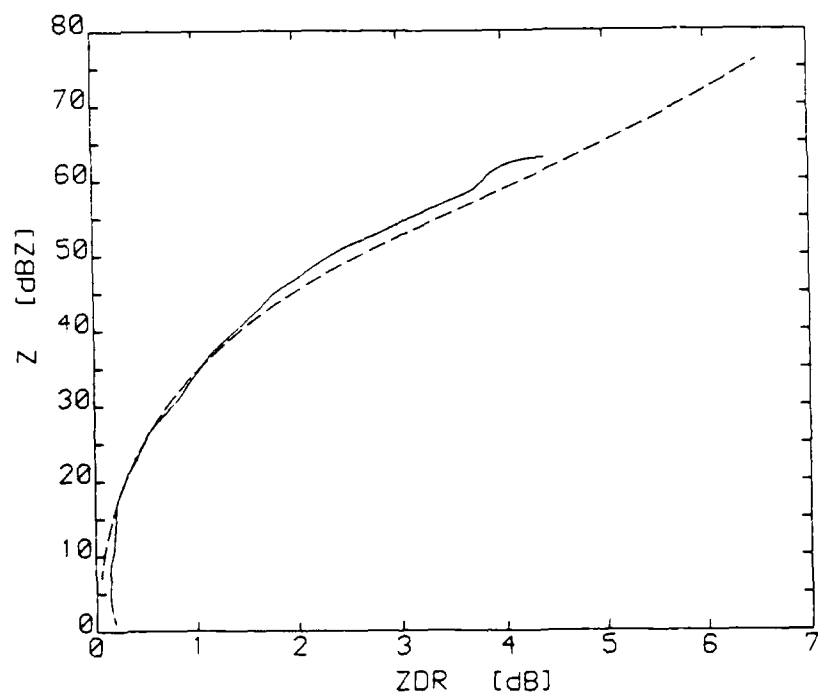


Figure 1

The value of the differential reflectivity (Z_{DR}) as a function of the radar reflectivity factor (Z). The dotted line is for theoretical values calculated for a Marshall-Palmer raindrop size distribution. The solid line is the average of 150000 radar data points collected on many different days in mature clouds; an average value of Z_{DR} is calculated for each 2dBZ increment in Z .

RHI SCAN ON 06/07/1983 AT 1607 UT
 TAPE 315 RASTER 67 SCAN 1 AZ = 148.0 deg

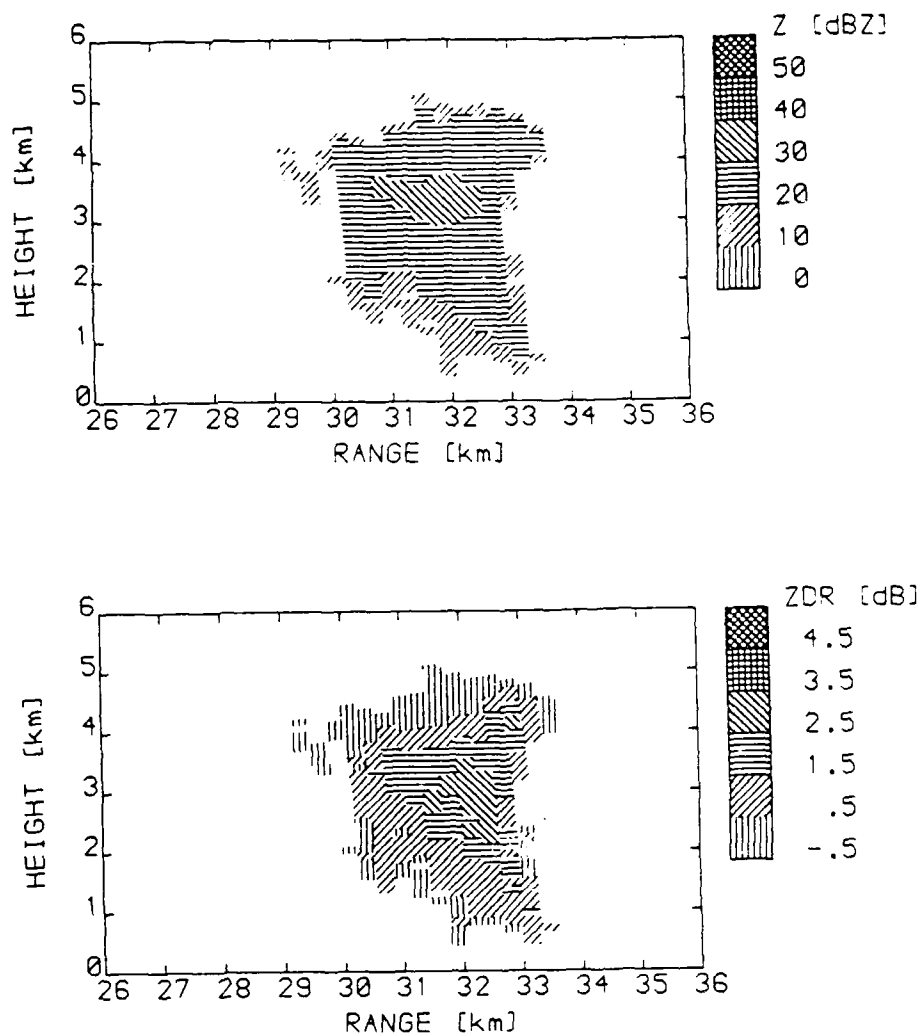


Figure 2

A vertical section through the most intense part of an isolated cell on 6 July 1983 at 1607 GMT. High positive Z_{DR} accompanies weak Z .

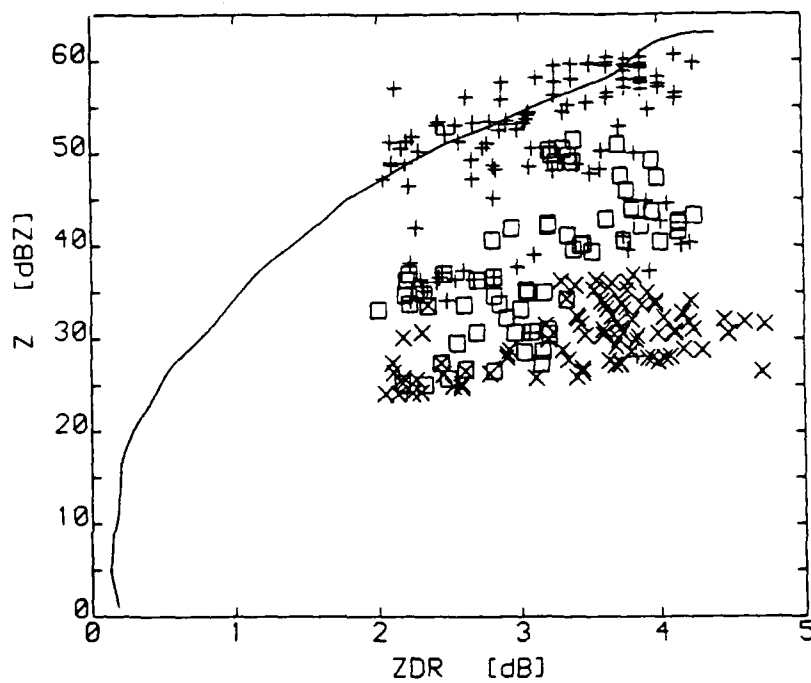


Figure 3

Evolution of the individual values of Z and Z_{DR} for three vertical sections of the cloud in Figure 2. To avoid cluttering up the diagram only data points with Z_{DR} above 2dB are plotted. x 1611 GMT, \square 1613 GMT and + 1619 GMT. The solid line is the average for rain on many days (Figure 1).

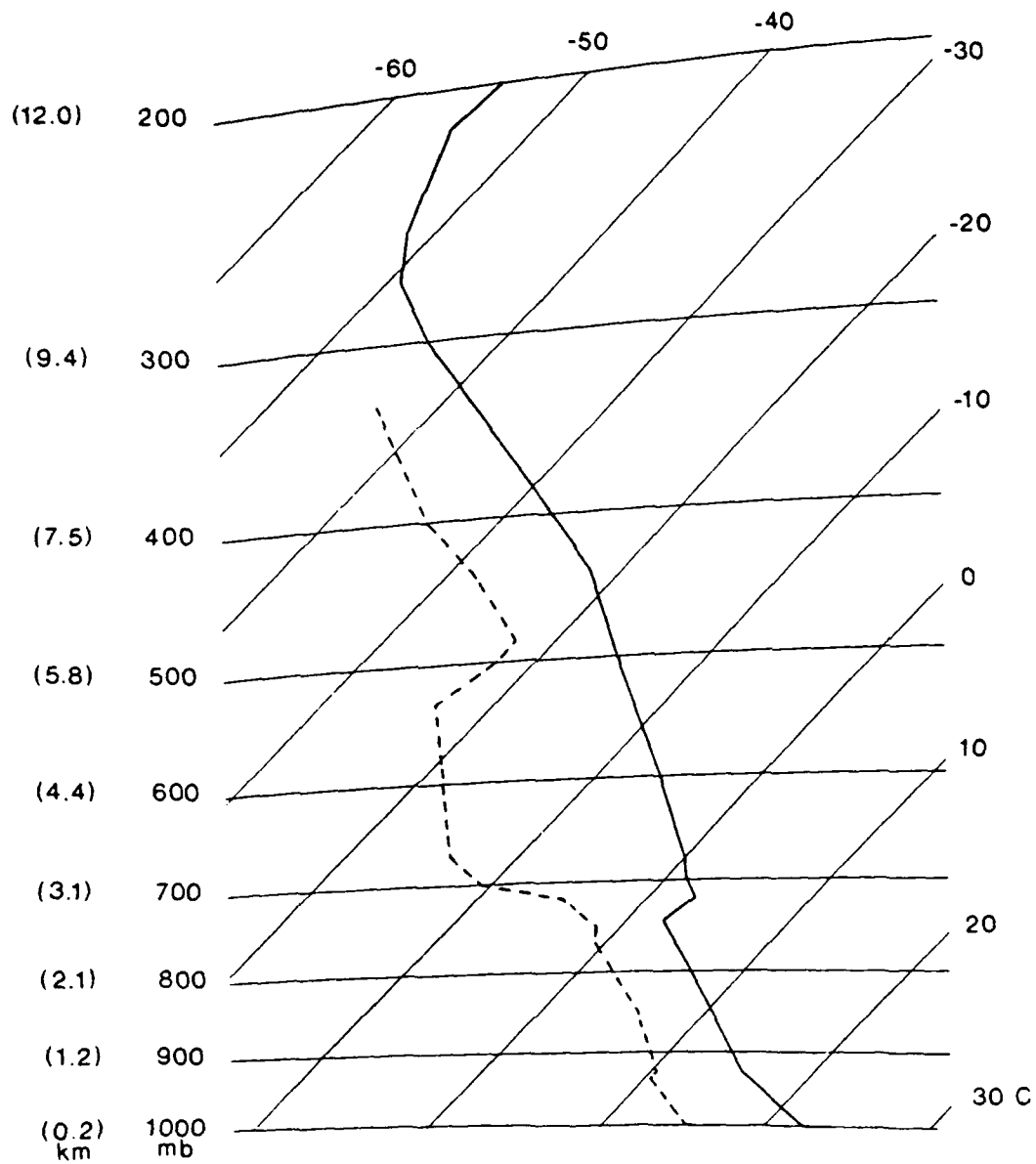


Figure 4

Sonde ascent for Crawley (80km East of Chilbolton) at 1200 on 20 June 1984.

PPI SCAN ON 20/06/1984 AT 1743 UT
 TAPE 337 RASTER 43 SCAN 1 EL = 1.5 deg

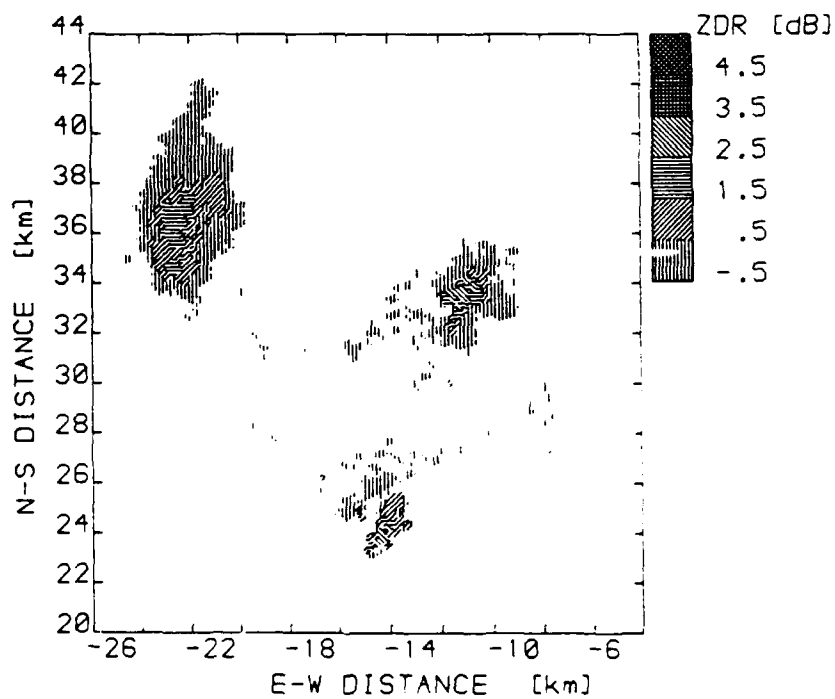
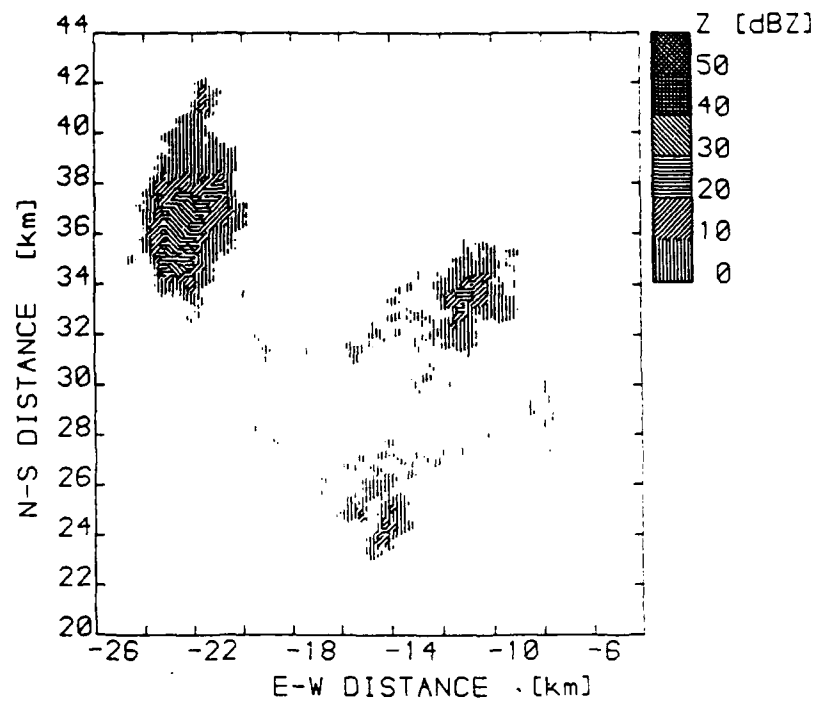


Figure 5

A 1° elevation PPI radar scan on 20 June 1984 at 1743 GMT showing various weak isolated echoes, two having anomalously high values of Z_{DR} .

RHI SCAN ON 20/06/1984 AT 1745 UT
TAPE 337 RASTER 44 SCAN 3 AZ = 342.5 deg

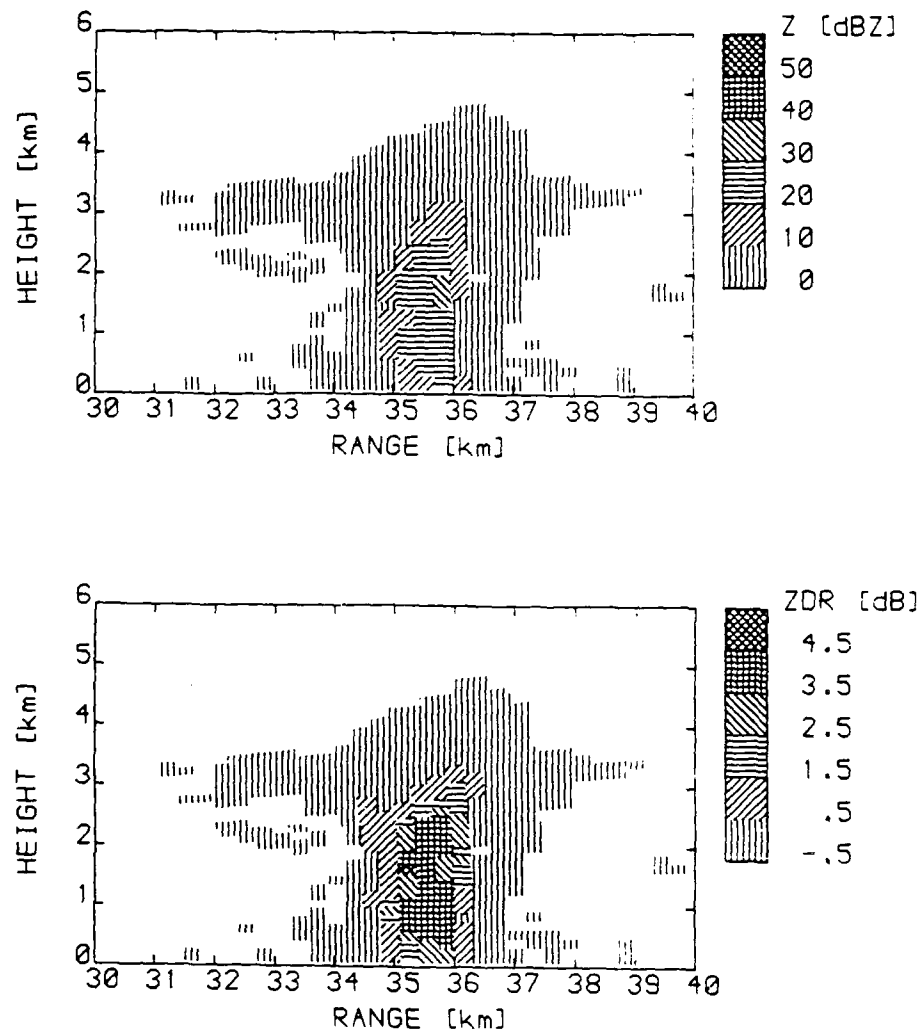


Figure 6

A vertical section on 20 June 1984 at 1745 through the most intense part of the isolated echo in Figure 5 which is 33km north of the radar.

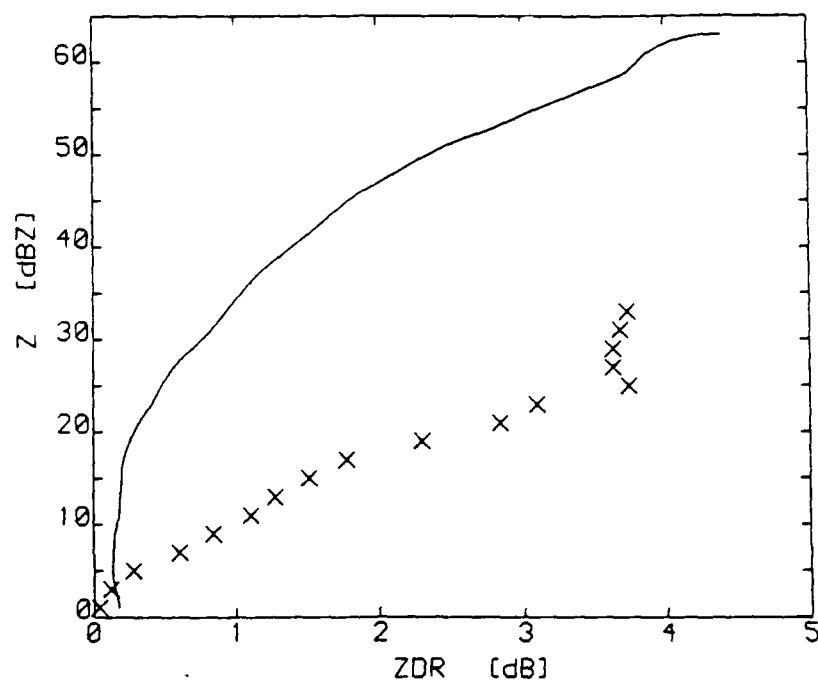


Figure 7

A plot of the average values of Z_{DR} for each 2dBZ increment in Z for 2700 data points obtained during twenty minutes observation of the echo in Figure 6. The solid line is the average for rain on many days (Figure 1).

RHI SCAN ON 20/06/1984 AT 1810 UT
 TAPE 337 RASTER 60 SCAN 1 AZ = 359.2 deg

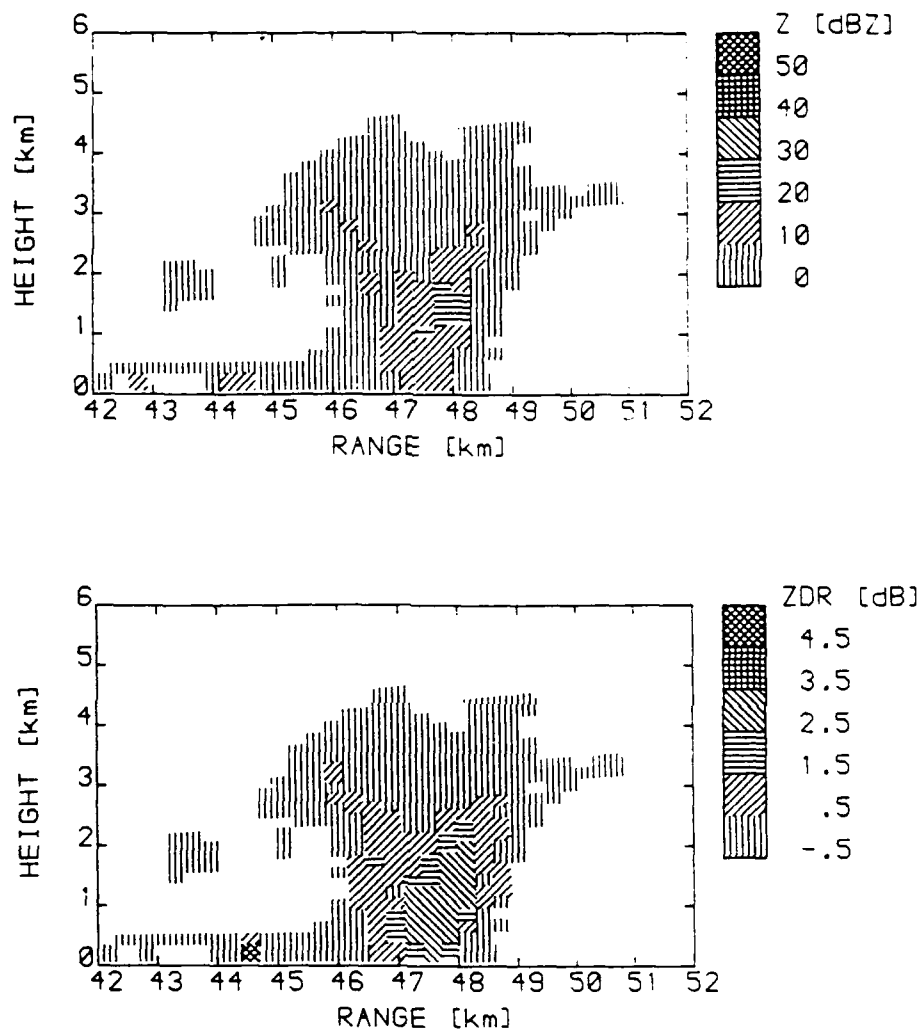


Figure 8

A vertical section on 20 June 1984 at 1810 through the most intense part of an isolated echo, which has developed since the PPI in Figure 5.

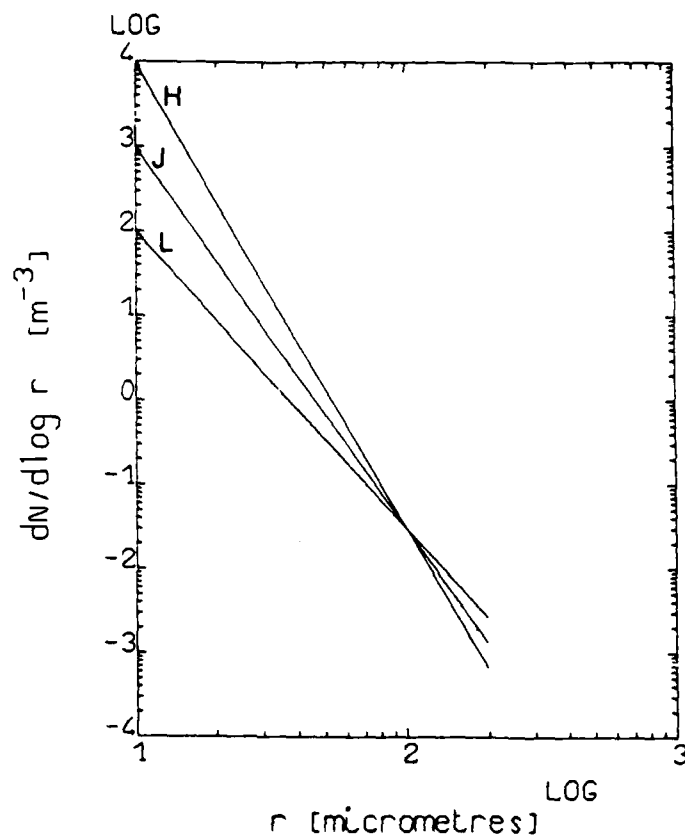


Figure 9

Ultra-giant nucleus spectra. J - the average of Junge (1972) data. H and L - other spectra used to test the model.

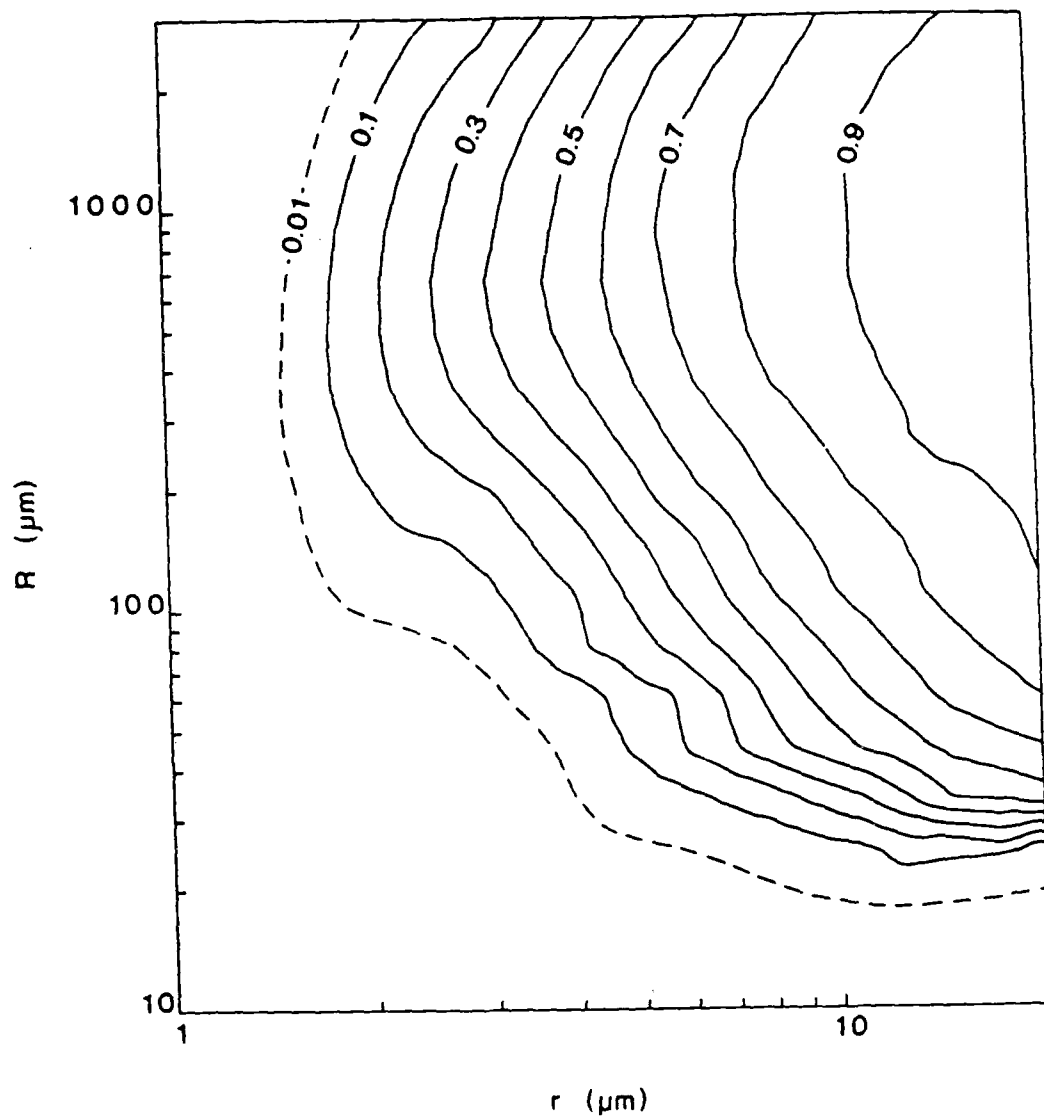


Figure 10

Collection efficiencies, $E(R, r)$, of the larger particles (radius R) for smaller droplets (radius r). These values are used in all subsequent Figures.

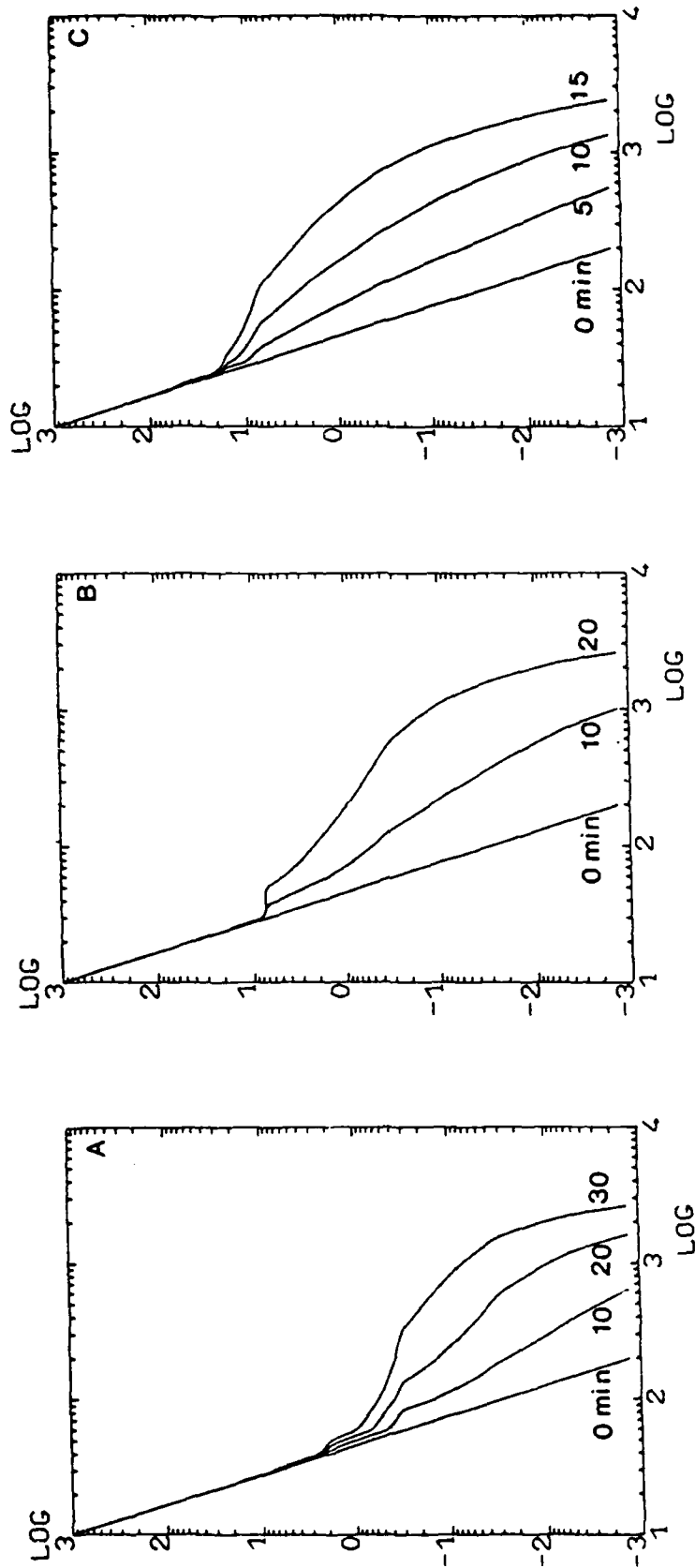


Figure 11

The development of the raindrop spectrum with time as an initial Junge ultra-giant nucleus spectrum (J) sweeps out cloud water having a LWC of 2 g m^{-3} . A) cloud droplet size $4 \mu\text{m}$, B) $6 \mu\text{m}$ and C) $10 \mu\text{m}$.

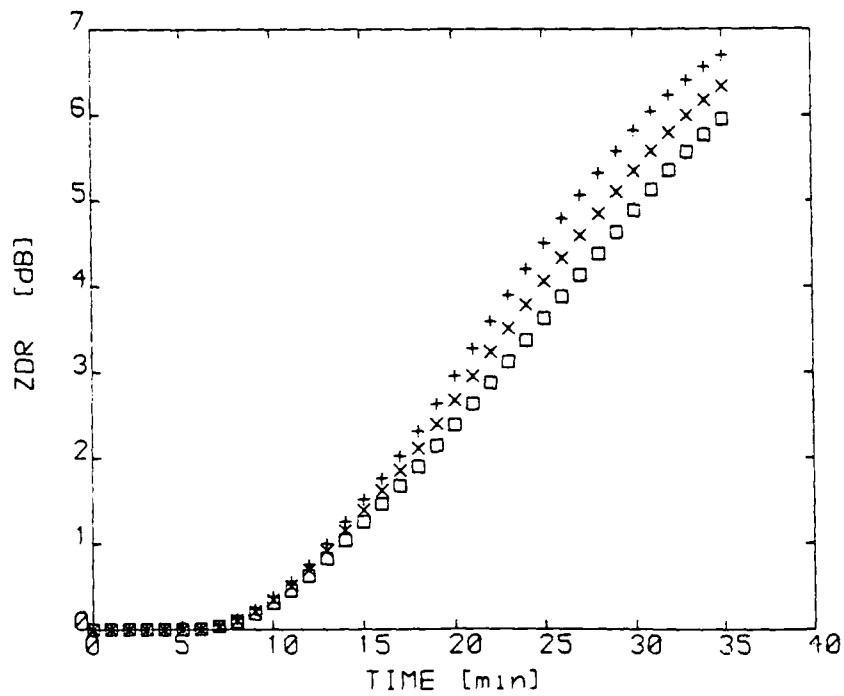
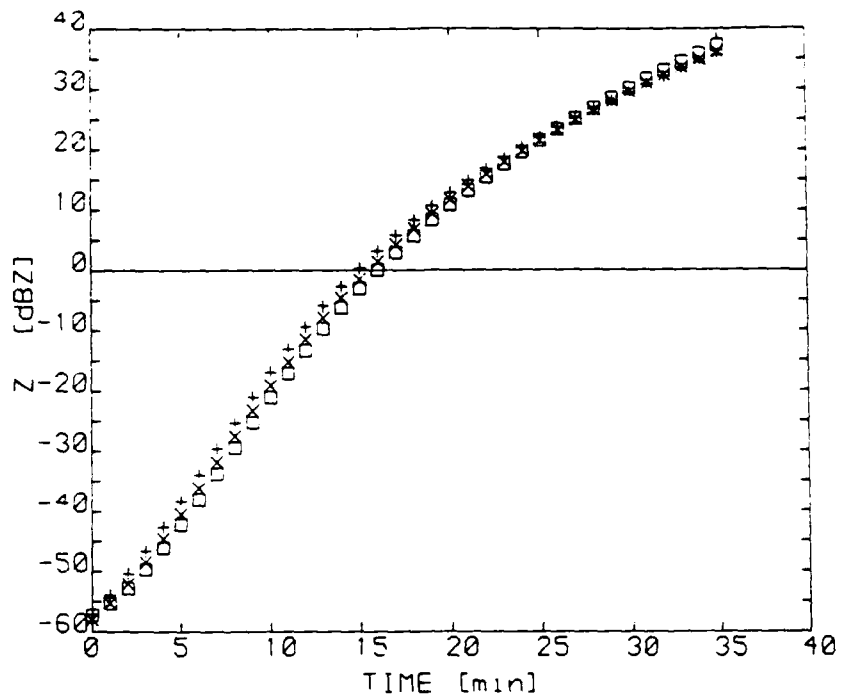


Figure 12

The growth of Z and Z_{DR} with time as the three nucleus spectra capture cloud droplets of radius 6 μm and LWC 2 g m^{-3} .
 \square , spectrum H; \times , spectrum J; $+$, spectrum L.

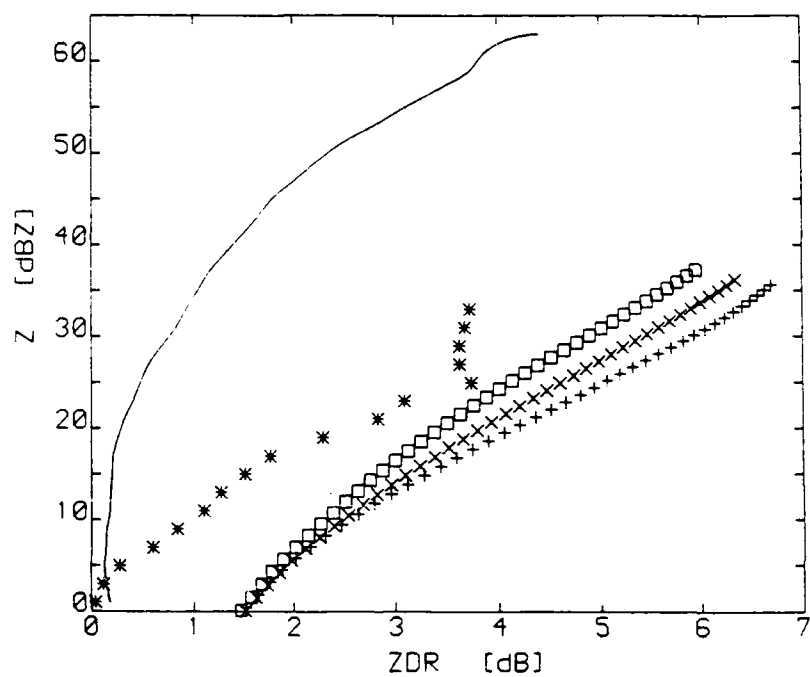
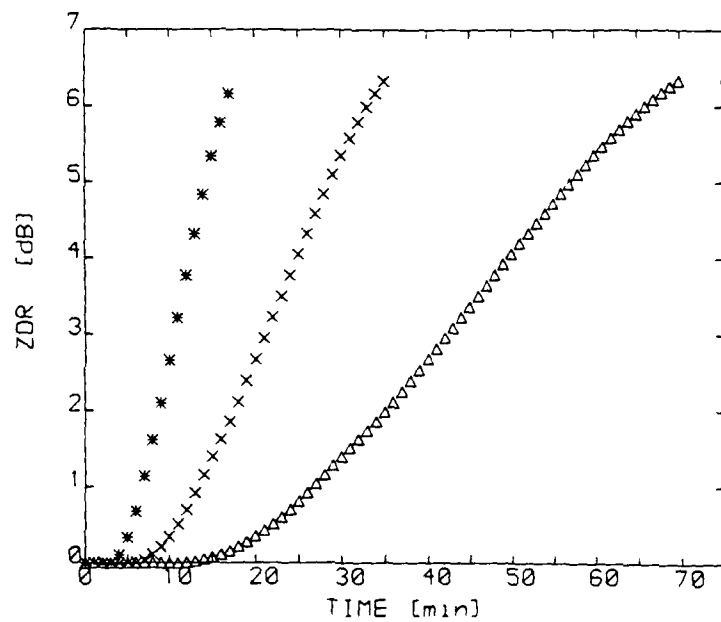
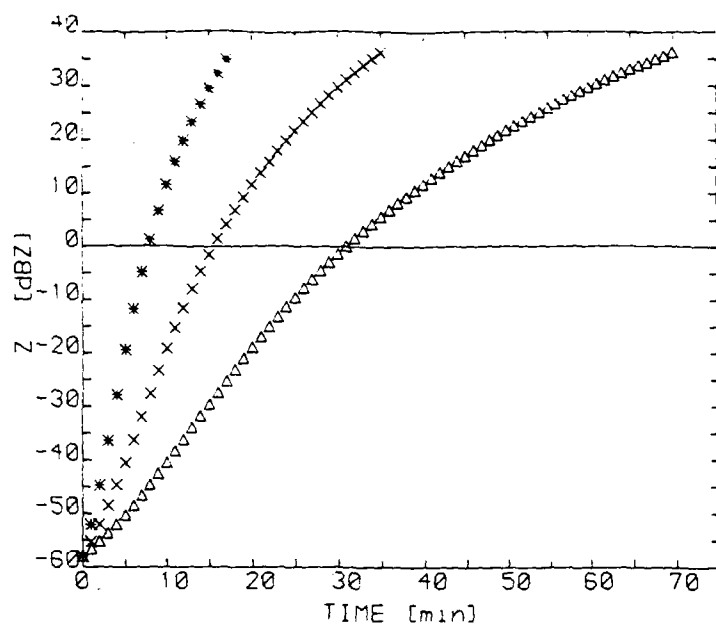


Figure 13 The values of Z_{DR} accompanying Z for the three different initial nucleus spectra H, J, and L growing under the conditions of Figure 12. The solid line is the average for rain on many days (from Figure 1). * - average for the echo on 20 June 1984 (from Figure 7). □, spectrum H; X, spectrum J; +, spectrum L.

Figure 14

The evolution of Z and Z_{DR} with time for clouds of differing liquid water content; Δ , 1 g m^{-3} ; \times , 2 g m^{-3} , and $*$, 4 g m^{-3} . Junge nucleus spectrum J. Cloud droplet radius $6 \mu\text{m}$.



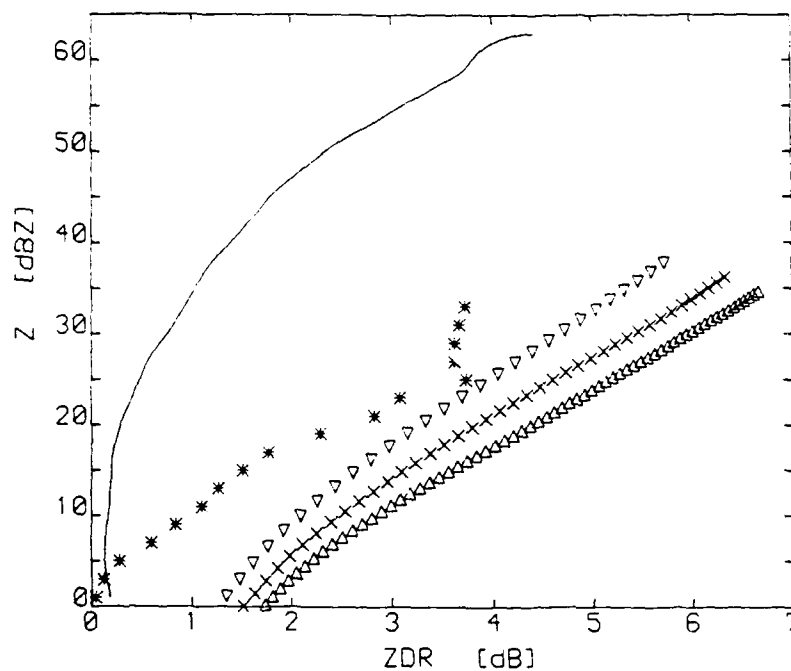


Figure 15

The values of Z_{DR} accompanying Z as the initial Junge spectrum, J , sweeps out cloud liquid water, L , of 2 g m^{-3} for differing radii of the small cloud droplets: Δ , $4\mu\text{m}$; X , $6\mu\text{m}$; and ∇ , $10\mu\text{m}$. Solid line is the average value for rain on many days.

* - average for the echo on 20 June 1984 (from Figure 7).

PART C

POLARIZATION RADAR MEASUREMENTS OF RAINDROP SIZE SPECTRA
AND RAINFALL RATES IN HEAVY RAIN

ABSTRACT

The differential reflectivity (ZDR) measures the mean shape of hydrometeors and provides an estimate of the mean size of raindrops. Observations of ZDR for rain may be combined with the conventional radar reflectivity factor (Z) and fitted to any two parameter raindrop size distribution and this information used to derive more accurate rainfall rates. In such work the precise shape of raindrops is a critical parameter. Recently available data suggest that large raindrops are more oblate than previously believed. These new shapes support the idea that ZDR values above 3.5dB can be attributed to rain. Average values of ZDR as a function of Z obtained in heavy rain by the Chilbolton radar agree very closely with those predicted using the new shapes. Statistics are also presented of the natural variability of raindrop spectra in heavy rain. Implications for the measurement of rainfall rates by radar are discussed.

INTRODUCTION

The radar reflectivity factor, Z , of rain measured by a conventional radar is not a unique function of the rainfall rate or the raindrop size distribution, but is given by the product ND^6 , where N is the concentration of drops of diameter D , summed over all the drop sizes present. Many different empirical relationships have been proposed relating the rainfall rate (R) to the radar reflectivity (Z). The use of one of these formulae is essentially equivalent to assuming a constant raindrop size distribution. Such relationships reflect an average long term dependence, but the actual rainfall predicted by an individual value of Z is typically in error by a factor of two because of natural fluctuations in the raindrop size spectra (Wilson and

Brandes, 1979).

Polarization diversity radar provides a second observable parameter, the differential reflectivity, which is related to the mean drop size spectra, and when this information is used in conjunction with Z, more accurate rainfall rates may be derived. The differential reflectivity (ZDR) is defined as:

$$ZDR = 10 \log (Z_H/Z_V) \quad (1)$$

where Z_H and Z_V are the radar reflectivity factors measured at horizontal and vertical polarizations, respectively. ZDR is related to the mean hydrometeor shape. For spherical particles, such as small raindrops, Z_H and Z_V are equal, and ZDR is zero. Larger raindrops are oblate to a degree which depends upon their size, so Z_H exceeds Z_V ; ZDR is positive, and its magnitude is related to the mean raindrop size present.

When observations of both Z and ZDR are available, then the data can be fitted to any two parameter raindrop size distribution. Raindrop size distributions are commonly of the exponential form:

$$N(D) = N_0 \exp (-3.67 D/D_0) \quad (2)$$

where D_0 is the equivolumetric raindrop diameter. Seliga and Bringi (1976) proposed that the value of D_0 may be derived from the magnitude of ZDR, and N_0 may then be found if Z is known. The use of an empirical Z-R relationship is equivalent to using a one parameter raindrop size distribution such as that proposed by Marshall-Palmer (1948), where N_0 is constant and equal to $8000 \text{ m}^3 \text{ mm}^{-1}$ and D_0 is a function of rainfall rate.

The differential reflectivity technique relies on a precise knowledge of the shapes of different sizes of raindrops. The Chilbolton radar (Cherry and Goddard, 1982) can measure ZDR to an accuracy of about 0.1dB which is equivalent to a change in raindrop axial ratio of about 0.01. Most ZDR measurements have been

interpreted using the laboratory based equilibrium raindrop shapes of Pruppacher and Pitter (1971) who quote errors of about 0.02 for the axial ratios of the smaller drops.

In a series of comparisons of Chilbolton radar data with a ground based disdrometer (Goddard and Cherry, 1984; and Goddard, Cherry and Bringi, 1983), significantly improved agreement was obtained if the drops below 3mm in size were made slightly more spherical than the shapes of Pruppacher and Pitter. The proposed changes in drop shapes were within the experimental error of the Pruppacher and Pitter measurements, for example the axial ratio of a 1mm drop was changed from 0.98 to 1.00. Recently, more accurate measurements of the shape of naturally occurring raindrops using airborne shadowgraph instruments (Chandrasekar et al, 1987) have confirmed that the shapes inferred from the radar are correct and the drops are indeed slightly more spherical than suggested by Pruppacher and Pitter.

In this paper we direct attention to heavier rainfall with values of Z above 40dBZ and rainfall rates generally above 10mm hr⁻¹. The precise shapes of raindrops larger than 4mm are uncertain, but are important for ZDR measurements in heavier rain. Doviak and Zrnica (1984) state that the maximum value of ZDR due to rain should be 3.5dB. This assertion is based upon Green's (1975) formula for the axial ratio of raindrops, which is very close to the measurements of Pruppacher and Pitter. Using these shapes a 6mm drop would be associated with a ZDR of 3.8dB and an 8mm drop 4.7dB; summing the weighted contribution of the various drops in a Marshall-Palmer raindrop size distribution leads to the conclusion that the ZDR of rain cannot exceed 3.5dB. Doviak and Zrnica (1984) suggest that higher values of ZDR result from a measurement related problem or are due to targets other than

raindrops and suggest they arise from ice particles which have very oblate shapes when they melt.

Values of ZDR above 3.5dB and as high as 6dB have been reported in convective showers (Illingworth et al, 1987) and in view of the above argument it seems logical to attribute such observations to melting ice particles. On closer examination other possibilities arise. Based on a statistical analysis of the high values of ZDR accompanying intense echoes at altitudes where rain is to be expected, Caylor and Illingworth (1986) hypothesised that raindrops larger than 4mm are more oblate than predicted by Pruppacher and Pitter. This suggestion was prompted by two findings. Laboratory measurements (Rasmussen et al, 1984) suggest that, unless the ice particles are initially extremely oblate, then the shapes during melting are no more distorted than those of the same sized water drop. Secondly, a limited series of aircraft measurements of large drops (Cooper et al, 1983) implied more oblate forms. Beard and Chuang (1987) have recently published more accurate measurements of the shape of large drops and in Section 2 of this paper we use these new shapes to calculate the values of ZDR to be expected for various raindrop size distributions. The predicted variation of the average values of ZDR as a function of Z using these new shapes is compared with the actual average values observed with the Chilbolton radar. The variation in the naturally occurring spectra around these mean values is discussed in Section 3. The implications of these results are explored in the final Section 4.

2. THE DIFFERENTIAL REFLECTIVITY OF HEAVY RAIN

2.1 Drop Shapes and Differential Reflectivity

The axial ratios for drops above 4mm proposed by Pruppacher and Pitter (1971) are compared with the more recent values obtained by Beard and Chuang (1987) in Table 1. The values of Pruppacher and Pitter have considerable scatter when experimental errors are considered, with, for example, drops between 7 and 8mm having ratios in the range 0.51 to 0.69. The uncertainties in axial ratios quoted for Beard and Chuang's model are less than 0.015. For raindrops larger than 2mm Beard and Chuang find that the axial ratio is nearly a linear function of size with a fall in axial ratio of about 0.06 for every millimeter increase in size. The 9mm drop shape entry in the table is taken from the graph in their paper and is consistent with the shape measured by Pruppacher and Beard (1970) in the low turbulence UCLA wind tunnel. The 10mm axial ratio is derived by extrapolation of the linear relationship and is not supported by direct evidence. Beard (1976) found that changes in pressure and temperature have a negligible effect on raindrop shape over all reasonable values to be found in the atmosphere.

The two drop shape models lead to different predicted magnitudes of ZDR for the larger raindrops. The values of ZDR in Table 1 are computed for the Beard and Chuang shapes using the simple Rayleigh-Gans theory which is strictly only applicable to the small drops, and the Mie-Gans theory which should be used when the drop diameter becomes a reasonable fraction of the radar wavelength. We are indebted to Dr Holt of the Department of Mathematics, Essex University for the Mie-Gans calculations which are carried out for water drops at 0°C and the Chilbolton frequency of 3.0765GHz. The values of ZDR using the exact theory are

only slightly higher than for Rayleigh scattering apart from drops above 8mm where the divergence is considerable.

2.2 Statistical Analysis of Radar Data

A simple prediction of the values of ZDR to be expected in rain is displayed in Figure 1 for a Marshall-Palmer raindrop size distribution with a value of N_0 of $8000\text{m}^{-3}\text{mm}^{-1}$. The two curves are obtained using the two drop shapes models in Table 1 for different values of D_0 in Equation 2 and terminating the raindrop spectrum at 8mm. The curves diverge for values of Z above 40dBZ; the Pruppacher and Pitter shapes leading to a maximum predicted value of 3.5dB, whereas the more oblate shapes suggest values of up to 4.5dB are possible.

The crosses in Figure 1 represent the average values of ZDR for each 2dBZ step in Z, obtained from measurements in rain made with the Chilbolton radar during summer convective storms on many different days. Isolated echoes smaller than 2km in diameter were not included in the analysis. During this time, the freezing level was at 3km or slightly above, and so, to minimise ambiguities due to melting ice particles, data were only analysed for altitudes below 1km. It is well established that in severe storms with intense reflectivities, values of ZDR close to zero can extend down to the ground; these signatures are interpreted as hail reaching the ground (e.g. Illingworth et al, 1986). These features are usually quite localised and easy to identify, and so any cell having values at 1km altitude where ZDR was below 1dB with Z above 40dBZ was excluded from the analysis. An example of the average values of ZDR for every 2dBZ step in Z for such a cell is shown in Figure 2, where the effect of the hail in reducing the mean values of ZDR for values of Z above 55dBZ is quite dramatic.

It has been argued that values of ZDR above 3.5dB should be attributed to raindrops containing melting ice cores (e.g. Doviak and Zrnic, 1984; Beard and Chuang, 1987). The evidence from the Chilbolton radar does not support this. Values of ZDR of up to 9dB have been observed in the bright band and are thought to result from melting snowflakes and ice crystals, but these only occur in stratiform clouds with a clearly defined melting layer. In convective storms our observations of many vertical profiles of Z and ZDR indicate that, as ice particles melt, the value of ZDR gradually increases from the zero value associated with graupel and hail, and reaches a maximum value reflecting the equilibrium shape of the raindrop when melting is complete. The ZDR profiles in convective clouds do not show a maximum associated with the final stages of melting followed by a collapse to a less oblate raindrop containing no ice. Laboratory studies of the melting of ice support this suggestion; Rasmussen et al (1984) show that ice spheres smaller than 9mm do not shed water, but that as melting proceeds they become progressively more oblate, finally assuming the shape of the equivalent diameter water drop. For spheres larger than 9mm an unstable torus of liquid water built up around the equator, but an ice particle falling in the free atmosphere would be free to tumble and would shed such a torus.

Values below 250m altitude were also excluded from the analysis in Figure 1, as these were likely to be affected by ground clutter. Even with this height restriction the quarter degree beamwidth Chilbolton radar still detected the occasional ground return, but the ZDR of such returns is easy to recognise, as the values of ZDR lie in the range +5dB to -5dB and changes by several dB between one 300m gate and the next (Hall et al, 1984).

To suppress this clutter, a ZDR reading was rejected if the change in ZDR at a neighbouring gate was more than 60%.

The average values of ZDR obtained, after the removal of ground clutter and ambiguities due to melting ice, are those displayed in Figure 1. This data, together with the sample size and standard deviations are summarised in Table 2. If we assume a normal distribution then the standard errors in the mean are only significant for the values of Z in the two highest ranges; these error bars are plotted in the figure.

The radar evidence is more consistent with the drop shapes proposed by Beard and Chuang and we shall use these sizes from now onwards. The errors in axial ratio of 0.015 are equivalent to a change in ZDR for the raindrops of 0.2dB, which is still larger than the estimated error of 0.1dB in the ZDR measurement made by the Chilbolton radar. The inferences made from the radar observations provide only indirect evidence. In the heavy rain the large drops contribute a large component to the total Z observed, and because the larger drops are the most oblate, the ZDR measurement is even more heavily influenced by the largest drops present in the spectra.

2.3 Analytic Forms of the Raindrop Spectrum

We have few direct observations of the concentration of the largest raindrops. The ground-based disdrometer described by Joss and Waldvogel (1967) is widely used for radar validation experiments, but the largest drop size recorded is 5.3mm; even if the size range was increased, a negligible number of any larger drops would be detected because of the small sample area of the instrument. The data displayed in Figure 1 were obtained for storms within 100km range of the Chilbolton radar, but the

number of such storms which would be above a single immobile ground-based disdrometer would be extremely small. This restriction does not apply to airborne instruments, and Willis (1984) reports raindrop spectra measured inside a hurricane where the rain rate was computed to be 169mm/hr, but unfortunately no data are presented for drops greater than 4mm. This device sampled 2m^3 of cloud every 10secs (1.3km of flight track); in the heaviest rain it sampled about 20 raindrops in the 4 to 5mm size range; extrapolating the exponential distribution indicates that such a device would not obtain a significant sample of 8mm drops. Recently, Beard et al (1986) have reported finding large raindrops within warm shallow clouds over Hawaii. On one occasion the drop diameter reached 8mm and the average concentration of raindrops in the 5 to 6mm range for the observations was about one per cubic meter. It appears that earlier suggestions that collision induced break-up would limit the maximum raindrop size to a few millimeters have been overemphasised.

Although it appears that large raindrops may well be found in heavy rain, and that such large raindrops would affect the values of Z and ZDR, it seems impossible to obtain an independent means of sampling such drops to check any radar inferences. We shall adopt a different approach, and test various forms of the raindrop size distribution to see which agrees most closely with the radar data. To compute the curves in figure 1, we assumed a D_{max} of 8mm, a constant N_0 of $8000 \text{ m}^{-3} \text{ mm}^{-1}$, and allowed D_0 to vary. We shall also explore the effect of fitting the data to a gamma distribution (Ulbrich and Atlas, 1984):

$$N(D) = N_0 D^m \exp(-(3.67+m)D/D_0) \quad (3)$$

The fourth variable, m , reflects the breadth of the size distribution.

Let us first consider the effect of truncating the exponential distribution. Joss and Waldvogel (1969) used a maximum value of 6mm but, in view of the above discussion, larger values such as the 9mm used in the ZDR calculations of Goddard and Cherry (1984) should be more realistic. In Figure 3 values of Z and ZDR are plotted for maximum drop sizes of 8, 9, and 10mm, with the value of N_0 kept at $8000 \text{ m}^{-3} \text{ mm}^{-1}$ throughout. The agreement of the predictions using the 10mm diameter cut-off with the average radar data is remarkable.

Figure 3 also explores the effect of the value of m in the gamma function. When $m = 0$ the gamma function reduces to the simple exponential, but some measurements indicate that natural raindrop spectra contain rather fewer of both the very large drops and the very small drops than would be the case for an exponential, and that a value of $m = 2$ is more appropriate (Ulbrich, 1983). Again N_0 is kept constant at $8000 \text{ m}^{-3} \text{ mm}^{-1}$, and the values for $D_{\text{max}} = 8$ and 10mm with $m=2$ are also plotted in Figure 3. The agreement with observation is less good; the lower predicted values of ZDR at high rain rates reflect the lower concentrations of the large raindrops in the narrower spectrum.

If four variables are used in the raindrop spectrum then, for only two observables, an infinite combination of values is possible. There is no reason, per se, to believe that the analytic form of the raindrop distribution should be the same for all rain rates, for example, N_0 can be adjusted to give the required value of Z for any value of ZDR. In the absence of any other radar observable parameters, the most sensible choice seems to be a pure exponential with a variable D_0 , but keeping N_0 at $8000 \text{ m}^{-3} \text{ mm}^{-1}$ and $D_{\text{max}} = 8$ or 10mm.

So far the values of ZDR have been computed for raindrops

at 0°C. The values for the larger drops are temperature dependent; for example, using the full MieGans theory an 8mm drop with axial ratio of 0.521 has a ZDR of 6.70dB at 0°C (Table 1) but 5.94dB at 10°. However, the change in ZDR is not a simple function of temperature. Computations are being carried out at +10°C and 10°C; this lower figure should be of interest when interpreting transient narrow columns of positive ZDR which extend up to 2km above the freezing level in vigorous convection. We have argued (Illingworth et al, 1987) that these are due to supercooled raindrops. These effects of temperature at S band (10cm) should be small, but could be more serious at C band (5.6cm). Computations at 5.636 GHz (A Holt, personal communication) show that, for the axial ratios in Table 1, a 7mm drop would have a ZDR of 5.87dB and 5.33dB at 0°C and 10°C, respectively; for an 8mm drop the values are 6.15dB and 5.42dB. Ambiguities will arise because at 10° ZDR is changing so slowly with drop size; the 8mm drop has a ZDR at 10°C considerably lower than the 7mm drop at 0°C.

3. Variability of Natural Raindrop Spectra.

In the previous section we concentrated upon obtaining average values of ZDR for a given magnitude of Z. Particular observations of Z and ZDR do not, of course, lie on this average curve; it is this fact which enables ZDR to be used as independent observable. The curve in Figure 1 for the Beard and Chuang drop shapes represents the best available estimate of the values of Z and ZDR for a value of $N_0 = 8000 \text{ m}^{-3} \text{ mm}^{-1}$ in the exponential raindrop size spectra of equation (1). For any particular observation of Z and ZDR, the value of D_0 can be derived from ZDR, and N_0 found from Figure 1, using the fact that Z scales linearly with N_0 .

Histograms of the frequency of occurrence of different values of ZDR for each interval of 2dBZ in Z are plotted in Figure 4. The mean values of ZDR of each histogram are those plotted in Figure 1. The width of the histograms can be used to estimate the variability of naturally occurring raindrop spectra. Histograms for values of Z less than 30dBZ are not presented because the resolution of ZDR obtainable by the radar is insufficient; histograms for Z above 60dBZ are not shown because the sample sizes are too small. An asymmetry of the distributions in Figure 4 is evident, with a long tail showing that values of ZDR many times the mean occasionally occur. This implies that values of N_0 are generally close to $8000 \text{ m}^{-3} \text{ mm}^1$, but that on occasion much lower values occur. The isolated first echoes analysed in Part A are not included in the 'average' data. The unusual characteristics of these first echoes may be re-emphasised with reference to Figure 4. In these isolated clouds Z values of 30 and 40dBZ were accompanied by ZDR values of 3 and 4dB, respectively; the statistical analysis presented in Figure 4 shows that for these two values of Z, 98% of the data in the sample were accompanied by ZDRs of a lower magnitude.

In view of the skewness of the ZDR histograms in Figure 4, the histograms were re-computed for $\text{Log}(ZDR)$. The results are displayed in Figure 5 and a greater symmetry of the distributions is apparent. This is confirmed by Table 2 which provides the values of standard deviations, skewness and kurtosis for the histograms in Figures 4 and 5. The skewness (defined as the ratio of the third moment to the cube of the standard deviation) of the $\text{log}(ZDR)$ distributions is about ten times less than that for the linear ZDR histograms for the range of Z from 30 to 50dBZ; above 50dBZ the difference is less clear, but this may be

affected by the smallness of the sample size. The kurtosis (the ratio of the fourth moment to the fourth power of the standard deviation) should be 3 for a normal distribution; higher values arise if the wings of the distribution are wider than for a normal distribution. Again, the value of kurtosis for the log (ZDR) histograms in the Z range 30-50dbZ are close to 3, whereas the linear ZDR histograms have much greater values. Kurtosis values for Z above 60dbZ are not meaningful because of the small sample size.

The statistics in Table 2 of the variability of spectra may be of use in interpreting conventional radar data, and for statistical studies of problems related to electromagnetic propagation in the lower troposphere.

5. DISCUSSION AND CONCLUSIONS

The precise shape of raindrops which should be used for the interpretation of ZDR measurements has been a matter of considerable debate. The results reported in this paper are compatible with the new, more accurate, shapes proposed by Beard and Chuang (1987). In the absence of any third observable reflecting the value of m in the gamma distribution, the most reasonable spectrum for interpreting the Z and ZDR observations is the exponential of equation (1) with a $D_{\max} = 8\text{mm}$. In heavy rain with Z values above 50dbZ there is an indication that a $D_{\max} = 10\text{mm}$ could be used.

Figure 6 compares the values of rain rate (R) as a function of ZDR using the original shapes of Pruppacher and Pitter and the new shapes of Beard and Chuang for an exponential size distribution. For a given ZDR the values of R scale linearly with Z. On the Figure curves for 10 and 100 mm/hr are plotted.

The new drop shapes lead to slightly lower rainfall rates for a given Z/ZDR combination; for example, for a ZDR of 3 and 3.7 dB the reductions are 26% and 44% respectively. The effect of using a D_{\max} of 10mm is marked with the dashed line and this uncertainty over choice of truncation limit only becomes significant for ZDR above 3dB, at 4db the reduction in deduced rain rate is about 25%.

In Part A we argued that values of ZDR of 6dB were compatible with a monodispersed distribution of large raindrops, and this interpretation is compatible with the shapes discussed in this paper. From a radar analysis, Caylor and Illingworth (1986) hypothesised that large raindrops must be more oblate; the more oblate shapes have now been confirmed independently, and gave more consistent agreement with the radar data. However, the extreme oblateness of the very large drops proposed by Caylor and Illingworth (1988) are too exaggerated, and those of Beard and Chuang (1987) should be used.

Rasmussen et al (1985) report laboratory experiments of drop shapes in the presence of a horizontal electric field. Appreciable changes in axial ratio occurred only for field above 200 kV m^{-1} and drops above 4mm; the measurements did not encompass drops larger than 5mm or fields other than the horizontal. It is generally believed that the field required to trigger lightning in the atmosphere is about 300 kV/m; regions where the field exceeds 200 kV/m are likely to be localised in both time and space, and are also more likely to occur where the hydrometeors are in the ice phase. The effects of electric fields on ZDR are likely to be small. However, if the lightning does occur in a region with large raindrops and high ZDR, a localised sudden change in ZDR might occur. Such a step change in ZDR might be

detected if the radar was not scanning, but was dwelling on the lower regions of an active storm. In view of the changing sensitivity of differently sized large raindrops to field changes, apparent in Rasmussen et al's (1985) results, a quantitative interpretation of any such ZDR jumps will probably not be possible.

In Part E of the report we discuss first results of a new polarisation parameter which may provide information on the parameter, m , in the gamma function which reflects the breadth of the raindrops size distribution. This additional variable promises to increase further the accuracy of rainfall estimates from polarisation radars.

REFERENCES

- Beard K V, (1976) Terminal velocity and shape of cloud and precipitation drops aloft. J Atmos Sci, 34, 851-864
- Beard K V and Chuang D (1987) A new model for the equilibrium shape of raindrops. J Atmos Sci, 44, 1509-1524.
- Beard D V, Johnson D B and Baumgardner D (1986) Aircraft observations of large raindrops in warm, shallow, convective clouds. Geophys. Res. Letters, 13, 991-994
- Caylor I J and Illingworth A J (1986) Observations of the growth and evolution of raindrops using dual-polarization radar. Preprints 22nd Conf Radar Meteor, Amer Meteor Soc, 88-91
- Chandrasekar V, Cooper W A and Bringi V N (1987) Axis ratios and oscillations of raindrops. Submitted to J Atmos Sci.
- Cherry S M and Goddard J W F (1982) Design features of dual polarisation radar. URSI Open Symposium on Multiple Parameter Radar Measurements of Precipitation, Bournemouth, UK, 23-27 Aug.
- Cooper W A, Bringi V N, Chandrasekar V, and Seliga T A (1983) Analysis of raindrop parameters using a 2D precipitation probe with application to differential reflectivity. Preprints 21st Conf Radar Meteorology, Amer Meteor. Soc., 448-493
- Doviak R J and Zrnic D S (1984) Doppler Radar and Weather Observation, Academic Press, Orlando, Florida.
- Goddard J W F and Cherry S M (1984) The ability of dual polarisation radar (coplanar linear) to predict rainfall rate and microwave attenuation. Rad Sci, 19, 201-208
- Goddard J W F, Cherry S M and Bringi V N (1983) Comparisons of dual-polarization radar measurements of rain with ground-based distrometer measurements. J Appl Met, 21, 252-256
- Green A W (1975) An approximation for the shape of large raindrops. J Appl Met, 14, 1578-1583.
- Hall M P M, Goddard J W F, and Cherry S M (1984) Identification of hydrometeors and other targets by dual-polarisation radar. Radio Sci, 19, 132-140
- Illingworth A J, Goddard J W F and Cherry S M (1986) Detection of hail by dual-polarization radar. Nature, 320, 431-433.
- Illingworth A J, Goddard J W F and Cherry S M (1987) Polarization radar studies of precipitation development in convective storms. Q J Roy Meteorol Soc, 113, 469-489.
- Joss J and Waldvogel A (1967) Ein Spektograph für Niederschlagstropfen mit automatischer Auswertung. A raindrop spectrometer with automatic readout. Pure Appl Geophys, 68, 240-246.
- Joss J and Waldvogel (1969) Raindrop Size Distribution and Sampling Size Errors. J Atmos Sci 26, 566-569

Marshall J S and Palmer W M K (1948) The distribution of raindrops with size. J Meteorol, 6,243-248.

Pruppacher H R and Beard K V (1970) A wind tunnel investigation of the internal circulation and shape of water drops falling at terminal velocity in air. Q J Roy Meteorol. Soc, 96,247-256

Pruppacher H R and Pitter R L (1971) A semi-empirical determination of the shape of cloud and rain drops. J Atmos Sci, 28, 86-94

Rasmussen R M, Levizzani V and Pruppacher H (1984) A wind tunnel and theoretical study of the melting behaviour of atmospheric ice particles: III Experiment and theory for spherical ice particles of radius above 500um. J Atmos Sci, 41,301-388.

Rasmussen R, Walcek C, Pruppacher H R, Mitra S K, Lew J, Levizzani, Wang P K and Barth (1985) A wind tunnel investigation of the effect of an external electric field on the shape of electrically uncharged rain drops. J Atmos Sci, 42, 1647-1652

Seliga T A and Bringi V N (1976) Potential use of radar differential reflectivity measurements at orthogonal polarizations for measuring precipitation. J Appl Met, 15, 69-76

Ulbrich C W (1983) Natural variations in the analytical form of the raindrop size distribution. J.Clim and Appl.Met,22,1764-1775.

Ulbrich C W and Atlas D (1984) Assessment of the contribution of differential polarization to improved rainfall measurements. Rad Sci, 19, 49-57

Willis P T (1984) Functional fits to some observed drop size distributions and parameterization of rain. J Atmos Sci, 41, 1648-1661.

Wilson J W and Brandes E A (1979) Radar measurements of rainfall - a summary. Bull Am Met Soc, 60,1048-1058

TABLE 1

Size	P-P shapes Axial Ratio	Axial Ratio	B and C Shapes ZDR(dB) (Raleigh Gans)	ZDR(dB) (Mie Gans)
4	0.762	0.778	2.49	
5	0.701	0.708	3.41	3.48
6	0.655	0.642	4.35	4.42
7	0.621	0.581	5.31	5.33
8	0.583	0.521	6.34	6.70
9	-	0.46	7.49	10.87
10	-	0.4	8.78	16.34

Values of axial ratio and ZDR for various sizes of raindrop. The Mie-Gans calculations are supplied by Dr Holt, Department of Mathematics, University of Essex, and apply to raindrops at 0°C and 3.0765 GHz. P-P shapes refer to Pruppacher and Pitter (1971), B and C to Beard and Chuang (1987).

TABLE 2

Z (dBZ)	\overline{ZDR} (dB)	LINEAR			$\overline{\log}$ ZDR	LOG		
		σ	Skew- ness	Kurto- sis		σ	Skew- ness	Kurto- sis
30-31	0.86	0.70	2.15	10.5	-0.17	0.31	-0.05	2.99
32-34	0.96	0.70	2.15	8.07	-0.11	0.30	-0.14	2.93
34-35	1.06	0.75	1.70	6.77	-0.07	0.29	-0.04	2.78
36-37	1.17	0.71	1.60	6.39	0.00	0.25	+0.06	2.84
38-39	1.31	0.72	1.50	5.80	0.06	0.22	+0.13	2.90
41-42	1.48	0.74	1.42	5.16	0.12	0.20	+0.25	2.68
43-44	1.65	0.75	1.35	4.87	0.18	0.18	+0.27	2.95
45-46	1.79	0.73	1.26	4.81	0.22	0.16	+0.27	3.20
47-48	2.01	0.75	0.98	3.80	0.27	0.16	+0.15	2.28
49-50	2.23	0.74	0.83	3.52	0.33	0.14	+0.07	2.60
51-52	2.48	0.76	0.86	3.59	0.37	0.13	0.09	2.45
53-54	2.81	0.83	0.92	4.10	0.43	0.12	0.17	2.89
55-56	3.10	0.87	0.70	3.33	0.47	0.12	0.06	2.41
57-58	3.45	0.92	0.23	2.34	0.52	0.12	-0.28	2.41
59-60	3.73	0.96	0.11	2.46	0.56	0.11	-0.41	2.41
61-62	3.88	0.91	-0.07	-	0.58	0.11	-0.52	-
63-64	4.41	0.67	-0.44	-	0.64	0.07	-0.58	-

The average values of differential reflectivity for each 2dBZ step in Z observed in heavy rain by the Chilbolton radar. The left-hand half of the table displays the mean, standard deviations (σ), skewness and kurtosis of the distributions of ZDR - see Figure 4 for the equivalent histograms. The right-hand side shows the equivalent parameters for $\log (ZDR)$ - see Figure 5 for the histograms.

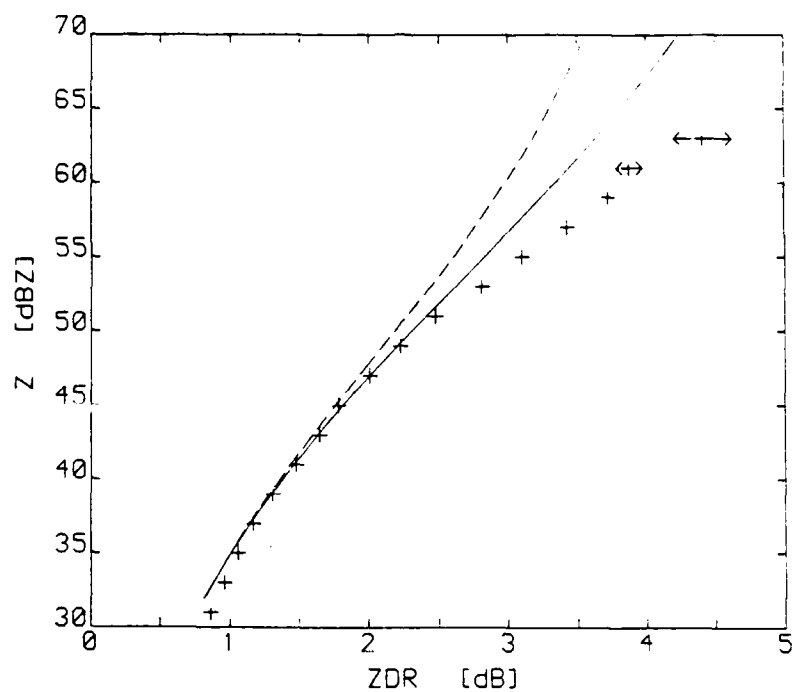


Figure 1. The variation of Z with ZDR for an exponential drop size distribution using two drop shape models. The solid line is the Beard and Chuang drop shapes and the dashed line is the Pruppacher and Pitter shapes. In both cases $D_m = 8\text{mm}$ and $N_0 = 8000\text{m}^{-3}\text{mm}^{-1}$. The crosses are averaged Chilbolton radar data collected from summer convective clouds.

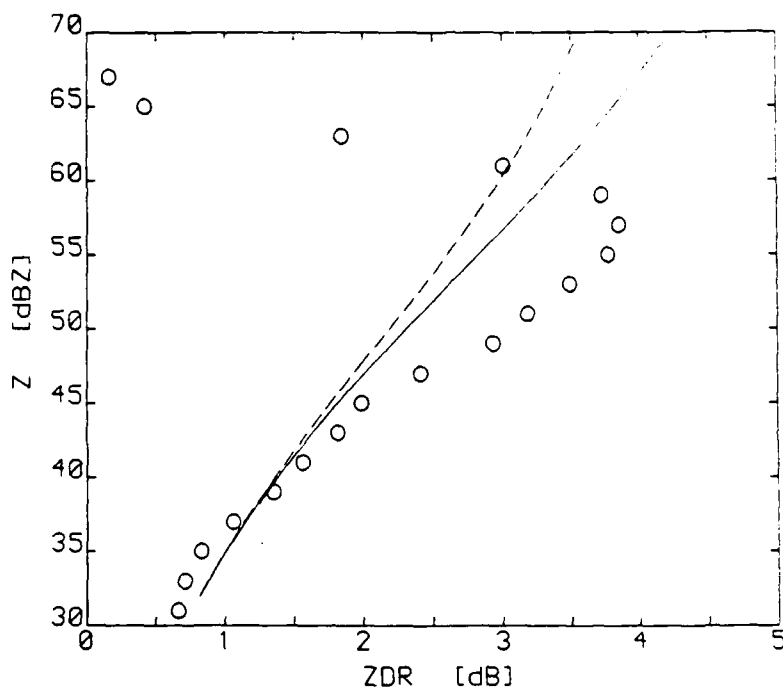


Figure 2. An example of the effect due to hail showing the significant decrease in ZDR at high Z values. The circles are averaged Chilbolton data from a storm on 6 July 1983 where a hail shaft was identified. The two lines are theoretical Z-ZDR relationships and are identical to those in Figure 1.

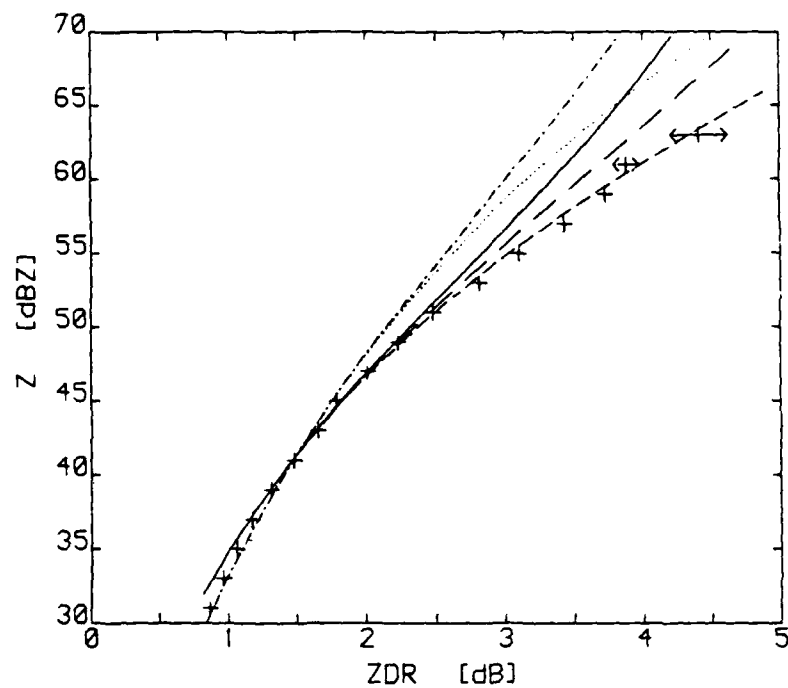


Figure 3. The relationship of Z with ZDR for variations in the parameters of the gamma drop size distribution. The solid line is $m = 0$, $D_m = 8\text{mm}$; the long dashed line is $m = 0$, $D_m = 9\text{mm}$; the short dashed line is $m = 0$, $D_m = 10\text{mm}$. The dotted line is $m = 2$, $D_m = 8\text{mm}$ and the dash-dot line is $m = 2$, $D_m = 10\text{mm}$. The Beard and Chuang drop shapes were used and $N_0 = 8000\text{m}^{-3}\text{mm}^{-1}$. The crosses are averaged Chilbolton data as in Figure 1.

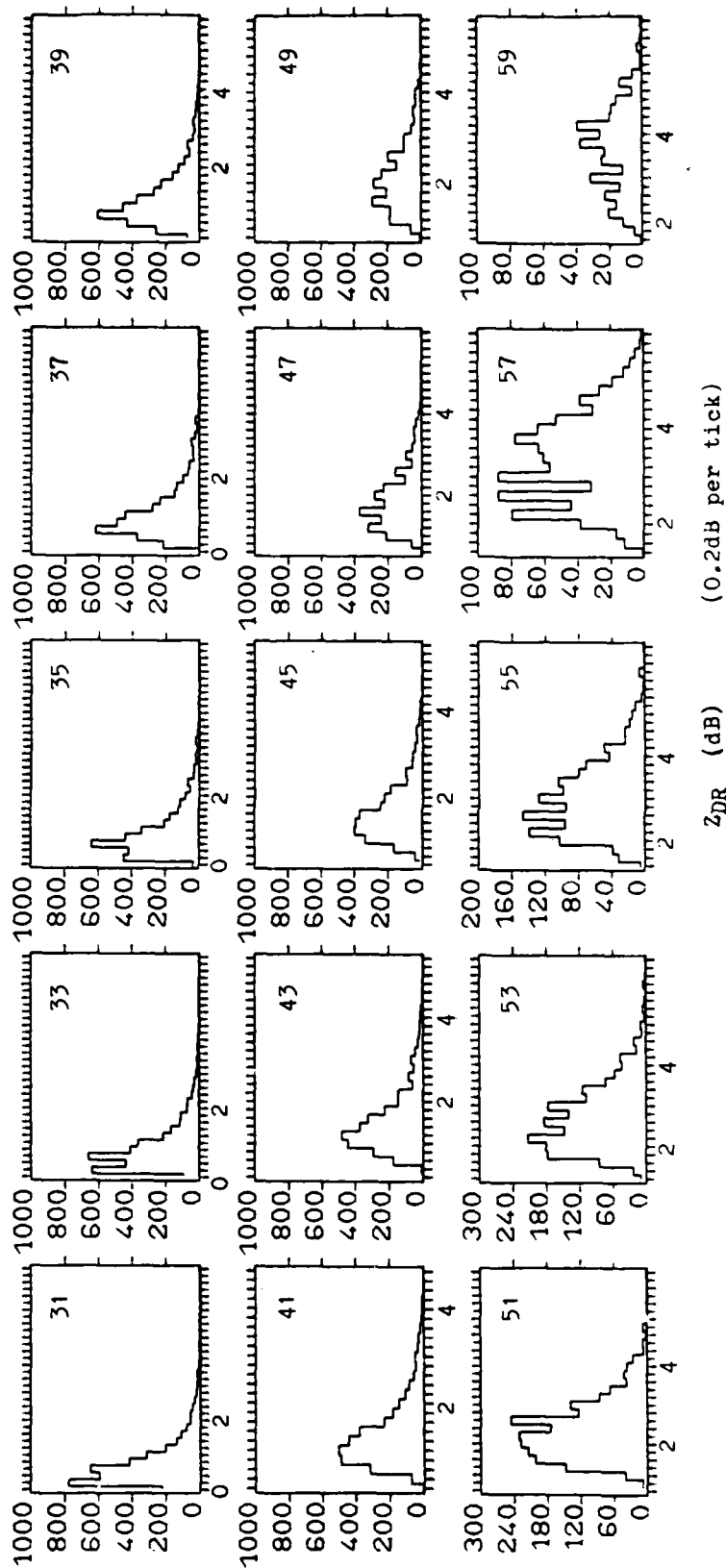


Figure 4. Histograms of the number of ZDR values associated with 2dB intervals in Z. The data were observed for summer convective clouds in 1983 and 1984. The number in the corner of each histogram indicates the center of the particular Z interval in units of dB.

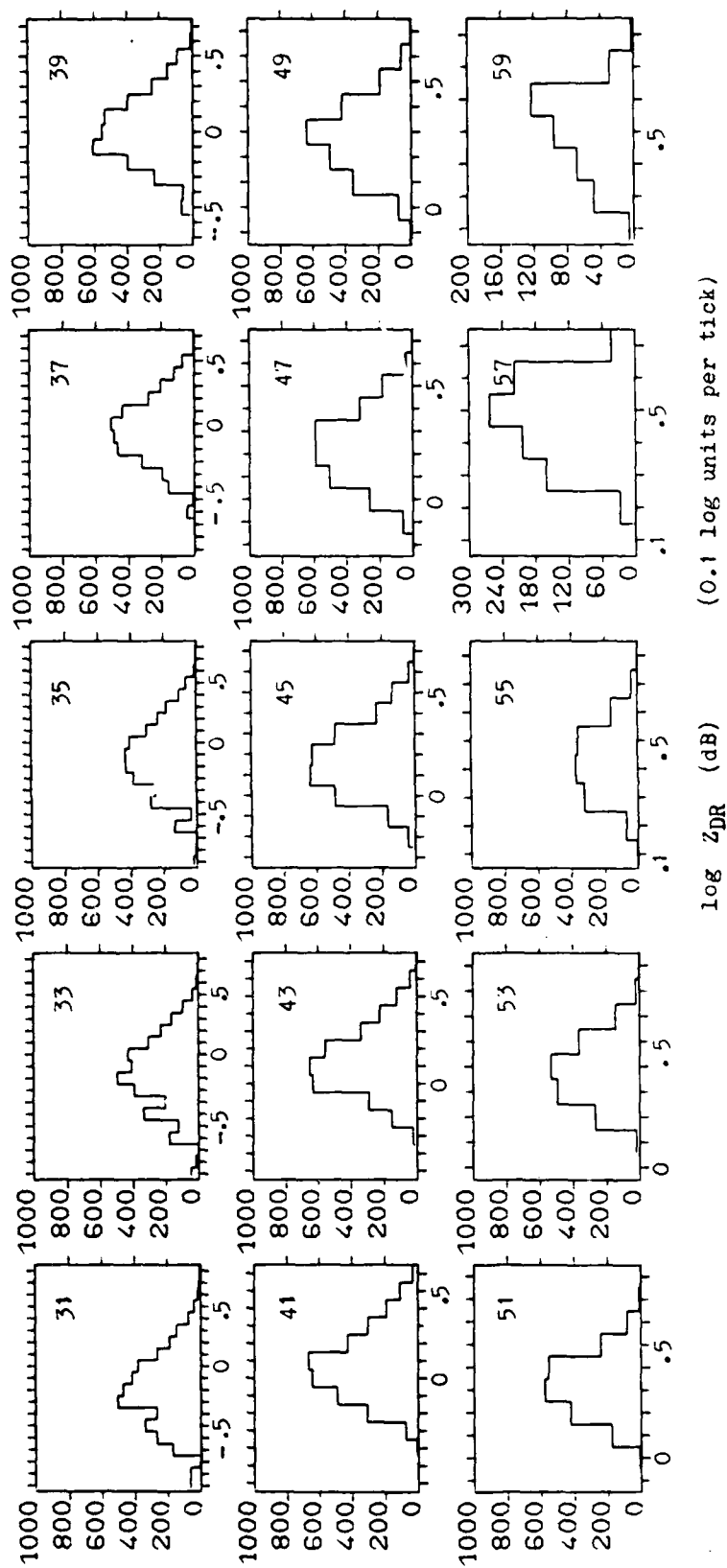


Figure 5. The histograms of Figure 4 replotted with logarithmic spaced ZDR bins.

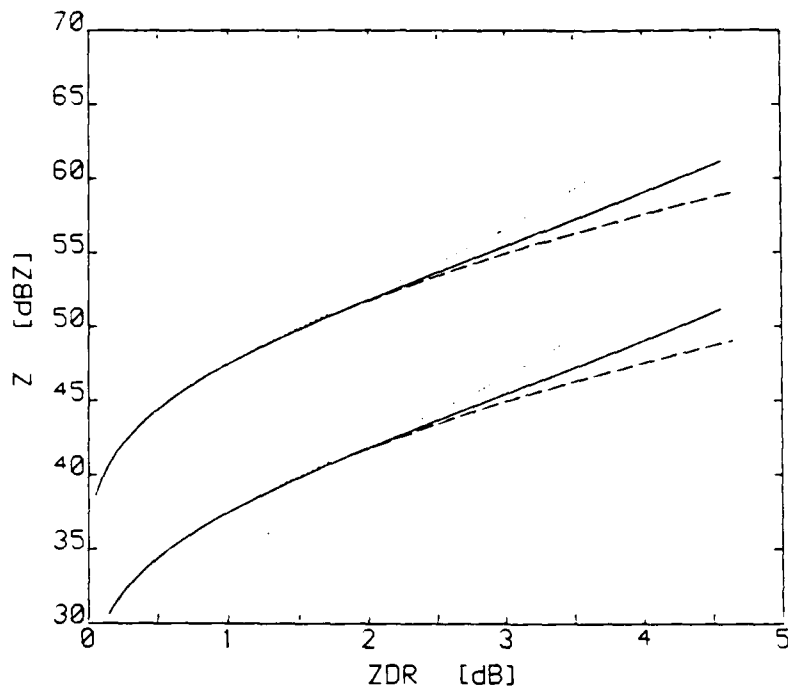


Figure 6. The variation of Z with ZDR expected for constant rainfall rates. The lower set of curves is for a rainfall rate of 10mm/hr and the upper set is for a rate of 100mm/hr. The solid line is the Beard and Chuang drop shapes and an exponential drop size distribution with $D_m = 8$ mm while the dashed line is for $D_m = 10$ mm. The dotted line shows the rainfall expected with the Pruppacher and Pitter shapes for an exponential distribution with $D_m = 8$ mm. $N_0 = 8000\text{m}^{-3}\text{mm}^{-1}$ in all cases.

PART D

ZDR ARTEFACTS DUE TO TRIPLE SCATTERING

Wilson and Reum (1988) describe a radar artefact which they have called a "flare echo". This spike or flare shaped echo typically has reflectivities of less than 20dBZ which extend downrange of some intense radar storm echoes. The mechanism causing this artefact can be explained with reference to Figure 1 from Wilson and Reum's paper. The flare is caused by scattering of the radar beam by the hydrometeors to ground, backscattering by the ground to the hydrometeors, and finally by the hydrometeors back to the radar. If the hydrometeors are a distance h above the ground, then the flare echo caused by the triple scattering is found a distance h behind the storm on the same radial. Wilson and Reum analysed the Doppler signature of these flares but did not consider any polarisation effects.

Figure 2 shows an RHI observed with the Chilbolton radar with a very obvious occurrence of hail at a range of 87 km where zero values of ZDR reach the ground. One puzzling feature is evident in this RHI: the column of positive ZDR inclined at 45° to the vertical extending from the ground at 88 km range to an altitude of 4 km at range of 91 km; values of ZDR in this column reach + 9dB and Z is less than 20dBZ.

These values of + 9dB for ZDR are the only data points gathered in clouds with the Chilbolton radar which are inexplicable in terms of known properties of hydrometeors and had been a cause for some concern. It is extremely reassuring to find that such ZDR values can be analysed in terms of the triple scattering model. When measuring ZV, the dipoles induced in the precipitation particles in the cloud have their axes in the vertical direction. A Rayleigh dipole does not radiate along its axis and so for ZV negligible power is reradiated to the ground. However, for ZH the induced dipole axis is horizontal and the triple

scattering mechanism will operate as shown in Figure 1. We conclude that the flare echo occurs only for ZH and will be absent in ZV, thus leading to positive ZDR artefacts.

Following the identification of the ZDR flare artefact in Figure 2 we have examined some data taken with the CP2 radar during the Maypole experiment in 1984 (supplied courtesy of P Herzegh, NCAR). On 13 June, 1984, the radar observed a severe damaging hailstorm over the Denver area and several of these positive ZDR artefacts have been identified behind the major Z echo. An example is given in Figure 3 where, at a range of 31 km and 6 km altitude the ZDR reaches + 12 dB. Such a magnitude cannot be due to precipitation and is clearly due to triple scattering from the high Z region at 26 km range and 5 km altitude. (Note that the ZDR hatching scale wraps around for ZDR above 5.5dB.)

The magnitude of ZDR resulting from the triple scattering depends on the background ZH and ZV in that region. For example, a ZDR of + 10 dB could be caused by a ZH of 20dBZ and a ZV of 10dBZ, with, in the absence of triple scattering ZH and ZV being both 10dBZ (ie. $ZDR = 0$). If the background level of ZH and ZV had been 30dBZ, then the triple scattering power would have been negligible in comparison, and no ZDR artefact would occur. Our experience with CP2 and the Chilbolton radar is that an echo of $Z = 60\text{dBZ}$, will give a flare echo having ZH of + 20dBZ, and so positive ZDR artefacts will only occur if the pre-existing ZH and ZV are equal to or less than 20dBZ.

The artefacts in Figures 2 and 3 are very obvious; more worrying would be regions on the far side of storms at altitudes of 2-3 km where ZDR is + 2 or 3 db, which could easily be mistaken for precipitation signatures. We are currently developing

a quantitative treatment to enable a precise analysis of such cases to be carried out.

Zrnic (1987) has shown that the triple scattered power is proportional to Z^2/λ^4 . Consequently, for the same geometry of echo as in Figures 2 and 3, but maximum echoes of $Z = 50\text{dBZ}$ instead of 60dBZ , the triple scattered power will be reduced from $ZH = 20\text{dBZ}$ to 0dBZ , and the artefacts should not cause a problem. Difficulties may arise at C-band, however; because of the wavelength dependence, the triple scattered power from the main echoes in Figures 2 and 3 will be increased by a factor of 16. As a consequence, the ZDR artefacts would be more extensive at 5.6cm and occur where values of the background Z are up to 30dBZ , instead of 20dBZ for the 10cm radar. At 10cm significant triple scattering artefacts only occur when Z exceeds 60dBZ in the main echo; at C-band significant artefacts are to be expected when Z is greater than 50dBZ ; echoes of 50dBZ are much more common and widespread than those of 60dBZ .

We plan to use this 10cm flare data to model the artefacts which would be produced at this shorter wavelength.

REFERENCES

- Wilson, J.W. and Reum, D. (1988) "The flare echo": Reflectivity and velocity signature. J. Ocean & Atmos. Tech. (to be published).
- Zrnic, D.S. (1987) Three-body scattering produces precipitation signatures of special diagnostic value. Rad. Sci. 22, 76-86.

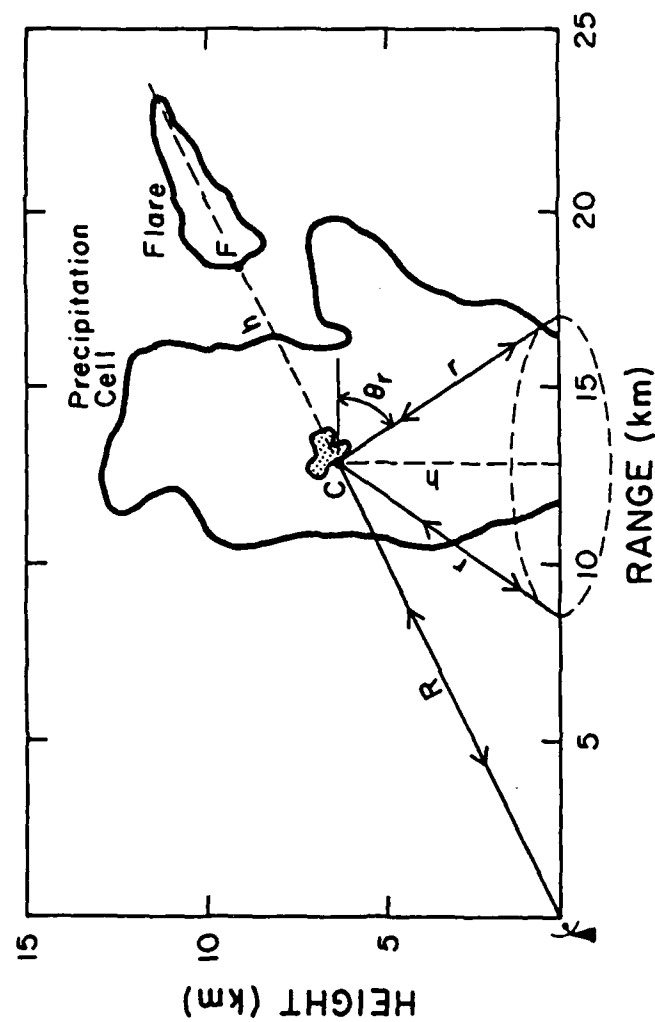


Figure 1 Schematic of the proposed radar signal path responsible for the flare echo. The precipitation cell and flare are as observed by CP-4 on 20 July 1986 near Huntsville, Alabama. The dark shading near point C represents the 60 dBZ_c core responsible for producing the flare echo. See text for further description.

(From Wilson and Reum, 1988)

RHI SCAN ON 06/07/83 AT 1336 UT
 TAPE 315 RASTER 3 SCAN 4 AZ = 66.0 deg

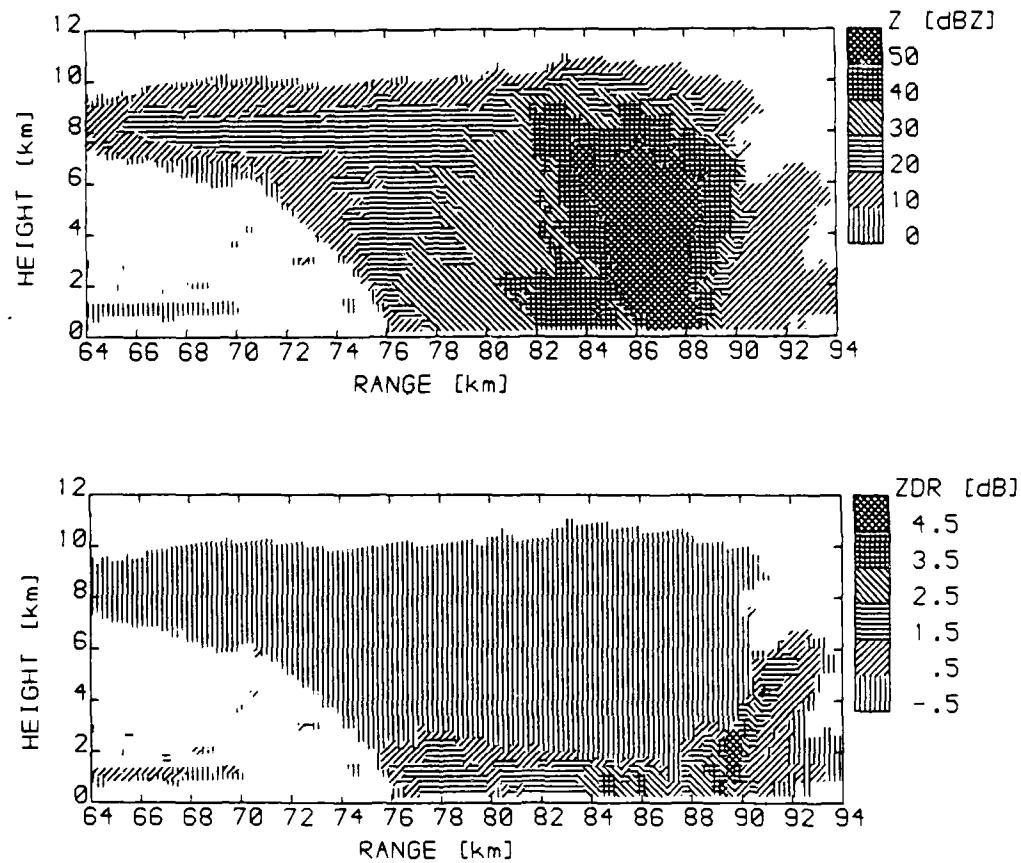


Figure 2. A vertical section of a cloud observed on 6 July 1983 at 1336 UT. A hail shaft is visible near the ground in ZDR at a range of 87km. The flare echo in ZDR extends upward from a range of about 88km.

RHI SCAN ON 13/06/84 AT 1719 MD
TAPE 573 RASTER 5 SCAN 2 AZ = 162.0 deg

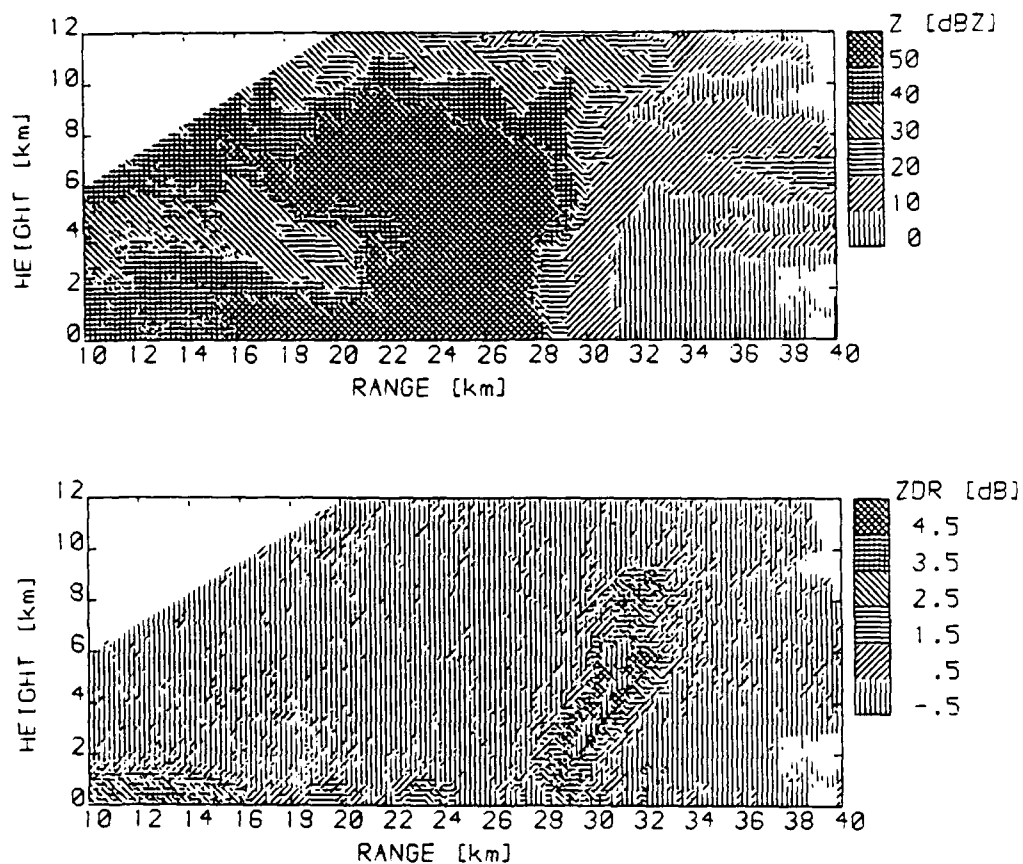


Figure 3. A vertical section of an intense convective cloud recorded by the NCAR CP-2 radar on 13 June 1984 at 1719 MD. The flare echo in ZDR extends upward beginning at a range of 28km. The negative ZDR in the center of the flare echo is due to wrap around of the positive ZDR scale.

PART E

RADAR MEASUREMENTS OF THE BREADTH OF THE SIZE DISTRIBUTION
OF PRECIPITATION PARTICLES

1. INTRODUCTION

In this note we summarise some first results of the time series radar data obtained at one range gate using radar pulses alternately polarised in the horizontal and vertical directions. We shall concentrate on the cross correlation of the time series data of ZH and ZV (the radar reflectivities measured with horizontal and vertical polarisations, respectively), which we shall call $p(H,V)$. If it is unity then all the precipitation particles are the same shape, whereas if a distribution of shapes is present the correlation falls. The shape of a drop is a unique function of its size, so if all the raindrops are the same size then $p(H,V) = 1$, as the size distribution of raindrops becomes broader $p(H,V)$ should fall.

In Section 2 we briefly review some of the properties of the fluctuating radar echo. This arises because the precipitation forms an incoherent target. We then outline how the correlation between the fluctuations in ZH and ZV should be related to the particle size spectrum. The data acquisition system for recording this time series data and the signal conditioning algorithms are described in Section 3. Some first results gathered during December 1987 are presented in Section 4. We shall show some examples of time series data from drizzle with a $p(H,V)$ of 0.99 and from the melting layer where $p(H,V)$ is only 0.43. Implications of these results and plans for further analysis and observations are discussed in Section 5.

A detailed technical description of the Chilbolton radar is to be found in Cherry and Goddard (1982). A discussion of the statistics of ZH and ZV is given by Bringi et al (1983).

2. THE CORRELATION OF ZH AND ZV: $p(H,V)$.

Precipitation particles form an incoherent target, the backscattered signal from an ensemble of precipitation particles fluctuates with a standard deviation equal to the mean value. This arises because the precipitation particles are continually moving relative to one another in space, and so the signal from each particle arrives at the antenna with a randomly changing phase. The resultant amplitude at the antenna from many particles obeys the same statistics as the drunken man's walk. Figure 1A shows the value of ZH recorded at one particular 75m range gate for each of 64 successive pulses transmitted with the same polarisation during a 210msec period of time. The straight line is the linear average of the 64 ZH samples leading to an estimate of ZH of $300 \text{ mm}^6 \text{ m}^{-3}$ or 25dBZ. The fluctuation in the sampled values of ZH as the particles reshuffle in space is clearly visible in the Figure. In this case successive transmitted pulses do not give independent estimates of ZH, and the decorrelation time is several times the pulse period. The decorrelation time of the signal is related to the width of the Doppler spectrum.

We are concerned with a new measurement which involves comparison of the fluctuations of the radar estimates of ZH and ZV obtained using transmitted pulses alternately polarised in the vertical and the horizontal. These alternate samples are displayed in Figure 1A for ZH, and Figure 1B for ZV for the same 75 meter gate during the same 210msec sample period. The average value of ZV for the 64 pulses is $305 \text{ mm}^6 \text{ m}^{-3}$, leading to an estimate of ZDR for this gate of -0.06dB. (Note that the absolute calibration of the radar is still being carried out and that both ZH and ZV may have an absolute error of several dBZ, but that the

relative errors are far less than this). The new information is obtained by examining the fluctuations in ZH and ZV, rather than merely calculating their average values obtained from the 64 pulse pairs during the 210msecs.

The principle of the method can be described with reference to Figure 2. For horizontally polarised radiation let us call the amplitude scattered by a single particle a_h , and the amplitude for vertically polarised radiation a_v . In the figure we consider just three particles, and for each radar pulse our estimate of ZH is obtained by squaring AH , the vector sum of the three values of a_h added with random phase; similarly ZV is derived from AV , the vector sum of the three values of a_v . If the ZH and ZV estimates are obtained in a time much shorter than the decorrelation time, then the a_h and a_v amplitudes for the scattered signal for each single particle will arrive with the same phase (Figure 2a). If we now wait for a time longer than the decorrelation time we can obtain two more independent samples of ZH and ZV with a new set of random phases for a_h and a_v (Figure 2b).

Figures 2a and 2b demonstrate the situation where all the particles are the same shape, in other words for each particle the ratio of a_h to a_v is always fixed (here we have chosen a factor of two). Figures 2a and b represent two pairs of ZH and ZV obtained for three particles having the same shape, each pair being an independent sample. For each pair the phases of the amplitudes (a_h and a_v) of each scatterer are the same, so the amplitude of the resultants AH and AV are in the same ratio as the components a_h and a_v . Consequently, ZH and ZV are always in the same ratio, they fluctuate together and the correlation coefficient, $p(H,V)$ is unity.

Figures 2c and 2d represent the more complicated arrangement when the particles have different shapes. In this case the ratio of a_h to a_v for each scatterer is not constant. Figure 2c shows a pair of samples of AH and AV taken in a time short compared to the decorrelation time, so that the a_h and a_v amplitude of each scatterer arrive with the same phase. Figure 2d shows another pulse pair taken after a time delay greater than the decorrelation time, the various values of a_h and a_v now add up with a new set of random phases, but because the ratio of a_h to a_v is not constant, the ratio of the resultants AH and AV is not the same as in Figure 2c. The estimates of ZH and ZV , obtained by squaring AH and AV , are not perfectly correlated and $p(H,V)$ falls.

The statistics that relate $p(H,V)$ to the spectral width of the particle size distribution are not simple. We have adopted the Monte Carlo approach. In this method we calculate the values of ZH and ZV expected from a distribution of precipitation particles by adding up the individual scattered signals arriving with random phase; the procedure is then repeated with a different set of random phases until an estimate of the correlation $p(H,V)$ can be made. This theoretical work is still in progress.

3. DATA ACQUISITION AND SIGNAL CONDITIONING.

The RAL radar system (Cherry and Goddard, 1982) amplifies the return signal using a swept gain to correct for range; this signal is then digitised every 250nsec equivalent to a 37.5m range resolution. Dedicated hardware forms a true linear average of the value of ZH and ZV for each 300m gate for 64 transmitted pulse pairs. Every 210mseconds these values are then recorded on magnetic tape for 512 range gates of 300m length. This degree of

spatial and time averaging yields an accuracy of 0.1dB in ZDR (Bringi et al, 1982).

The UMIST system for recording the time series information samples the digitised return signal every 500nsec. This is equivalent to a gate resolution of 75m - the maximum resolution for the 0.5 microsecond transmitted pulse. An estimate of ZH or ZV is recorded at 64 of these gates for 64 transmitted pulse pairs forming an 8k block of data every 210 mseconds. This data arrives in short bursts and is stored in a dual port ram, which acts as a buffer so that the data can be fed to a tape recorder in the streaming mode. The average data rate is about 40,000 bytes per second, or 100Mbytes an hour. Currently a 3600' tape lasts for 40 minutes of continuous recording.

For processing limited amounts of data the magnetic tapes are played back into an IBM PC AT equivalent with an arithmetic co-processor. Figure 3A shows a raw time series for 64 pulses of ZV at one 75m gate. This series is typical in that it is clear to the eye that one or two of the data points in the time series are affected by some interference or noise problem. Developing an automatic algorithm which can detect these spikes and correct them is quite a challenging task. These noise spikes have a negligible effect on the average values of ZH and ZDR calculated for the 210 msecond sample period at the 75m gate; if they are identified by eye and replaced by a linear interpolated data point the changes in the ZDR value is less than 0.03dB. However the presence of these spikes does lead to appreciable reductions in $p(H,V)$, the correlation of ZH and ZV.

We suspect that these spikes are due to real signals being picked up by the antenna. An extensive study has shown a pattern to the spikes; they tend to occur at a sequence of nearly

consecutive gates for just a few of the transmitted pulses out of the 64 pulses in the series. This is consistent with bursts of noise lasting about 100 mseconds. The strategy developed to correct for these 'flyers', has been to analyse the time series for all 64 gates in the 8k data block so that obvious flyers may be identified; once a transmitted pulse has been found to produce flyers at several gates, the data from all 64 gates for this pulse are removed and replaced by an interpolated datum point at each gate. This procedure is necessary because the noise pulse is itself noisy. This problem can be seen in Figure 3A. At this gate the large spike 110 mseconds into the time series can easily be identified. However, the noise pulse after 25 mseconds is much less obvious, and if time series data at this gate alone were available the small noise signal could not be identified, although its presence does lead to a significant degradation of $p(H,V)$. Figure 3B shows the result of using this algorithm on the noisy data in Figure 3A. This noise removal algorithm is very slow and means of speeding it up are under active study. In the next Section we shall consider correlations obtained at one range gate for a single RHI through the melting layer, this data analysis represents a minute fraction of the data set acquired in the past few weeks.

4. FIRST RESULTS OF $p(H,V)$

We shall now discuss the correlation data obtained at one gate for an RHI through stratiform rain with a distinct melting layer. Figure 4 shows the values of Z and ZDR for the RHI obtained on 16 December 1987 where a melting layer at an altitude of 1.9km is visible in both Z and ZDR . A vertical section of Z , ZDR and $p(H,V)$ at a range of 9.9km is plotted in Figure 5; the

observations are linear averages obtained over four neighboring range gates. The time-series data displayed in other figures are for a single range gate having a sample volume of about 40m by 40m by 75m.

The bright band in Z is quite pronounced in Figure 5, with the maximum value of Z over 15dBZ higher than in the rain below; the Z of dense ice only increases by 7dB when it becomes wet, so this larger change must be caused by very low density ice becoming wet. A reasonable interpretation is that they are snowflakes. The ZDR data shows that the bright band in ZDR is about 200m below that in Z , a common occurrence for higher Z values in stratiform clouds, the melting snowflake apparently reaching its maximum degree of oblateness after it has started to collapse. The value of $p(H,V)$ is close to unity in the ice above the melting layer and in the rain below but falls to 0.4 where ZDR is a maximum; a plausible explanation is that the large oblate half-melted snowflakes are coexisting with smaller fully melted spherical raindrops. ZDR is zero in the rain, implying that all the raindrops are essentially spherical; according to our interpretation, in such a region $p(H,V)$ must be close to one, any values appreciably below unity would be regarded with suspicion. A zero value of ZDR in the ice above the freezing layer can be due to low density ice particles which will scatter as if they were of spherical shape, or to tumbling aspherical particles; in this case the high values of $p(H,V)$ indicate the former.

Figure 1, referred to earlier, where the correlation is 0.99 is taken in the rain at an altitude of 520m; while the time series in Figure 6 shows a correlation of 0.97 in the ice just above the melting layer with a ZDR of 1.35dB. Figure 7 shows the low correlation of 0.43 in the melting layer. An additional

feature is immediately obvious in Figure 7, the ZH time series appears much more noisy than the ZV data. Perusal of other time series data in the bright band confirms this impression. Such an effect needs to be quantified, but consideration of the shapes of the particles in the melting layer suggests that such a feature is quite reasonable; if the melting layer contains oblate half melted snowflakes and spherical raindrops, then the vertical dimensions of the raindrops and the oblate melting snowflakes will be similar, but these two types of particles will have a wider range of horizontal dimensions. Figure 7 suggests that it may be possible to derive a fifth independent parameter from the time series data - the difference in the frequency spectra of the time series for ZH and ZV may be related to the distribution of horizontal and vertical dimensions of the scattering particles. We shall discuss this further in the next section.

5. CONCLUSIONS

The results discussed in Section 4 show that it is possible to derive meaningful values of $p(H,V)$ from the time series data. Much work remains to be done. The identification of the source of noise responsible for the 'flyers' (an example is given in Figure 2) needs to be pursued; if the noise is external to the radar and cannot be removed then we need to find less computationally intensive means of removing the noise spikes.

We have presented data of low correlations in the melting layer. If the method is to be used for providing an estimate of the spectral width of raindrop spectra, we need firstly to demonstrate that the value of $p(H,V)$ falls in heavy rain when ZDR is positive. Secondly, it must be shown that $p(H,V)$ is an independent observable and is not functionally related to ZDR. Because

wintertime rain in the UK tends to be light we have not yet recorded time series data of rain with an appreciable ZDR. The validation of such a technique requires an independent confirmation of the raindrop spectrum. Some time series data have already been gathered over a ground-based disdrometer. During the summer of 1988 it should be possible to record heavier rain over the disdrometer. Cooperative flights with the Met Office C-130 are planned for the summer of 1988 to check radar inferences of particle types. This aircraft is equipped with a 2-D probe which provides a direct measurement of the size and shape of precipitation particles.

In Section 4 we commented that, in the melting layer, the frequency spectra of the fluctuation in the ZH and ZV time series data were different, and that this was consistent with a broad distribution of horizontal dimensions of melting hydrometeors in the melting layer and a more limited range of vertical dimensions. This asymmetry of the noise warrants further examination. Consider the situation of non-spherical particles of hail or graupel which are tumbling as they fall, if the tumbling is random then the distribution of the vertical and horizontal diameters will be similar and the noise spectra of ZH and ZV should be identical. Any differences in the noise spectra should reflect a lack of symmetry in the fall mode. One is tempted to speculate that this fifth parameter might be of use in identifying hail above the freezing level to complement the ZDR method of locating hail when it is close to the ground.

REFERENCES

Bringi V N, Seliga T A and Cherry S M (1983) Statistical properties of the dual-polarization differential reflectivity (ZDR) radar signal. IEEE Trans Geo and Remote Sens, GE-21, 215-220

Cherry S M and Goddard J W F (1982) Design features of dual polarisation radar, URSI, Open Symposium on Multiple Parameter Radar Measurements of Precipitation, Bournemouth UK, 23-27 Aug.

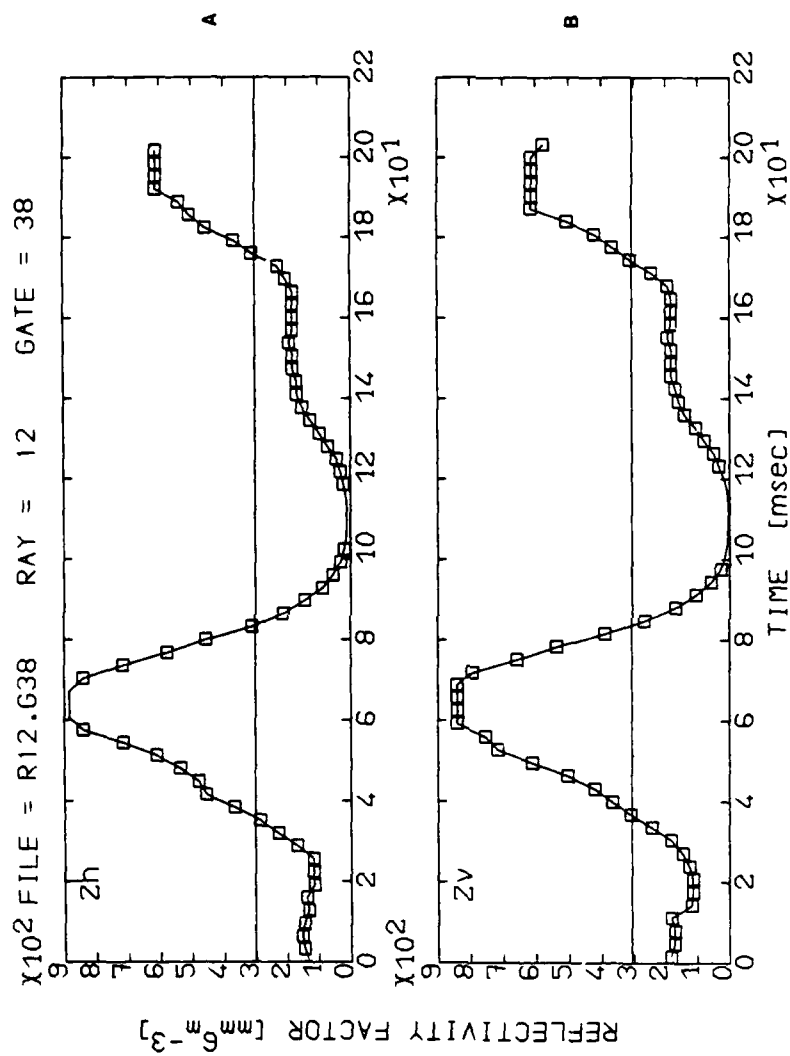
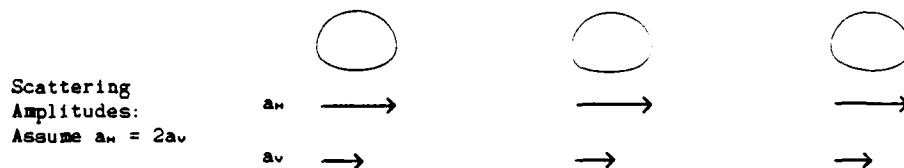


Figure 1. A time series for Z_h and Z_v observed in drizzle at an altitude of 0.52km and a range of 9.9km. The correlation coefficient, $\rho(H,V)$, between Z_h and Z_v is 0.990.

Figure 2. Diagrammatic explanation of the correlation of Z_h and Z_v : ρ_{hv} .

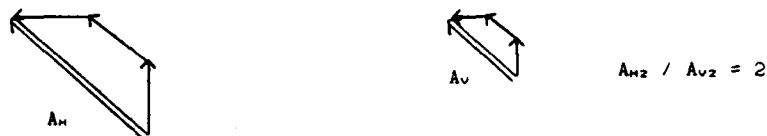
Three Particles of the Same Shape



A) First estimate of A_h and A_v



B) Second estimate of A_h and A_v



$A_{h1}/A_{v1} = A_{h2}/A_{v2}$ for identical shaped particles which implies $\rho_{hv} = 1$

Three Particles of Dissimilar Shape



C) First estimate of A_h and A_v (For convenience use only angles of 0°)



D) Second estimate of A_h and A_v



$A_{h1}/A_{v1} \neq A_{h2}/A_{v2}$ for dissimilar shaped particles which implies $\rho_{hv} < 1$

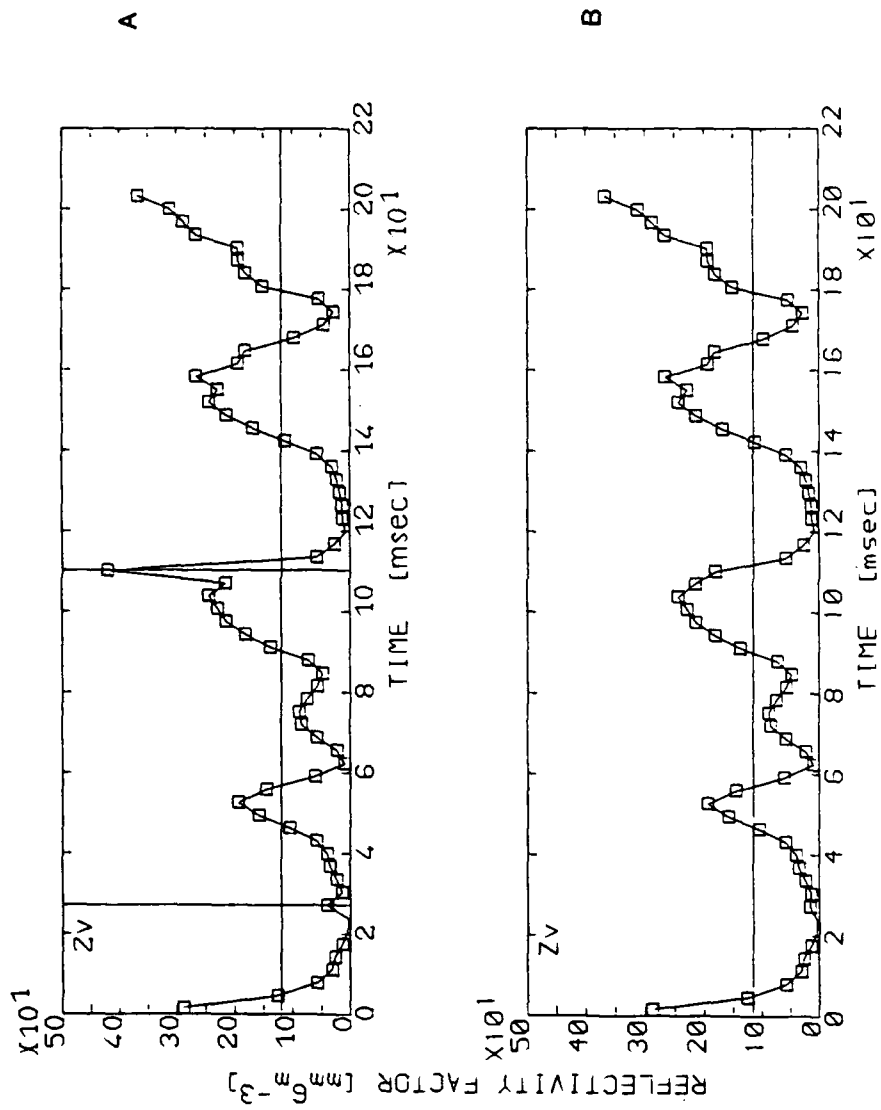


Figure 3. Plot A is an example of a Zv time series showing two fliers marked by vertical lines. Plot B is the same Zv time series after being processed by an automated flyer editing program.

RHI SCAN ON 16/12/87 AT 0645 UT
TAPE 111 RASTER 215 SCAN 1 AZ = 154.0 deg

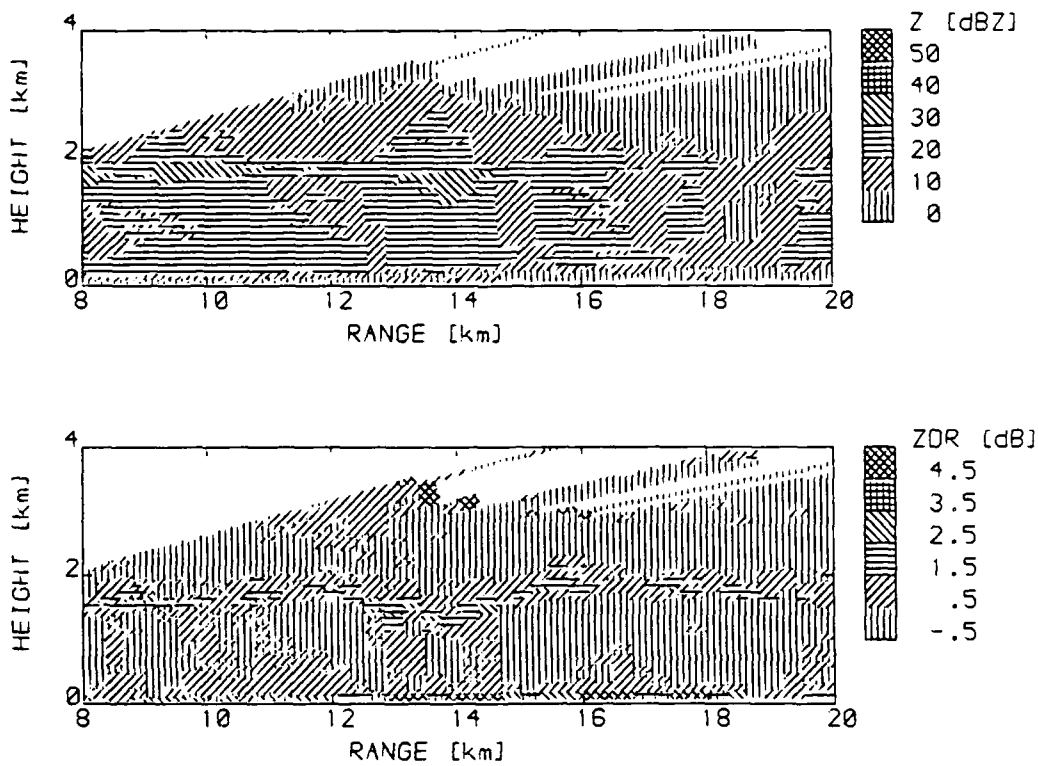


Figure 4. A vertical section on 16 December 1987 at 0645 UT showing stratiform cloud producing light precipitation. A radar bright band is visible, particularly in ZDR, at a height of about 1.9km.

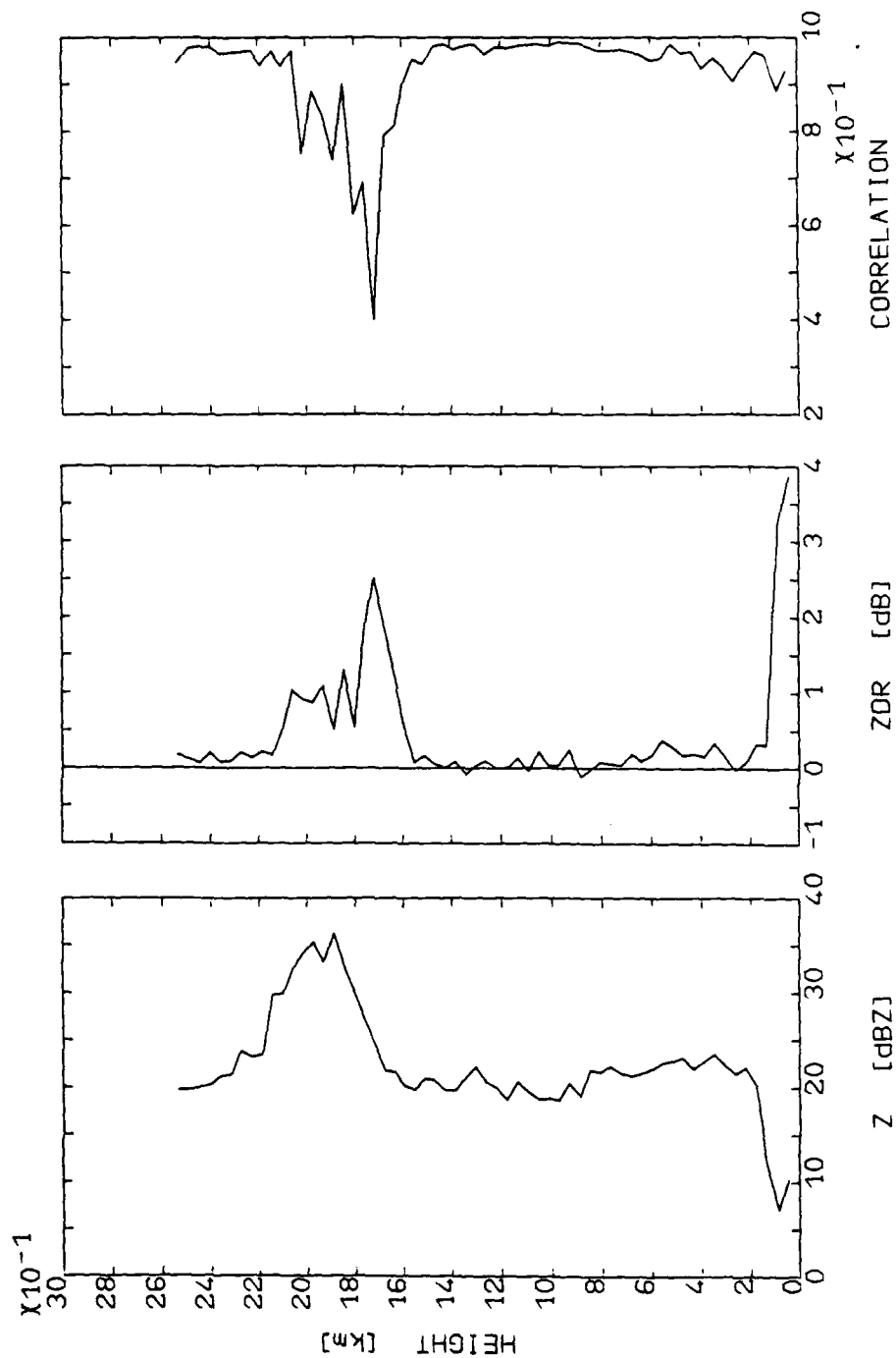


Figure 5. A profile of the vertical structure in Z, ZDR and $\rho(H,V)$ at a range of 9.9km for the RHI in Figure 4. The bright band is obvious between a height of 1.6km and 2.2km. The profile is taken at a single 300m wide range gate.

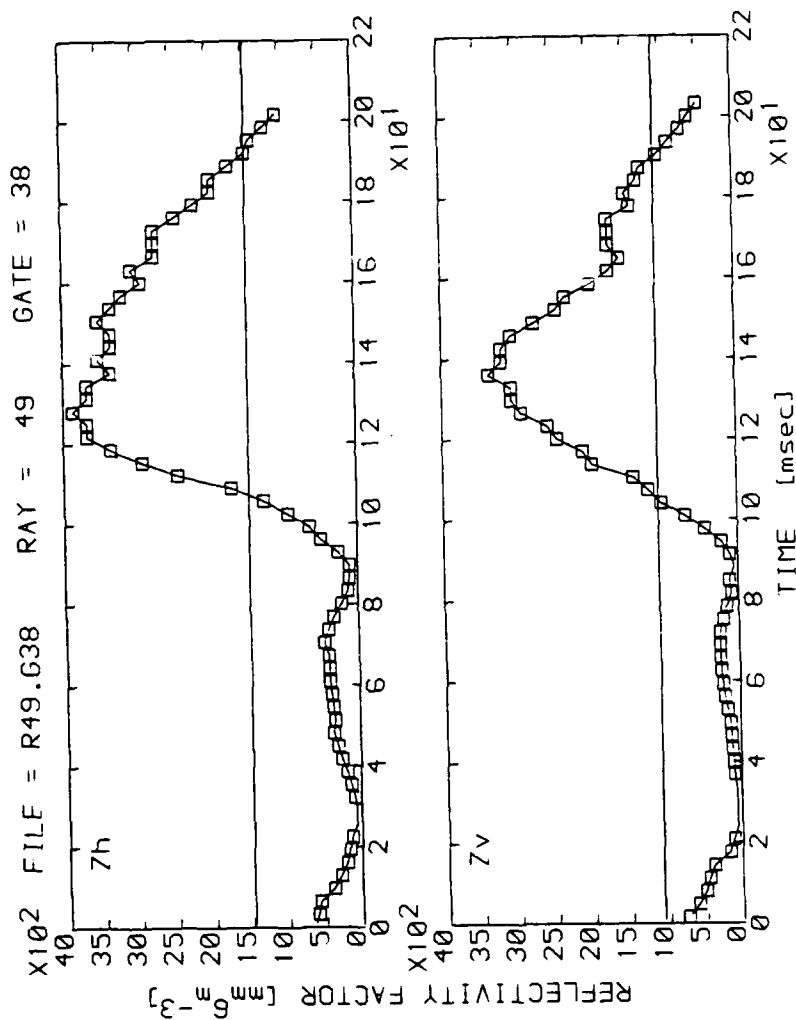


Figure 6. A time series for 7h and 7v observed in snow at a height of 2.06km and 9.9km range from the RHI of Figure 4. The correlation coefficient, $\rho(H,V)$, is 0.969.

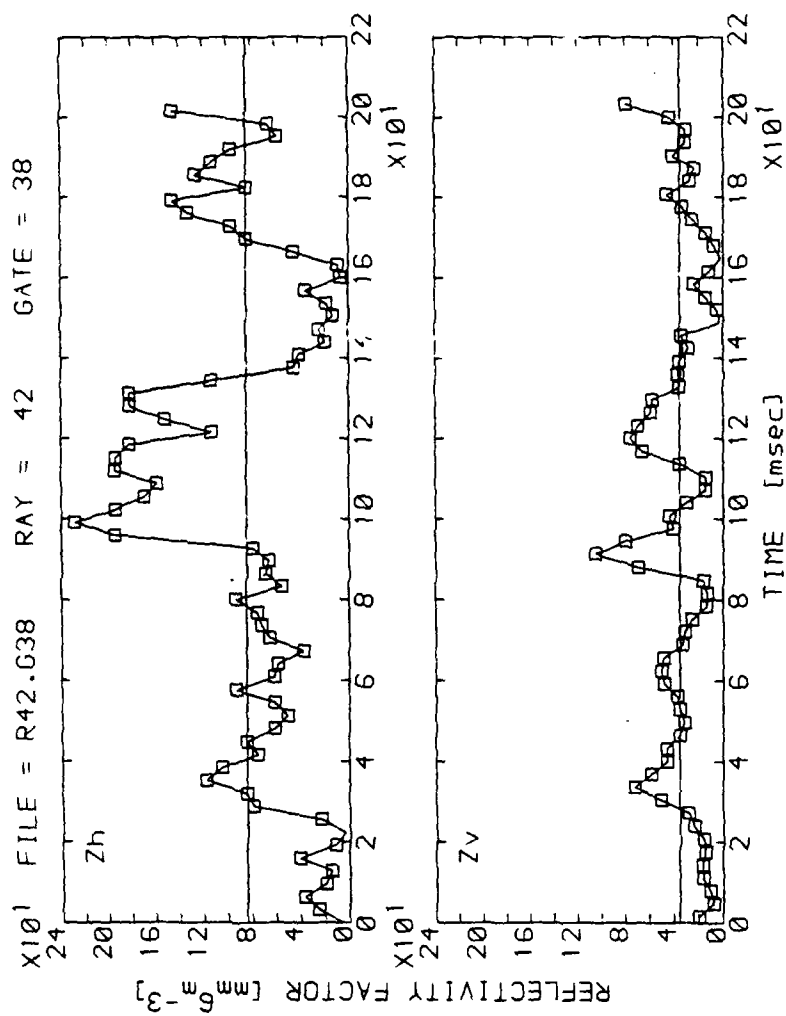


Figure 7. Z_h and Z_v time series with a correlation coefficient of 0.426 observed in the melting layer of the RHI in Figure 4. The range is 9.9km and the height is 1.76km.